



**BIMODAL HYBRID CONTROL OF RIGID-BODY ATTITUDE
BASED ON UNIT QUATERNIONS**

PAULO PERCIO MOTA MAGRO

**TESE DE DOUTORADO EM ENGENHARIA DE SISTEMAS ELETRÔNICOS E
DE AUTOMAÇÃO
DEPARTAMENTO DE ENGENHARIA ELÉTRICA**

**FACULDADE DE TECNOLOGIA
UNIVERSIDADE DE BRASÍLIA**

UNIVERSIDADE DE BRASÍLIA
FACULDADE DE TECNOLOGIA
DEPARTAMENTO DE ENGENHARIA ELÉTRICA

**BIMODAL HYBRID CONTROL OF RIGID-BODY ATTITUDE BASED
ON UNIT QUATERNIONS**

**CONTROLE HÍBRIDO BIMODAL DE ATITUDE DE CORPOS
RÍGIDOS BASEADO EM QUATÉRNIOS UNITÁRIOS**

PAULO PERCIO MOTA MAGRO

**ORIENTADOR: PROF. JOÃO YOSHIYUKI ISHIHARA
COORIENTADOR: PROF. HENRIQUE CEZAR FERREIRA**

TESE DE DOUTORADO EM ENGENHARIA DE SISTEMAS
ELETRÔNICOS E DE AUTOMAÇÃO

PUBLICAÇÃO: PPGEA.TD-121/17

BRASÍLIA/DF: SETEMBRO - 2017

UNIVERSIDADE DE BRASÍLIA
FACULDADE DE TECNOLOGIA
DEPARTAMENTO DE ENGENHARIA ELÉTRICA

BIMODAL HYBRID CONTROL OF RIGID-BODY ATTITUDE BASED
ON UNIT QUATERNIONS

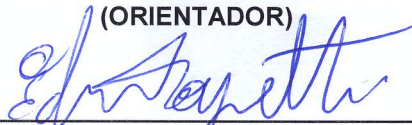
PAULO PERCIO MOTA MAGRO

TESE DE DOUTORADO SUBMETIDA AO DEPARTAMENTO DE ENGENHARIA ELÉTRICA DA
FACULDADE DE TECNOLOGIA DA UNIVERSIDADE DE BRASÍLIA, COMO PARTE DOS
REQUISITOS NECESSÁRIOS PARA A OBTENÇÃO DO GRAU DE DOUTOR.

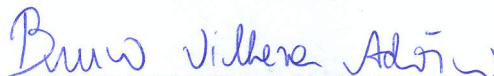
APROVADA POR:



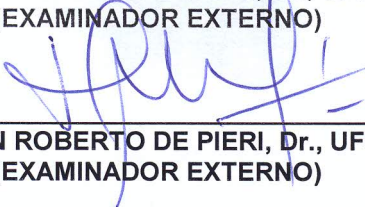
JOAO YOSHIYUKI ISHIHARA, Dr., ENE/UNB
(ORIENTADOR)



EDUARDO STOCKLER TOGNETTI, Dr., ENE/UNB
(EXAMINADOR INTERNO)



BRUNO VILHENA ADORNO, Dr., UFMG
(EXAMINADOR EXTERNO)



EDSON ROBERTO DE PIERI, Dr., UFSC
(EXAMINADOR EXTERNO)

Brasília, 12 de setembro de 2017.

FICHA CATALOGRÁFICA

MAGRO, PAULO PERCIO MOTA

Bimodal hybrid control of rigid-body attitude based on unit quaternions [Distrito Federal] 2017.

vi+88 p., 210 x 297 mm (ENE/FT/UnB, Doutor, Engenharia Elétrica, 2017).

Tese de doutorado – Universidade de Brasília, Faculdade de Tecnologia.

Departamento de Engenharia Elétrica

1. Hybrid system

2. Attitude control

3. Robustness

4. Unit quaternion

I. ENE/FT/UnB

II. Título (série)

REFERÊNCIA BIBLIOGRÁFICA

MAGRO, P. P. M. (2017). Bimodal hybrid control of rigid-body attitude based on unit quaternions, Tese de doutorado, Publicação PPGEA.TD-121/17, Departamento de Engenharia Elétrica, Universidade de Brasília, Brasília, DF, vi+88.

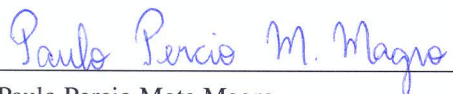
CESSÃO DE DIREITOS

AUTOR: Paulo Percio Mota Magro

TÍTULO: Bimodal hybrid control of rigid-body attitude based on unit quaternions.

GRAU: Doutor ANO: 2017

É concedida à Universidade de Brasília permissão para reproduzir cópias desta tese de doutorado e para emprestar ou vender tais cópias somente para propósitos acadêmicos e científicos. O autor reserva outros direitos de publicação e nenhuma parte dessa tese de doutorado pode ser reproduzida sem autorização por escrito do autor.



Paulo Percio Mota Magro

Departamento de Eng. Elétrica (ENE) - FT

Universidade de Brasília (UnB)

Campus Darcy Ribeiro

CEP 70919-970 - Brasília - DF - Brasil

*To my lovely wife Marcia
and my son Philippe*

ACKNOWLEDGMENTS

After getting my master's degree title, eighteen years ago, and after nineteen years of hard work on designing and programming instruments in the Process Control and Instrumentation area, I decided it was time to start a new journey of life. Back to university, I spent the last four years keeping up with the advances in Control Theory and Mathematics and working on the studies that make up this thesis. So far, it has been a tough and delightful experience, all at the same time.

Starting with my wife, Marcia Magro, I would like to thank her for all the support given since I first met her, in the end of my graduation course.

Also, I would like to express my gratitude to Prof. João Yoshiyuki Ishihara and Prof. Henrique Cezar Ferreira. To Prof. Ishihara for all his worthwhile guidance and his valuable classes that fulfilled my expectations. To Prof. Henrique for his assistance whenever necessary.

I register my acknowledgments to my fellow students Hugo T. Kussaba, Luis Felipe C. Figueredo (now postdoctoral researcher) and Henrique Marra Menegaz (now assistant professor of Faculdade do Gama - UnB) for the amiable mood, spicity of cooperation and enthusiasm, features that certainly inspired me to proceed my research in a focused and determined way.

For those, not mentioned here, who somehow helped me travel this road, my special thanks.

Lastly, I am grateful to the Cordenação de Aperfeiçoamento de Pessoal de Nível Superior (CAPES) for the doctoral scholarship and to the researchers of Laboratório de Automação e Robótica (LARA) for all the help given.

ABSTRACT

Title: Bimodal hybrid control of rigid-body attitude based on unit quaternions

Author: Paulo Percio Mota Magro

Supervisor: Prof. João Yoshiyuki Ishihara

Co-Supervisor: Prof. Henrique Cezar Ferreira

**Programa de Pós-graduação em Engenharia de Sistemas Eletrônicos e de Automação
Brasília, September 12th, 2017**

The main objective of this thesis is the development of a hybrid controller capable of solving the rest-to-rest attitude control problem with better performance than the hysteretic hybrid controller of literature in terms of settling time or energy consumption. The hybrid nature of the controller, in this case, is an essential requirement to achieve global control robust against measurement noise and to prevent undesirable effects such as unwinding and chattering. The attitude is represented by a unit quaternion since it provides the minimum number of parameters that does not present representation singularities.

It is proposed two distinct controllers, both with two binary logic variables for the control of attitude. The first designed controller, named HY, has the main variable determined by an on-off control with hysteresis that indicates which quaternion representation of the reference attitude should be followed and the other variable determined by an on-off control without hysteresis that indicates the chattering prone region. This scheme offers more opportunities of updating the main variable than the hysteretic hybrid controller, for instance, when there is an abrupt variation in the reference attitude. As a consequence, the body is more likely to being pulled towards the shortest rotation direction. However, this strategy restricts the way the controller is implemented (jumps can not have higher priority than flows).

In the second proposed controller, called bimodal, both variables are determined by an on-off control with hysteresis. The main variable indicates which quaternion representation of the reference attitude should be followed and the other variable indicates the chattering prone region. This strategy eliminates restrictions on the way the controller is implemented, but makes the dynamics of these variables more complex, since one variable influences the behavior of the other. The resulting effect is that the hysteresis width of the on-off control for the main variable adapts according to the state of the other variable being either equal or half of the value of the hysteresis width parameter. This controller is a middle term solution in terms of cost between the memoryless discontinuous and the hysteretic hybrid control.

It is presented a formal proof that the two proposed controls lead to global stability without unwinding and are robust against measurement noise. The effectiveness of the controllers is shown through simulations. The results indicate that the proposed controllers have advantages when the initial and final angular velocities are low. In the case of the bimodal controller, even for other initial angular velocities, the energy consumption of the system is, on average, lower compared to the hysteretic hybrid controller. Better performances in terms of energy consumption occur when the hysteresis band is larger as is the case when cheaper sensors are used or in noisy electromagnetic environments.

As an extension of the results mentioned above, two other contributions were proposed. One of them refers to the problem of attitude synchronization of a network of rigid bodies (agents). A distributed control with globally asymptotically stability property and robustness against noise measurement was proposed for an undirected connected network (cyclic or acyclic) of agents. The other one is related to the kinematic control of the pose of a rigid body within the unit dual quaternion group. It was proposed an extension of the bimodal attitude controller for the pose. For both cases, formal proofs are presented and simulation results illustrate the advantages of the proposed controllers.

Keywords: *Hybrid system, Attitude control, Robustness, Unit quaternion.*

RESUMO

Título: Controle híbrido bimodal de atitude de corpos rígidos baseado em quatérnios unitários

Autor: Paulo Percio Mota Magro

Orientador: Prof. João Yoshiyuki Ishihara

Coorientador: Prof. Henrique Cezar Ferreira

Programa de Pós-graduação em Engenharia de Sistemas Eletrônicos e de Automação

Brasília, 12 de setembro de 2017

Esta tese tem como objetivo principal o desenvolvimento de um controlador híbrido capaz de resolver o problema de regulação de atitude de um corpo rígido (a partir do repouso) com melhor desempenho que o controlador híbrido hysterético existente na literatura em termos de tempo de estabilização ou consumo de energia. A natureza híbrida do controlador é um requisito essencial para se obter um controle global e robusto a ruídos de medição e impedir efeitos indesejáveis como *unwinding* e *chattering*. A representação da atitude é feita com quatérnio unitário por possuir o menor número de parâmetros (quatro) que não apresenta singularidades.

Propõe-se dois controladores distintos, ambos com duas variáveis de estado lógicas binárias, para o controle de atitude. O primeiro controlador, denominado HY, tem a variável principal determinada por um controle *on-off* com histerese para indicar qual representação em quatérnio da atitude de referência deve ser seguida e uma outra variável determinada por um controle *on-off* sem histerese para indicar a proximidade à região crítica sujeita a *chattering*. Esse esquema oferece mais oportunidades de atualização da variável principal que o controlador híbrido hysterético, por exemplo quando há uma variação abrupta na atitude de referência. Isso reduz as chances do corpo seguir na direção da rotação mais longa. Contudo, essa estratégia impõe restrições na forma como o controlador é implementado (*jumps* não podem ter prioridade sobre *flows*).

No segundo controlador proposto, denominado bimodal, ambas as variáveis são determinadas por um controle *on-off* com histerese. A variável principal indica qual representação em quatérnio da atitude de referência deve ser seguida e a outra variável indica a proximidade à região crítica sujeita a *chattering*. Essa estratégia elimina as restrições sobre a forma de implementação do controlador, porém torna a dinâmica dessas variáveis mais complexas, dado que uma variável interfere no comportamento da outra. O efeito resultante é que a banda de histerese do controle *on-off* referente à variável principal, se adapta de acordo com o estado da outra variável, sendo ora igual, ora a metade do valor do parâmetro banda de histerese. Esse controlador é uma solução intermediária em termos de custo entre o controlador descontínuo e o controlador híbrido hysterético.

São apresentadas provas formais da estabilidade global do sistema e de sua robustez contra ruídos de medição para ambos os controladores propostos. A eficácia dos controladores é mostrada por meio de simulações. Os resultados indicam que os controladores propostos apresentam vantagens quando a velocidade angular inicial e final é baixa. No caso do controlador bimodal, mesmo para outras velocidades angulares iniciais, o consumo de energia do sistema é, em média, inferior quando comparado com o controlador híbrido hysterético. Melhores desempenhos em termos de consumo de energia ocorrem quando a banda de histerese é maior como no caso em que são usados sensores mais baratos ou em ambientes onde há muito ruído eletromagnético.

Como extensão dos resultados anteriormente citados, foram propostas mais duas contribuições. A primeira refere-se ao problema de sincronização de atitude de uma rede de corpos rígidos (agentes). Foi proposto um controle distribuído com propriedade de estabilidade global e assintótica e robustez contra ruídos de medição para uma rede de agentes representada por um grafo não direcionado e conexo (cíclico ou acíclico). A segunda está relacionada com o controle cinemático da pose de um corpo rígido dentro do grupo de quatérnio dual unitário. Foi proposta uma extensão do controlador de atitude bimodal para pose. Em ambos os casos as provas formais são apresentadas e resultados de simulação ilustram as vantagens dos controladores propostos.

Palavras-chave: *Sistemas híbridos, Controle de atitude, Robustez, Quatérnio unitário.*

CONTENTS

1	INTRODUCTION	1
1.1	CONTRIBUTIONS	3
1.2	MANUSCRIPT ORGANIZATION	4
2	PRELIMINARIES	6
2.1	ATTITUDE OF A RIGID BODY	6
2.2	QUATERNION	7
2.3	KINEMATICS AND DYNAMICS OF RIGID BODY ATTITUDE	8
2.4	ATTITUDE CONTROL PROBLEM	9
2.5	DUAL QUATERNION	9
2.6	KINEMATICS OF RIGID BODY MOTION	10
2.7	HYBRID SYSTEM FRAMEWORK	10
3	DISCONTINUOUS AND HYSTERETIC CONTROLLERS	12
3.1	GLOBAL STABILIZATION BY CONTINUOUS FEEDBACK	12
3.2	GLOBAL STABILITY VIA DISCONTINUOUS KINEMATIC ATTITUDE CONTROL	13
3.3	ROBUSTNESS PROBLEM	14
3.4	DISCONTINUOUS ATTITUDE CONTROL	16
3.5	HYSTERETIC HYBRID ATTITUDE CONTROL	17
3.6	PROBLEM DEFINITION	19
4	FIRST PROPOSED HYBRID ATTITUDE CONTROLLER (HY)	21
4.1	STABILITY ANALYSIS	22
4.2	CHATTERING ANALYSIS	25
4.3	SIMULATION RESULTS	27
4.4	CHAPTER CONCLUSIONS	28
5	PROPOSED BIMODAL HYBRID ATTITUDE CONTROLLER	30
5.1	STABILITY ANALYSIS	32
5.2	CHATTERING ANALYSIS	35
5.3	SIMULATION RESULTS	37
5.3.1	RIGID BODY	37
5.3.2	QUADROTOR MINI-HELICOPTER	39
5.3.3	SPACECRAFT	41
5.4	CHAPTER CONCLUSIONS	44
6	ROBUST GLOBAL DISTRIBUTED ATTITUDE CONTROL FOR MULTIPLE RIGID BODIES	46
6.1	PRELIMINARIES	46
6.1.1	ATTITUDE KINEMATICS AND DYNAMICS OF A GROUP OF N-AGENTS	46
6.1.2	GRAPH THEORY	47
6.1.3	MULTIPLE AGENTS ATTITUDE COORDINATION CONTROL	47
6.2	PROPOSED HYBRID ATTITUDE CONTROLLER	48
6.3	STABILITY ANALYSIS	49
6.4	SIMULATION RESULTS	53
6.5	CHAPTER CONCLUSIONS	55

7 DUAL QUATERNION-BASED BIMODAL GLOBAL CONTROL FOR ROBUST RIGID-BODY POSE KINEMATIC STABILIZATION	59
7.1 HYSTERETIC HYBRID CONTROLLER	59
7.2 PROPOSED BIMODAL HYBRID CONTROLLER	59
7.3 STABILITY ANALYSIS	60
7.3.1 CHATTERING ANALYSIS	62
7.4 SIMULATION RESULTS	63
7.5 CHAPTER CONCLUSIONS	63
8 CONCLUSIONS	67
8.1 FUTURE WORK	67
BIBLIOGRAPHY	69
 APPENDICES	
A RESUMO ESTENDIDO EM LÍNGUA PORTUGUESA	74
B PROOFS OF SOME LEMMAS	79
C PUBLICATIONS	88

List of Figures

1.1	Examples of areas where the global attitude control can be applied: underwater vehicle and aerospace vehicle.	1
2.1	Body frame, reference frame and fixed-reference frame example.	6
2.2	Example of a solution trajectory to a hybrid system. Solid curves indicate flow and dashed arcs indicate jumps.	11
3.1	Example of a strategy to stabilize the arm of a clock needle at point A.	13
3.2	State space representation of the discontinuous controller. Arrows indicate the direction of rotation so the attitude is regulated to $\mathbf{1}$ or $-\mathbf{1}$	14
3.3	System behavior for the discontinuous controller when no noise is present in the output y and when the output is corrupted by noise.	17
3.4	State space representation of the hysteretic controller (with one state variable \bar{h}). Arrows indicate the direction of the “proportional” term of the torque (dependent on \bar{h}) so the attitude is regulated to $\mathbf{1}$ or $-\mathbf{1}$. The parameter δ represents the hysteresis half-width of the on-off control for state \bar{h}	18
3.5	Comparison of the system behavior when the discontinuous controller and the hysteretic controller are applied to highlight the longer rotation direction determined by the hysteretic controller.	19
3.6	Comparison of the system behavior when the discontinuous controller and the hysteretic controller are applied to highlight the behavior when the initial condition of the system is not at rest.	19
4.1	Graphical representation of sets C_2 and D_2	21
4.2	State space representation of η_e and $\ \epsilon_e\ $ and the proposed regulation with two state variables (\bar{h} and m). The parameter δ represents the hysteresis half-width of the on-off control for state \bar{h}	22
4.3	Graphical representation of the jump map for h^+ and m^+	26
4.4	Comparison between the discontinuous controller and the proposed HY controller.	28
4.5	Comparison between the hysteretic controller and the proposed HY controller.	29
5.1	Graphical representation of sets C_2 and D_2	31
5.2	State space representation and the proposed regulation with two state variables (\bar{h} and m). Arrows indicate the direction of the “proportional” term of the torque (dependent on \bar{h}) so the attitude is regulated to $\mathbf{1}$ or $-\mathbf{1}$. The hysteresis half-width of the on-off control for state \bar{h} is $\delta/2$ when $m = 1$ and δ when $m = -1$	31
5.3	Graphical representation of the jump map for h^+ and m^+	36
5.4	Difference between the energy spent when the bimodal and the hysteretic controller is applied ($\Delta\mathcal{E}$) as a function of the initial conditions, represented by $\eta_e(0)$ and Ω	38
5.5	Comparison between the hysteretic and the proposed bimodal controller for a relatively high initial angular velocity norm.	39
5.6	Comparison between the discontinuous and the proposed bimodal controller for the quadrotor.	40
5.7	Comparison between the hysteretic and the proposed bimodal controller for the quadrotor.	41
5.8	Comparison between the hysteretic and the proposed bimodal controller for the spacecraft. Initial condition $\eta_e = -0.4$ and η_σ near -0.1	43
5.9	Comparison between the hysteretic and the proposed bimodal controller for the spacecraft. Initial condition $\eta_e = 0.4$ and η_σ near -0.1	44

5.10	Difference between the energy spent when the bimodal and the hysteretic controller is applied ($\Delta\mathcal{E}$) as a function of the initial conditions, represented by $\eta_e(0)$ and Ω	45
6.1	Agent i state space representation and the proposed regulation. The hysteresis half-width of the on-off control for state h_i is δ_i	49
6.2	Topology of communication.	54
6.3	Evolution of the first component of the attitude of the agents in the first scenario. In the upper graphic (continuous controller), a specific noise of magnitude lower than 0.2 was applied to agent 4 between 0.6 and 10 s. The lower graphic refers to the hybrid controller.	56
6.4	Evolution of the attitude $\mathbf{q}_{i0} = (\eta_{i0}, \epsilon_{i0})$ of the agents in the second scenario, where $\epsilon_{i0} = (\epsilon_{i0x}, \epsilon_{i0y}, \epsilon_{i0z})$. The graphics on the left refers to the continuous controller and the others on the right to the hybrid one.	57
6.5	Evolution of the angular velocity $\boldsymbol{\omega}_i = (\omega_{ix}, \omega_{iy}, \omega_{iz})$ of the agents in the second scenario. The graphics on the left refers to the continuous controller and the others on the right to the hybrid one.	58
7.1	State space representation of the hysteretic controller (with one state variable h). Arrows indicate the direction of the rotation so the attitude is regulated to $\mathbf{1}$ or $-\mathbf{1}$	60
7.2	State space representation of the bimodal controller (with two state variables, h and m). Arrows indicate the direction of the rotation so the attitude is regulated to $\mathbf{1}$ or $-\mathbf{1}$	61
7.3	Rotation comparison between the discontinuous and bimodal controllers.	64
7.4	Evolution of the translation components of $\mathbf{p} = p_x\hat{\mathbf{i}} + p_x\hat{\mathbf{j}} + p_x\hat{\mathbf{k}}$ for the discontinuous and bimodal controllers.	64
7.5	Rotation comparison between the hysteretic and bimodal controllers.	65
7.6	Evolution of the translation components of $\mathbf{p} = p_x\hat{\mathbf{i}} + p_x\hat{\mathbf{j}} + p_x\hat{\mathbf{k}}$ for the hysteretic and bimodal controllers.	65
B.1	Geometrical representation of distance d from $\mathbf{q} = (m, \epsilon_m)$	82

LIST OF SYMBOLS AND NOTATIONS

Symbols and notations for scalars, vectors, matrices and quaternions

a, b, c, \dots	scalars are represented by lowercase plain letters;
$\mathbf{a}, \mathbf{b}, \mathbf{c}, \dots$	vectors are represented by lowercase bold letters;
A, B, C, \dots	matrices are represented by uppercase plain letters;
$\mathbf{a}, \mathbf{b}, \mathbf{c}, \dots$	unit quaternions are represented by lowercase bold letters;
$\mathbf{A}, \mathbf{B}, \mathbf{C}, \dots$	quaternions are represented by uppercase bold letters;
$\hat{\mathbf{a}}, \hat{\mathbf{b}}, \hat{\mathbf{c}}, \dots$	unit norm vectors are represented by lowercase bold letters with a hat over the letter;
$\ \cdot\ $	Euclidean vector norm;
$\langle \cdot, \cdot \rangle$	inner product;
I_3	identity matrix of dimension 3;
A^T	transpose of matrix A ;
$\text{diag}(\mathbf{v})$	diagonal matrix with the diagonal elements being the components of vector \mathbf{v} ;
\dot{V}	time derivative of function V ;
∇V	gradient of Lyapunov function V ;
\circ	quaternion multiplication operation or dual quaternion multiplication operation;
\otimes	Kronecker product;
\times	cross-product operation between two three-dimensional vectors;
ε	dual unit;
\mathbf{q}^{-1}	inverse of the unit quaternion \mathbf{q} ;
\mathbf{q}^*	conjugate of the unit quaternion \mathbf{q} ;
$\Re(\mathbf{q}), \Im(\mathbf{q})$	the real and imaginary components of the unit quaternion \mathbf{q} ;
$\mathbf{0}$	null vector or quaternion $(0, \mathbf{0})$;
$\underline{\mathbf{q}}^*$	conjugate of the unit dual quaternion $\underline{\mathbf{q}}$;
$\Re(\underline{\mathbf{q}}), \Im(\underline{\mathbf{q}})$	real and imaginary components of the unit dual quaternion $\underline{\mathbf{q}}$.

The only exception refers to Lyapunov function candidates, represented by uppercase plain letter V .

Symbols and notation related to sets and groups

\mathbb{R}	set of real numbers;
\mathbb{R}^n	set of n-tuples of real numbers (x_1, x_2, \dots, x_n) for $x_i \in \mathbb{R}, i = \{1, \dots, n\}$;
\mathbb{H}	set of quaternions;
\mathbb{S}^3	set of unit quaternions, i.e. the unit 3-sphere;
\mathbb{H}_0	set of pure imaginary quaternions;
\mathbb{S}^n	hypersphere of \mathbb{R}^{n+1} ;
\mathbb{B}	closed unit ball in the Euclidean norm of appropriate dimension;
$\underline{\mathbb{H}}$	set of dual quaternions;
$\underline{\mathbb{S}}$	set of unit dual quaternions;
$\mathbb{B}(0, r)$	open ball of radius r in the Euclidean norm of appropriate dimension;
A, B, C, \dots	sets are represented by uppercase plain letters;
$A \setminus B$	set difference operation, i.e., the set of all members of A that are not members of B ;
$V^{-1}(A)$	preimage or inverse image of the set A ;
\overline{A}	closure of set A ;
$\overline{\text{co}}A$	closed convex hull of set A ;
$\text{SO}(3)$	group of rigid body rotations, i.e., the 3-dimensional special orthogonal group;
$\text{SE}(3)$	group of rigid body motions, i.e., the 3-dimensional special Euclidean group;
$\cdot \times \cdot$	Cartesian product of two sets.
X	set $\mathbb{S}^3 \times \mathbb{R}^3$;
X_c	set $\{-1, 1\}$.

1

INTRODUCTION

Rigid body attitude control is an important issue in aerospace vehicle projects (aircraft and spacecraft) as well as in underwater vehicles, ground vehicles, robotic systems, and some other applications [1] (see Figure 1.1). In a variety of applications, changes in operating points are necessary and consequently rest-to-rest motion is a common desired objective [2]. In particular, when arbitrary excursions in attitude are allowed or desired, the rest-to-rest global attitude control problem arises [1].

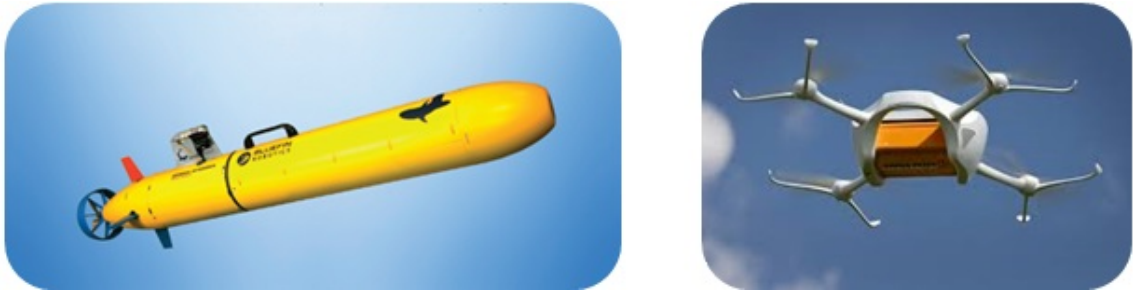


Figure 1.1: Examples of areas where the global attitude control can be applied: underwater vehicle and aerospace vehicle.

The requirement of globality in this problem results in no simple solution due to the nature of the group of all attitudes, $SO(3)$. It is known that any 3-parameter attitude representation as Euler angles has the drawback of having singularities [3], being valid only locally. In this context, unit quaternion has gained interest since it provides attitude using the minimum number of parameters that does not present representation singularities¹.

The state space of unit quaternions, however, is a double covering of the $SO(3)$ – a pair of antipodal unit quaternions corresponds to the same attitude in $SO(3)$ – which leads, when a continuous quaternion based controller is used, to the undesirable phenomenon known as *unwinding*, where the body may start at rest arbitrarily close to the desired final attitude and yet rotate through large angles before coming to rest [5]. The unwinding occurrence can be avoided if one uses a (memoryless) discontinuous state feedback, such as the ones suggested by Fjellstad and Fossen [6], Fragopoulos and Innocenti [7] or Wie and Barba [8]. Although global asymptotic stabilization is achieved, the discontinuous nature of the controller introduces a chattering phenomenon, that consists of multiple jumps (of states) occurring at the same time and may occur in the presence of measurement noise when the system is in a region near 180° away from the reference attitude [9].

A globally stabilizing attitude control robust to measurement noise can be achieved with a hysteresis-based hybrid controller proposed by Mayhew et al. [10], hereafter called the hysteretic controller, using one binary logic variable. The hysteresis width covers the chattering prone region and can be designed for a given maximum noise magnitude. Compared with the memoryless discontinuous control, the hysteresis-based control assures no chattering with the cost of imposing longer rotation trajectories for some initial attitudes leading to a higher average settling time or energy consumption.

In order to have lower energy consumption for the hysteresis-based controller, one can try to reduce the noise level received in the controller by using expensive high-precision sensors and/or attitude estimates relied on some estimator as, for example, Kalman or particle filter. Although these solutions are effective in some situations, there are others in which some expressive noise should be expected. On the one hand, one can consider the increasing demand for solutions with low-cost components. Since filters – and in particular, the

¹This type of singularity contrasts with the mechanical singularity in mechanical systems [4].

particle filter – are computationally expensive [11], for embedded processors with low memory and processing resources, usually a less effective simplified estimator should be used, resulting in higher attitude estimation noise. On the other hand, inexpensive sensors result in higher noise levels. For example, in the experiments of Gebre-Egziabher et al. [12], one can notice noise amplitudes around 10 degrees. If further, the system is under electromagnetic disturbance or its angular velocity is fast, the noise level may be even higher [13].

In this study it was sought a robust globally stabilizing controller which would represent a better solution in terms of cost when compared with the fixed width hysteresis control. Reduction of costs represented by average settling time or energy consumption is important, for instance, in satellites and any other battery-operated systems [14]. It is proposed two hybrid controllers with two binary logic variables (one more than the hysteretic controller) for the rest-to-rest control of attitude represented by quaternions. The main variable indicates which quaternion representation of the reference attitude should be followed and the auxiliary one indicates when the current attitude is far from the chattering prone region. The main idea of the first controller is to increase the opportunities to update the main variable when compared with the hysteretic controller. This is accomplished by the updates induced by the second logic variable. The second controller, called bimodal, was devised from the experience gained with the former. Its main idea is to provide the controller with some adaptive property to the hysteresis width rather than using a fixed width as in the hysteretic controller [10]. By introducing a more complex dynamics, the second variable also embodied the hysteresis adaptive function.

As an extension of the results described above, two other contributions were proposed: one on attitude synchronization control for a network of rigid bodies (agents) and the other one on kinematic control for rigid-body pose within the group of unit norm dual-quaternions.

Regarding the former extension, much research has been developed on attitude coordination control in the last 10-15 years [15, 16, 17, 18, 19]. Compared with single-agent systems, multi-agent systems have special advantages due to its cooperation, such as higher feasibility, accuracy, robustness, scalability, flexibility, robustness, lower cost etc. and have a wide range of applications such as environmental monitoring, search and rescue, space-based interferometers, material handling and so on [20].

As mentioned above, the problem of robust and global attitude stabilization for a single rigid body has been solved a few years ago [21], but the network scenario arises much more challenges due to the inherent inter-agent interactions. Up to now, the great majority of the studies on attitude synchronization strategy provides at most an almost global asymptotic stable control as in [18, 17] and when it provides global control, it is not robust to measurement noise.

To the best of the author knowledge, the only study on attitude synchronization of multiple agents that achieves robust global synchronization is the one of Mayhew et al. in 2012 [21]. It assumes that each agent has access only to the relative attitude between its neighbors and to its angular velocity relative to the body frame. Its goal is to achieve stability of a synchronized state (which is not a specific absolute reference attitude) using a hybrid feedback scheme. The advantage of not requiring inertial attitude measurements has the cost of achieving synchronization only for connected and acyclic networks [22]. Actually, there exists a physical obstacle to the global convergence when the graph contains cycles [22, Theorem 1].

In this study, it is proposed a distributed attitude synchronization control with globally asymptotically stability property and robustness against noise measurement for an undirected connected network (cyclic or acyclic) of agents. The strategy uses a quaternion representation of the inertial attitude and the hysteretic hybrid controller with one binary logic variable, suggested by Mayhew et al. [10], for each agent, to solve the known problems arisen when continuous or discontinuous state-feedback laws are employed such as presence of unstable states, unwinding phenomenon and chattering.

Regarding the latter extension, the Lie groups of rigid body motions $SE(3)$ arises naturally in the study of aerospace and robotic systems. Stemming from the seminal work of Brockett [23] about control theory on general Lie groups, much of the literature has been devoted to the control of systems defined on $SE(3)$.

Although it is usual to design controllers for this system using matrices to represent elements of this Lie group [24, 25], it has been noted by some authors that controllers designed using another type of representation, namely, the unit dual quaternions ($\text{Spin}(3) \times \mathbb{R}^3$), which double covers $\text{SE}(3)$, may have advantages regarding computational time and storage requirements [26, 27].

It is important to note that since in this case the state space of a dynamical system is a general manifold, some difficulties to design a stabilizing controller to the system can be expected. Actually, the problem of robust and global pose stabilization of a rigid body is not simple, but, to a certain extent, analogous to the attitude problem.

Firstly, there is no continuous feedback controller capable of globally asymptotically stabilizing an equilibrium point on the manifold of the unit dual quaternion group [28].

Secondly, as the Lie group of unit dual quaternions is a double cover for the Lie group of rigid body motions $\text{SE}(3)$ [29, 28], it leads, when a continuous dual quaternion based controller is used, to a phenomenon similar to the “unwinding” in $\text{SO}(3)$ [5]: the body may start at rest arbitrarily close to the desired final pose and yet travel to the farther stable point before coming to rest.

Lastly, even using a (memoryless) discontinuous state feedback, it is impossible to achieve robust global asymptotic stabilization of a disconnected set of points resulted from the double covering of the $\text{SE}(3)$ [10, 9].

There are few works on unwinding avoidance in the context of pose stabilization using unit dual quaternions [29, 30, 31, 32]. All of them are based on a discontinuous feedback approach and are prone to chattering for initial conditions arbitrarily close to the discontinuity.

Inspired on the hysteresis-based hybrid control of Mayhew et al. [10] applied to attitude control stabilization, Kussaba et al. [28] extended it to render both coupled kinematics—attitude and translation—stable. However, this pose controller suggested by Kussaba et al. [28] inherits the same cost, aforementioned, of imposing longer rotation trajectories for some initial attitudes leading to a higher average settling time or energy consumption. The problem of energy consumption also aggravates in this context, as the coupled translation and rotation movements consume more energy [28].

To reduce this cost, it is proposed a bimodal hybrid control law that combines the bimodal controller proposed above for the attitude control problem and the control suggested by Kussaba et al. [28] so it represents a compromise in terms of cost between the memoryless discontinuous controller and the hysteretic one.

1.1 CONTRIBUTIONS

The contributions of this manuscript are:

1. It is stated and proved a theorem about the problem faced by a discontinuous attitude controller in the presence of measurement noise in the unit quaternion space (see Theorem 3.4, page 15). This result is a correction for a theorem in [10]. In that work, the system is corrupted by noise but the measured variable does not belong to the unit quaternion space. Consequently, the system model loses physical sense.
2. It is presented a global hybrid control of rigid-body attitude that is robust against measurement noise that is oriented for the rest-to-rest control of attitude represented by quaternions (see Chapter 4). The proposed controller extends a hysteretic hybrid controller of literature by introducing a new binary logic variable state. The controller is able to detect when the reference changes abruptly and when the current attitude is far from the reference on the initial instant. This way, it has more opportunities to determine which quaternion representation of the reference attitude should be followed compared with the hybrid

hysteretic controller of literature and is more likely to take the shorter rotation direction. This study was presented at the XII Simpósio Brasileiro de Automação Inteligente - SBAI 2015 and an online publication of the respective article is available at <http://swge.inf.br/SBAI2015/anais/413.pdf>.

3. It is proposed another global hybrid control strategy for rigid-body attitude that is robust against measurement noise (i.e., without chattering) using a bimodal controller (see Chapter 5). It is oriented for the rest-to-rest control of attitude represented by quaternions, however it may present advantages in other scenarios too. Among the global controllers, it is expected to be the most interesting choice when the attitude noise level is significant as for example when low cost components are used or when the system is under an electromagnetically noisy environment. The controller has two binary logic variable states. By adapting the hysteresis width, it reduces the region where the hysteretic controller determines the longer rotation direction without compromising the robustness and is a middle term solution in terms of cost between the memoryless discontinuous and the hybrid hysteretic control. An article about this study has been published in the Journal of the Franklin Institute [33].
4. It is proposed a distributed attitude synchronization control with globally asymptotically stability property and robustness against noise measurement for an undirected connected network (cyclic or acyclic) of agents (rigid bodies) (see Chapter 6). Due to the inherent inter-agent interactions, the controller design is much more challenging. In literature, the great majority of the controllers suggest continuous or discontinuous state-feedback laws. Since when restricted to a unique rigid body these types of control strategies lead to systems with known problems such as unstable states, unwinding phenomenon and chattering, it is expected that the multi-agent system presents even worse performance. To solve these problems, the proposed control uses the hysteretic hybrid feedback of literature with one binary logic variable for each agent and a stricter condition for the hysteresis width parameter. An article about this study has been submitted to the International Journal of Systems Science.
5. It is proposed a global hybrid control strategy for the rigid-body pose kinematic problem that is robust against measurement noise. The dual quaternion-based hybrid controller suggested in literature extends the quaternion-based hysteretic controller which is known to have a region in the state space where the control law pulls the body toward the longer rotation direction. The proposed strategy adapts the bimodal attitude controller of Chapter 5 to the rigid-body pose system in order to reduce the average settling time or energy consumption. In this context, the problem of energy consumption is aggravated as the coupled translation and rotation movements consume more energy (see Chapter 7). This study was presented at the *American Control Conference - ACC 2017* and the article has been published [34].

1.2 MANUSCRIPT ORGANIZATION

The manuscript is organized as follows:

The second chapter introduces the reader to the kinematic and dynamic equations for rigid-bodies attitude and to the kinematic equation for rigid-bodies motion. Besides, it briefly explains the hybrid system representation.

The third chapter describes the discontinuous controller and the hysteretic hybrid controller found in literature. It also demonstrates a theorem relative to the chattering problem faced by a discontinuous controller in the presence of measurement noise.

Chapters 4 and 5 present the HY hybrid controller and bimodal hybrid controller with their respective stability and chattering analysis.

Chapter 6 and 7 refer to two distinct subjects that naturally arise from the rigid-body attitude control matter.

Chapter 6 addresses the rigid-body attitude control applied to multi-agent systems in a cooperative control. It describes the proposed controller based on the hybrid hysteretic controller of literature and proves that it robustly globally asymptotically stabilizes the synchronized state. Chapter 7 focuses on the rigid-body pose kinematic stabilization. It shows the proposed bimodal hybrid controller and the proofs of control stability and robustness.

Chapter 8 presents the concluding remarks and suggestions for future work.

Appendix A presents the extended summary in Portuguese language. Appendix B shows the proofs of the lemmas used along the text. Appendix C lists the papers published in or submitted to journals and conferences.

2

PRELIMINARIES

2.1 ATTITUDE OF A RIGID BODY

The expression “attitude of an object” is usually used in Geometry and means the orientation of such object in space [35, 36]. Rigid body is a completely “undistortable” body. More formally, a rigid body is a collection of particles such that the distance between any two particles remains fixed, regardless of any motions of the body or forces exerted on it [37]. In general, the attitude is described by the relationship between two right-handed Cartesian coordinate frames, one frame, called body frame, attached to the rigid body and the other one, called reference frame, with the same origin as the first, but having its axes parallel to a fixed-reference or inertial frame [4, 38, 36]. According to Figure 2.1, the fixed-reference frame is $O_r x_r y_r z_r$, the body frame is $Ouvw$ and the reference frame is $Oxyz$, whose axes Ox , Oy and Oz are, by definition, parallel to the axes $O_r x_r$, $O_r y_r$ and $O_r z_r$ of the fixed-reference frame and whose origin coincides with the one of the body frame.

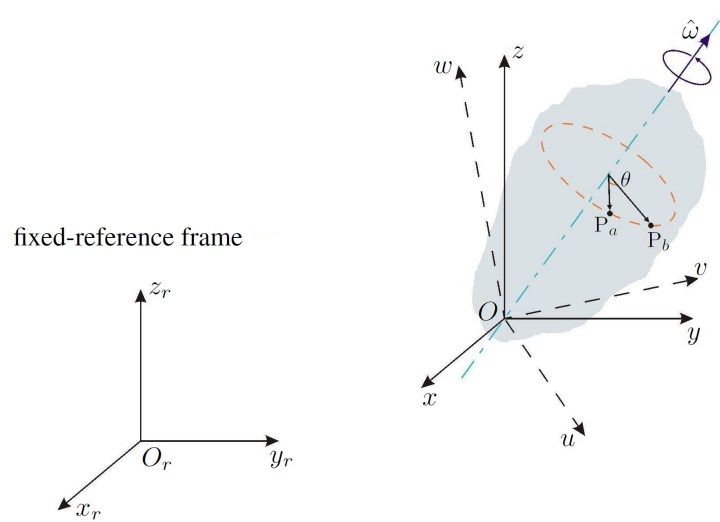


Figure 2.1: Body frame, reference frame and fixed-reference frame example.

The attitude can be represented in several ways. One of them is the rotation matrix, which can be interpreted as an operator that transforms the coordinates of a point from one frame to another one (passive transformation). For instance, suppose, initially, that the body frame coincides with the reference frame and after a determined period of time (the final moment), the body has rotated an angle θ about axis $\hat{\omega}$. Figure 2.1 illustrates the rotation motion of a body point from point P_a to P_b . Let \mathbf{p}_a and \mathbf{p}_b be the vectors that represent the coordinates of points P_a and P_b relative to a frame. As the body frame is attached to the body, $\mathbf{p}_b = \mathbf{p}_a$, relative to the body frame. However, relative to the reference frame,

$$\mathbf{p}_b = R\mathbf{p}_a. \quad (2.1)$$

The rotation matrix R transforms vector \mathbf{p}_a , which represents the position of point P_b relative to the body frame, into vector \mathbf{p}_b that represents the position of the same point P_b , relative to the reference frame.

The rotation matrix forms a group known as the special orthogonal group of order 3, or as the rotation group on \mathbb{R}^3 ,

$$\text{SO}(3) = \{R \in \mathbb{R}^{3 \times 3} : R^T R = R R^T = I, \det R = +1\}.$$

An element of $\text{SO}(3)$ can be parametrized by $\mathcal{R} : \mathbb{R} \times \mathbb{S}^2 \longrightarrow \text{SO}(3)$, defined as

$$\mathcal{R}(\theta, \hat{\omega}) = \exp(S(\hat{\omega})\theta),$$

where $\theta \in \mathbb{R}$ represents an angle, $\hat{\omega} \in \mathbb{S}^2$ is a rotation axis, $\mathbb{S}^n = \{\mathbf{x} \in \mathbb{R}^{n+1} : \mathbf{x}^T \mathbf{x} = 1\}$ and

$$S(\mathbf{x}) = \begin{bmatrix} 0 & -x_3 & x_2 \\ x_3 & 0 & -x_1 \\ -x_2 & x_1 & 0 \end{bmatrix}, \quad (2.2)$$

for $\mathbf{x} \in \mathbb{R}^3$. Equivalently, an element of $\text{SO}(3)$ can be parametrized by the Rodrigues formula [37]

$$\mathcal{R}(\theta, \hat{\omega}) = I + \sin(\theta)S(\hat{\omega}) + (1 - \cos(\theta))S(\hat{\omega})^2.$$

2.2 QUATERNION

The quaternion algebra is a four dimensional associative division algebra over \mathbb{R} invented by Hamilton [39], which naturally extends the algebra of complex numbers. It can represent rotations in a similar way as the complex numbers in the unit circle can represent planar rotations [37, pages 33,34]. The elements $1, \hat{i}, \hat{j}, \hat{k}$ are the basis of this algebra, satisfying

$$\hat{i}^2 = \hat{j}^2 = \hat{k}^2 = \hat{i}\hat{j}\hat{k} = -1. \quad (2.3)$$

The set of quaternions is defined as

$$\mathbb{H} \triangleq \left\{ \eta + \mu_1 \hat{i} + \mu_2 \hat{j} + \mu_3 \hat{k} : \eta, \mu_1, \mu_2, \mu_3 \in \mathbb{R} \right\}.$$

For ease of notation, the quaternion is denoted as $\mathbf{Q} \in \mathbb{H}$, where

$$\mathbf{Q} = \eta + \boldsymbol{\mu}, \quad \text{with} \quad \boldsymbol{\mu} = \mu_1 \hat{i} + \mu_2 \hat{j} + \mu_3 \hat{k}$$

and may be decomposed into a real component and an imaginary component: $\Re(\mathbf{Q}) \triangleq \eta$ and $\Im(\mathbf{Q}) \triangleq \boldsymbol{\mu}$ such that $\mathbf{Q} = \Re(\mathbf{Q}) + \Im(\mathbf{Q})$.

Another commonly used notation is

$$\mathbf{Q} = (\eta, \boldsymbol{\mu}),$$

with a scalar component $\eta \in \mathbb{R}$ and a vector component $\boldsymbol{\mu} = (\mu_1, \mu_2, \mu_3) \in \mathbb{R}^3$.

The sum of two quaternions, $\mathbf{Q}_a = (\eta_a, \boldsymbol{\mu}_a)$ and $\mathbf{Q}_b = (\eta_b, \boldsymbol{\mu}_b)$, is defined as

$$\mathbf{Q}_a + \mathbf{Q}_b = (\eta_a + \eta_b, \boldsymbol{\mu}_a + \boldsymbol{\mu}_b)$$

and the multiplication of two quaternions is defined as

$$\mathbf{Q}_a \circ \mathbf{Q}_b = (\eta_a \eta_b - \boldsymbol{\mu}_a^T \boldsymbol{\mu}_b, \eta_a \boldsymbol{\mu}_b + \eta_b \boldsymbol{\mu}_a + \boldsymbol{\mu}_a \times \boldsymbol{\mu}_b).$$

The conjugate of a quaternion \mathbf{Q} is given by $\mathbf{Q}^* = (\eta, -\boldsymbol{\mu})$ and the norm of a quaternion, by

$$\|\mathbf{Q}\| = \sqrt{\mathbf{Q} \circ \mathbf{Q}^*} = \sqrt{\eta^2 + \boldsymbol{\mu}^T \boldsymbol{\mu}} = \sqrt{\eta^2 + \mu_1^2 + \mu_2^2 + \mu_3^2}.$$

Pure imaginary quaternions are given by the set

$$\mathbb{H}_0 \triangleq \{\mathbf{Q} \in \mathbb{H} : \Re(\mathbf{Q}) = 0\}$$

which are very convenient to represent vectors of \mathbb{R}^3 . Thus, an Euclidean vector $\mathbf{p} \in \mathbb{R}^3$ can be represented in the same way as the quaternion $\mathbf{p} \in \mathbb{H}_0$ or as $(0, \mathbf{p}) \in \mathbb{H}_0$, using the other notation with the scalar component zeroed.

Unit quaternions¹ are defined as the quaternions that lie in the subset

$$\mathbb{S}^3 \triangleq \{\mathbf{q} \in \mathbb{H} : \|\mathbf{q}\| = 1\}.$$

The inverse of $\mathbf{q} \triangleq (\eta, \boldsymbol{\epsilon})$ equals its conjugate, $\mathbf{q}^{-1} = \mathbf{q}^* = (\eta, -\boldsymbol{\epsilon})$. Thus, $\mathbf{q} \circ \mathbf{q}^{-1} = \mathbf{q}^{-1} \circ \mathbf{q} = \mathbf{1} = (1, \mathbf{0})$, $\mathbf{0} = (0, 0, 0)$.

The set \mathbb{S}^3 forms, under multiplication, the Lie group Spin(3), whose identity element is $\mathbf{1}$ and group inverse is given by the quaternion conjugate \mathbf{q}^* .

Given the unit quaternion

$$\mathbf{q} = \left(\cos \frac{\theta}{2}, \hat{\boldsymbol{\omega}} \sin \frac{\theta}{2} \right), \quad (2.4)$$

the mapping $\mathcal{R} : \mathbb{S}^3 \longrightarrow \text{SO}(3)$ is defined by

$$\mathcal{R}(\mathbf{q}) = I + 2\eta S(\boldsymbol{\epsilon}) + 2S(\boldsymbol{\epsilon})^2. \quad (2.5)$$

Note that $\mathcal{R}(\mathbf{q}) = \mathcal{R}(-\mathbf{q})$. As the unit quaternions \mathbf{q} and $-\mathbf{q}$ represent the same rotation, the unit quaternion group double covers the rotation group SO(3).

The transformation from \mathbf{p}_a to \mathbf{p}_b , achieved by applying operator R in (2.1), can also be obtained by using the unit quaternion \mathbf{q} defined in (2.4) and equation [41, page 520]

$$(0, \mathbf{p}_b) = \mathbf{q} \circ (0, \mathbf{p}_a) \circ \mathbf{q}^*. \quad (2.6)$$

2.3 KINEMATICS AND DYNAMICS OF RIGID BODY ATTITUDE

Consider a rigid body with inertia matrix J in a rotational motion due to the action of some external torque $\boldsymbol{\tau} \in \mathbb{R}^3$. Consider also two frames: the reference frame and the body frame attached to the rigid body. Given that \mathbf{q} represents the rigid-body attitude $R \in \text{SO}(3)$, defined as the relative rotation of a body frame to a reference frame, the quaternion kinematic equation² is given by

$$\dot{\mathbf{q}} = \frac{1}{2} \mathbf{q} \circ (0, \boldsymbol{\omega}), \quad (2.7)$$

where $\boldsymbol{\omega} \in \mathbb{R}^3$ is the angular velocity expressed in the body frame.

The angular velocity rate is calculated using the dynamic equation (Euler's equation),

$$J\dot{\boldsymbol{\omega}} = S(J\boldsymbol{\omega})\boldsymbol{\omega} + \boldsymbol{\tau}, \quad (2.8)$$

written in body coordinates [37, page 167], i.e., the torque is expressed in the body frame and the inertia matrix is constant and calculated in the body frame (see Lemma B.1).

¹Along the text, the use of unit quaternions follows the Hamilton convention [40], that is, elements of the quaternion are ordered with real part first, quaternion algebra satisfies $\hat{\mathbf{i}}^2 = \hat{\mathbf{j}}^2 = \hat{\mathbf{k}}^2 = \hat{\mathbf{i}}\hat{\mathbf{j}}\hat{\mathbf{k}} = -1$ (2.3), operation $\mathbf{q} \circ (0, \mathbf{v}) \circ \mathbf{q}^*$ performs a passive transformation of vector \mathbf{v} components from local to global frame.

²For further details about rigid-body kinematic and dynamic equations refer to [37, 42].

2.4 ATTITUDE CONTROL PROBLEM

The attitude control problem may be established as a function of the attitude error. Supposing that $\mathbf{q}_d \in \mathbb{S}^3$ represents the desired constant attitude reference (the desired angular velocity is $\boldsymbol{\omega}_d \equiv \mathbf{0}$), the attitude error is given by $\mathbf{q}_e = (\eta_e, \boldsymbol{\epsilon}_e) = \mathbf{q}_d^* \circ \mathbf{q} \in \mathbb{S}^3$ and the kinematic equation is described by (Lemma B.2)

$$\dot{\mathbf{q}}_e = \frac{1}{2} \mathbf{q}_e \circ (0, \boldsymbol{\omega} - \mathcal{R}(\mathbf{q}_e)^T \boldsymbol{\omega}_d) = \frac{1}{2} \mathbf{q}_e \circ (0, \boldsymbol{\omega}). \quad (2.9)$$

Let $X = \mathbb{S}^3 \times \mathbb{R}^3$ and $\bar{x} = (\mathbf{q}_e, \boldsymbol{\omega}) \in X$. Since each physical attitude $R \in \text{SO}(3)$ is represented by a pair of antipodal unit quaternions $\pm \mathbf{q} \in \mathbb{S}^3$, the objective of the control becomes to stabilize the set

$$A = \{(\mathbf{1}, \mathbf{0}), (-\mathbf{1}, \mathbf{0})\} \subset X$$

for the following system

$$\dot{\bar{x}} = \begin{bmatrix} \dot{\mathbf{q}}_e \\ \dot{\boldsymbol{\omega}} \end{bmatrix} = F(\bar{x}, \boldsymbol{\tau}), \quad F(\bar{x}, \boldsymbol{\tau}) \triangleq \begin{bmatrix} \frac{1}{2} \mathbf{q}_e \circ (0, \boldsymbol{\omega}) \\ J^{-1}(S(J\boldsymbol{\omega})\boldsymbol{\omega} + \boldsymbol{\tau}) \end{bmatrix}, \quad (2.10)$$

by means of an appropriate choice of a feedback torque law $\boldsymbol{\tau}$, which has as information the output of the system (2.10) given by

$$y = (\mathbf{q}, \boldsymbol{\omega}), \quad (2.11)$$

that is, \mathbf{q} and $\boldsymbol{\omega}$ are measured. Note that together with the desired reference, \mathbf{q}_d , the state $\bar{x} = (\mathbf{q}_e, \boldsymbol{\omega})$ is available for feedback.

2.5 DUAL QUATERNION

Similarly to how the quaternion algebra was introduced to address rotations in the three-dimensional space, the dual quaternion algebra was introduced by Clifford [43] and Study [44] to describe rigid body movements. This algebra is constituted by the set

$$\mathbb{H} \triangleq \{\mathbf{q} + \varepsilon \mathbf{q}' : \mathbf{q}, \mathbf{q}' \in \mathbb{H}\},$$

where \mathbf{q} and \mathbf{q}' are called the primary part and the dual part of the dual quaternion and ε is called the dual unit which is nilpotent—that is, $\varepsilon \neq 0$ and $\varepsilon^2 = 0$. Given $\underline{\mathbf{q}} = \boldsymbol{\eta} + \boldsymbol{\mu} + \varepsilon(\boldsymbol{\eta}' + \boldsymbol{\mu}')$, define $\Re(\underline{\mathbf{q}}) \triangleq \boldsymbol{\eta} + \varepsilon \boldsymbol{\eta}'$ and $\Im(\underline{\mathbf{q}}) \triangleq \boldsymbol{\mu} + \varepsilon \boldsymbol{\mu}'$, such that $\underline{\mathbf{q}} = \Re(\underline{\mathbf{q}}) + \Im(\underline{\mathbf{q}})$. The dual quaternion conjugate is $\underline{\mathbf{q}}^* \triangleq \Re(\underline{\mathbf{q}}) - \Im(\underline{\mathbf{q}}) = \mathbf{q}^* + \varepsilon \mathbf{q}'^*$.

The multiplication of two dual quaternions $\underline{\mathbf{q}}_1 = \mathbf{q}_1 + \varepsilon \mathbf{q}'_1$ and $\underline{\mathbf{q}}_2 = \mathbf{q}_2 + \varepsilon \mathbf{q}'_2$ is given by

$$\underline{\mathbf{q}}_1 \circ \underline{\mathbf{q}}_2 = \mathbf{q}_1 \circ \mathbf{q}_2 + \varepsilon(\mathbf{q}_1 \circ \mathbf{q}'_2 + \mathbf{q}'_1 \circ \mathbf{q}_2).$$

The subset of dual quaternions

$$\underline{\mathcal{S}} = \{\mathbf{q} + \varepsilon \mathbf{q}' \in \mathbb{H} : \|\mathbf{q}\| = 1, \mathbf{q} \circ \mathbf{q}'^* + \mathbf{q}' \circ \mathbf{q}^* = 0\} \quad (2.12)$$

forms a Lie group [45] called unit dual quaternions group, whose identity is $\underline{\mathbf{1}} = \mathbf{1} + \varepsilon \mathbf{0}$, $\mathbf{0} = 0 + 0\hat{i} + 0\hat{j} + 0\hat{k}$ and group inverse is the dual quaternion conjugate. The constraint $\mathbf{q} \circ \mathbf{q}'^* + \mathbf{q}' \circ \mathbf{q}^* = 0$ in (2.12) implies that

$$\boldsymbol{\eta} \boldsymbol{\eta}' + \boldsymbol{\mu}^T \boldsymbol{\mu}' = 0. \quad (2.13)$$

An arbitrary rigid body displacement characterized by a rotation $\mathbf{q} \in \text{Spin}(3)$, followed by a translation $\mathbf{p} = p_x \hat{i} + p_y \hat{j} + p_z \hat{k} \in \mathbb{H}_0$ expressed in the body frame, is represented by the unit dual quaternion [29, 46]

$$\underline{\mathbf{q}} = \mathbf{q} + \varepsilon \frac{1}{2} \mathbf{q} \circ \mathbf{p}. \quad (2.14)$$

As the displacement $\underline{\mathbf{q}}$ is equally described by $-\underline{\mathbf{q}}$, the unit dual quaternions group double covers SE(3).

2.6 KINEMATICS OF RIGID BODY MOTION

Let \mathbf{q} represent the rigid-body attitude $R \in SO(3)$, defined as the relative rotation of a body-fixed frame to a reference frame and $\mathbf{p} \in \mathbb{H}_0$ represent the translation expressed in the body frame. The unit dual quaternion $\underline{\mathbf{q}}$, given by (2.14), describes the coupled attitude and position and the kinematic equation of a rigid body motion is given by [46]

$$\dot{\underline{\mathbf{q}}} = \frac{1}{2} \underline{\mathbf{q}} \circ \underline{\boldsymbol{\omega}}, \quad (2.15)$$

where $\underline{\boldsymbol{\omega}} = \boldsymbol{\omega} + \varepsilon \boldsymbol{\omega}'$ is called twist and is given by

$$\underline{\boldsymbol{\omega}} = \boldsymbol{\omega} + \varepsilon [\dot{\mathbf{p}} + \boldsymbol{\omega} \times \mathbf{p}], \quad (2.16)$$

$\boldsymbol{\omega} \in \mathbb{H}_0$ is the angular velocity expressed in the body frame and $\dot{\mathbf{p}} \in \mathbb{H}_0$ is the velocity expressed in the body frame.

Note that due to the principle of transference the kinematic equations (2.7) and (2.15) are similar [47]. It is straightforward to notice that (2.15) embodies both equation (2.7) and $\dot{\mathbf{p}} = \boldsymbol{\omega}' - \boldsymbol{\omega} \times \mathbf{p}$.

The principle of transference may mislead one to think that every theorem in quaternions can be transferred to another theorem in dual quaternions by a transference process. This is shown by counterexamples in [47]. Therefore, properties and phenomena related to quaternion motions like topological obstructions and unwinding may not follow by direct use of transference and have to be verified for dual quaternions [28].

2.7 HYBRID SYSTEM FRAMEWORK

Since a model of a hybrid dynamical system requires a description of the continuous-time dynamics, the discrete-time dynamics and the regions on which these dynamics apply, the general model of a hybrid system \mathcal{H} is in the form [48]

$$\mathcal{H} : \begin{cases} \dot{x} \in F(x), & x \in C, \\ x^+ \in G(x), & x \in D, \end{cases} \quad (2.17)$$

where x represents the state of the hybrid system, $\dot{x} \in F(x)$ is a differential inclusion that describes the flow, i.e., the behavior of the hybrid system while in the set C and $x^+ \in G(x)$ is a difference inclusion that describes the jumps, i.e., the behavior of the hybrid system while in the set D . The notation x^+ represents the state x just after transition. The objects of the model are named as follows: C is the flow set, F is the flow map, D is the jump set and G is the jump map [49].

Figure 2.2 shows a solution trajectory example [48]. A solution trajectory to a hybrid system is parametrized by both t , the amount of time passed, and j , to account for the number of jumps that have occurred. Subsets of $E \subset [0, \infty) \times \{0, 1, 2, \dots\}$ can correspond to the domain of evolutions of hybrid systems and are called hybrid time domains. More specifically, a subset E is a compact hybrid time domain if

$$E = \bigcup_{j=0}^{J-1} ([t_j, t_{j+1}], j)$$

for some finite sequence of times $0 = t_0 \leq t_1 \leq t_2 \leq \dots \leq t_J$ while E is a hybrid time domain if it is a union of a finite or infinite sequence of intervals $[t_j, t_{j+1}] \times \{j\}$ with the last interval (if existent) in the form $[t_j, T)$ for $T \in \mathbb{R}$ or in the form $[t_j, \infty)$ [49].

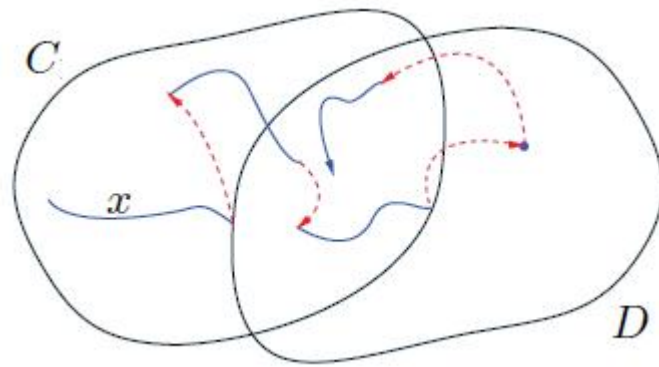


Figure 2.2: Example of a solution trajectory to a hybrid system. Solid curves indicate flow and dashed arcs indicate jumps.

3

DISCONTINUOUS AND HYSTERETIC CONTROLLERS

Attitude control of a rigid body is a typical nonlinear control problem and has been studied for decades [50, 8, 10], motivated especially by aerospace applications that involve maneuvers or attitude stabilization [1]. It is also an important problem in underwater vehicles projects, ground vehicles, robotic systems etc [1].

Probably, the first systematic study of spacecraft attitude control began in 1952, which was documented in unpublished form only (and classified as “secret”) [51]. Beforehand, in the second half of 1940’s, many studies in this area were sponsored by U.S. government agencies. In the open literature, one of the first paper appeared in 1957 (the launch year of Sputnik, the world’s first artificial Earth satellite). It described the problem of actively controlling one of the axes orientation of an artificial satellite so that it remains pointed downward toward the Earth [51].

By 1970, anticipating future spacecraft needs, rapid and large angle reorientation was already subject to study [52]. Later on, in 1985, it was published one of the first papers suggesting a discontinuous control feedback to achieve global attitude control [8]. Finally, only 26 years afterwards, in 2011, Mayhew et al. [10] noted that for the control of [8], it is possible to find a small measurement noise which is able to induce chattering of the state and presented a hybrid feedback control law that solved the global asymptotic stabilization problem and was robust to measurement noise.

3.1 GLOBAL STABILIZATION BY CONTINUOUS FEEDBACK

Bhat and Bernstein [5] proved that the attitude can not be globally stabilized by means of continuous feedback using Theorem 3.1 below and the fact that $SO(3)$ is a compact manifold, .

Let \mathcal{M} be a manifold of dimension m and consider a continuous vector field f on \mathcal{M} .

Theorem 3.1 From [4, Theorem 1]

Suppose $\pi : \mathcal{M} \rightarrow \mathcal{Q}$ is a vector bundle on \mathcal{Q} , where \mathcal{Q} is a compact, r -dimensional manifold with $r \leq m$. Then there exists no equilibrium of f that is globally asymptotically stable.

An easier way to understand the impossibility of global attitude stabilization using continuous time-invariant feedback is shown in [1, page 38] using the illustration of Figure 3.1. In this case, the manifold is the circle \mathbb{S}^1 and the problem refers to the attitude stabilization of the arm of the clock needle using a continuous feedback. To stabilize in configuration A, a continuous force vector field, tangent to the circle, was constructed to rotate the needle. Since the upper and lower half of the circle point in opposite direction, the vector force field must vanish somewhere – at point B in this case. Thus, a second unstable equilibrium point is created, an unstable one. Similarly, continuous time-invariant closed-loop vector fields create multiple closed-loop equilibria on the rotation group $SO(3)$ and the unit quaternion group \mathbb{S}^3 .

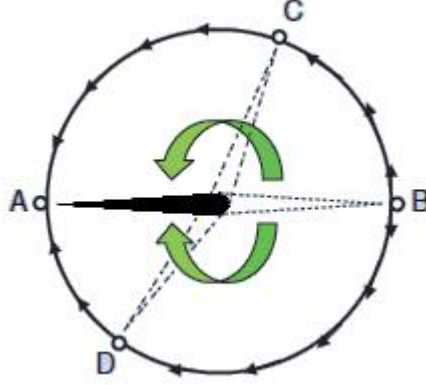


Figure 3.1: Example of a strategy to stabilize the arm of a clock needle at point A.

3.2 GLOBAL STABILITY VIA DISCONTINUOUS KINEMATIC ATTITUDE CONTROL

To simplify the problem presentation, only the kinematic attitude control is considered at first. That is, the system is described by equation (2.9) and the goal is to design an angular velocity feedback ω to stabilize the set $A_k = \{\mathbf{q}_e = \mathbf{1} \text{ or } \mathbf{q}_e = -\mathbf{1}\}$. The discontinuous feedback is motivated by the following Lyapunov function:

$$V(\mathbf{q}_e) = 2(1 - |\eta_e|).$$

Function V is positive definite on \mathbb{S}^3 with respect to A_k , since $V(\mathbb{S}^3 \setminus A_k) > 0$ and $V(A_k) = 0$. Considering the following control law

$$\omega(\mathbf{q}_e) = -\bar{h}\epsilon_e, \quad (3.1)$$

where $\bar{h} = \text{sgn}(\eta_e)$ and

$$\text{sgn}(\eta_e) \triangleq \begin{cases} -1, & \eta_e < 0, \\ 1, & \eta_e \geq 0, \end{cases} \quad (3.2)$$

the time derivative of V is $\dot{V}(\mathbf{q}_e) = -\|\epsilon_e\|^2$, which is negative definite. Note that this control law pulls the body toward the shortest rotation direction (see Figure 3.2).

The closed-loop had been proved to be globally asymptotically stable¹ [7]. However, when the initial condition of the system is near the discontinuity – i.e., near $\eta_e = 0$, a region near 180° away from the reference attitude –, measurement noise can cause chattering, which consists of multiple jumps (of states) occurring at the same time and keep the state near the discontinuity indefinitely [10]. Let $\mathbf{R} = (\eta_r, \epsilon_r) \in \mathbb{H}$ represent the noise such that $\mathbf{q}_m = (\mathbf{q}_e + \mathbf{R}) \in \mathbb{S}^3$ be the attitude corrupted by noise \mathbf{R} at instant t . Note that if η_e is near 0, the sign of $\eta_e + \eta_r$ and the sign of η_e can be different inducing the controller to change \bar{h} . This way, the discontinuous controller is not robust to measurement noise.

¹As function V is not a continuously differentiable, LaSalle's Theorem [53, page 117] can not be applied.

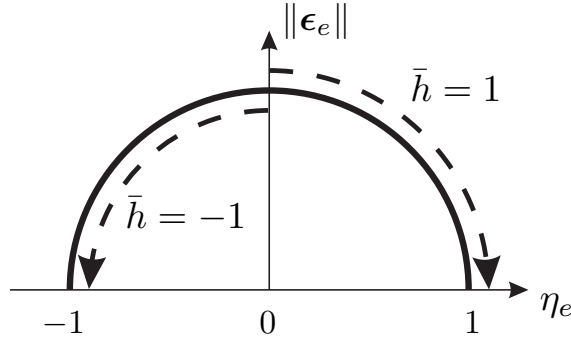


Figure 3.2: State space representation of the discontinuous controller. Arrows indicate the direction of rotation so the attitude is regulated to $\mathbf{1}$ or $-\mathbf{1}$.

3.3 ROBUSTNESS PROBLEM

As mentioned in the previous section, in case of a discontinuous feedback law, when the initial condition of the system is near the discontinuity, measurement noise can cause chattering and keep the state near the discontinuity indefinitely [9, 10]. See example of chattering behavior in Figure 3.3 (Section 3.4). Therefore, the stability is not robust to arbitrarily small measurement noise. To simplify notation, \mathbf{q}_e will be denoted as \mathbf{q} in this chapter.

Theorem 3.2 of Sanfelice et al. [9] proves this fact for a generic space. Before it is enunciated, it follows some definitions.

Let $O \subset \mathbb{R}^n$ be an open set and let $\mathcal{M}_i \subset \mathbb{R}^n$, $i \in \{1, \dots, m\}$, $m > 1$, be sets satisfying $\bigcup_{i=1}^m \mathcal{M}_i = O$. Let $\mathcal{M} \triangleq \bigcup_{i,j,i \neq j} \overline{\mathcal{M}_i} \cap \overline{\mathcal{M}_j}$, where $\overline{\mathcal{M}_i}$ is the closure of set \mathcal{M}_i .

Definition 3.1. [9, Definition 2.1] A Carathéodory solution to the system $\dot{\mathbf{x}} = f(\mathbf{x})$, where $\mathbf{x} \in \mathbb{R}^n$ is the state and $f : \mathbb{R}^n \rightarrow \mathbb{R}^n$, on an interval $I \subset [0, \infty)$ is an absolutely continuous function $\mathbf{x} : I \rightarrow \mathbb{R}^n$ that satisfies $\dot{\mathbf{x}}(t) = f(\mathbf{x}(t))$ almost everywhere on I . Given a piecewise constant function $\mathbf{e} : I \rightarrow \mathbb{R}^n$, a Carathéodory solution to the system $\dot{\mathbf{x}} = f(\mathbf{x} + \mathbf{e})$ on I is an absolutely continuous function \mathbf{x} that satisfies $\dot{\mathbf{x}}(t) = f(\mathbf{x}(t) + \mathbf{e}(t))$ for almost every $t \in I$; equivalently, for every $t_0 \in I$, $\mathbf{x}(t)$ satisfies

$$\mathbf{x}(t) = \mathbf{x}(t_0) + \int_{t_0}^t f(\mathbf{x}(\tau) + \mathbf{e}(\tau))d\tau, \quad \forall t \in I.$$

Theorem 3.2 From [7, Theorem 2.6]

Let $\varepsilon > 0$ and let \mathcal{K} satisfy $\mathcal{K} + \mathbb{B}(0, 2\varepsilon) \subset O$. Then, for each $\mathbf{x}_0 \in (\mathcal{M} + \mathbb{B}(0, \varepsilon)) \cap \mathcal{K}$ there exists a piecewise constant function $\mathbf{e} : [0, \infty) \rightarrow \mathbb{B}(0, \varepsilon)$ and a Carathéodory solution \mathbf{x} to $\dot{\mathbf{x}} = f(\mathbf{x} + \mathbf{e})$ starting at \mathbf{x}_0 such that $\mathbf{x}(t) \in (\mathcal{M} + \mathbb{B}(0, \varepsilon))^a$ for all $t \in [0, \infty)$ such that $\mathbf{x}(\tau) \in \mathcal{K}$ for all $\tau \in [0, t]$.

^aThe sum of sets follows Minkowski sum definition, i.e., $A + B = \{\mathbf{a} + \mathbf{b} : \mathbf{a} \in A, \mathbf{b} \in B\}$.

Besides, Sanfelice et al. [9] affirmed that this theorem can be extended to systems of the form $\dot{\mathbf{x}} = f(\mathbf{x}, \kappa(\mathbf{x} + \mathbf{e}))$, with $f(\cdot, \mathbf{u})$ locally Lipschitz uniformly over \mathbf{u} 's in the range of κ .

Mayhew et al. [10] also proved this fact (robustness problem) for the discontinuous control law $\boldsymbol{\omega}(\mathbf{q}) = -\text{sgn}(\eta)\boldsymbol{\epsilon}$ (3.1). They stated the following theorem.

Theorem 3.3 From [8, Theorem 3.2]

Let $\omega(\mathbf{q}) = -\text{sgn}(\eta)\epsilon$, $\mathcal{M} \triangleq \{\mathbf{q} \in \mathbb{S}^3 : \eta = 0\}$. Then for each $\alpha > 0$ and each $\mathbf{q}_0 \in \mathcal{M}^* \triangleq (\mathcal{M} + \alpha\mathbb{B}) \cap \mathbb{S}^3$, there exists a measurable function $e : [0, \infty) \rightarrow \alpha\mathbb{B}$ and a Carathéodory solution $\mathbf{q} : [0, \infty) \rightarrow \mathbb{S}^3$ to $\dot{\mathbf{q}} = \frac{1}{2}\mathbf{q} \circ (0, \omega(\mathbf{q} + e))$ satisfying $\mathbf{q}(0) = \mathbf{q}_0$ and $\mathbf{q}(t) \in \mathcal{M}^*$ for all $t \in [0, \infty)$.

This theorem affirms that applying the discontinuous control law, if the initial condition of the system is near the discontinuity ($\mathbf{q}_0 \in \mathcal{M}^*$), there exist a noise of magnitude not higher than α such that the state will remain near the discontinuity indefinitely. A point that stands out from these two theorems is that the feedback variable when corrupted by the measurement noise has no guarantee to belong to the space of the variable. For instance, the noise function suggested by Mayhew et al. [10] is $e = (-\alpha\text{sgn}(\eta), \mathbf{0})$. Note that the feedback depends on $(\mathbf{q} + e) \notin \mathbb{S}^3$, which is not an attitude quaternion representation and is a physical inconsistency.

As a contribution of this manuscript, in the sequel, a new theorem is stated and proved about the existence of such noise function for the case the sum $\mathbf{q} + e$ is restricted to \mathbb{S}^3 .

Theorem 3.4

Let $\omega(\mathbf{q}) = -\text{sgn}(\eta)\epsilon$, $\mathcal{M} \triangleq \{\mathbf{q} \in \mathbb{S}^3 : \eta = 0\}$. Then for each $0 < \alpha < \sqrt{2}$ and each $\mathbf{q}_0 \in \mathcal{M}^* \triangleq (\mathcal{M} + \mathbb{B}(0, \alpha)) \cap \mathbb{S}^3$, there exists a measurable function $e : [0, \infty) \rightarrow \mathbb{B}(0, \alpha)$ and a Carathéodory solution $\mathbf{q} : [0, \infty) \rightarrow \mathbb{S}^3$ to $\dot{\mathbf{q}} = \frac{1}{2}\mathbf{q} \circ (0, \omega(\mathbf{q} + e))$ satisfying $\mathbf{q}(0) = \mathbf{q}_0$, $(\mathbf{q} + e) \in \mathbb{S}^3$ and $\mathbf{q}(t) \in \mathcal{M}^*$ for all $t \in [0, \infty)$.

Proof. The idea of the proof is to find function e such that the direction of $\omega(\mathbf{q} + e)$ is opposite to the direction of $\omega(\mathbf{q})$. This way, the body always moves toward the longest rotation direction and gets stuck at $\eta = 0$.

Let $\mathbf{q}(t) = (\eta, \epsilon)$. From Lemma B.5, it is known that the scalar component of \mathbf{q} is limited to

$$|\eta| < \alpha \sqrt{1 - \frac{\alpha^2}{4}} =: m. \quad (3.3)$$

The range of m depends on α , which is restricted to $0 < \alpha < \sqrt{2}$. Note that $0 \leq |\eta| < m < 1$.

In order to make the direction of $\omega(\mathbf{q} + e)$ opposite to the direction of $\omega(\mathbf{q})$, let $e(t) = (\eta_r, \epsilon_r)$ be defined as

$$\eta_r = -\eta + \beta(\eta - \text{sgn}(\eta)m), \quad (3.4)$$

where $\beta \in (0, 1)$ so the sign of the sum $\eta + \eta_r = \beta(\eta - \text{sgn}(\eta)m)$ is opposite to the sign of η (Lemma B.6), i.e.,

$$\text{sgn}(\eta + \eta_r) = -\text{sgn}(\eta). \quad (3.5)$$

The value of ϵ_r can be obtained using Lemma B.7, so as to ensure that $\|e(t)\|$ is the minimum for the predefined value of η_r which satisfies $(\mathbf{q}(t) + e(t)) \in \mathbb{S}^3$. Thus,

$$\epsilon_r = \left(\sqrt{\frac{1 - (\eta + \eta_r)^2}{1 - \eta^2}} - 1 \right) \epsilon. \quad (3.6)$$

The proof that $\|e(t)\| < \alpha$ follows directly from Lemma B.8.

To end the demonstration, following is the proof that the attitude $\mathbf{q}(t) \in \mathcal{M}^*$ for all future time.

Let $\Omega \triangleq \{\mathbf{q} \in \mathbb{S}^3 : \eta \leq \alpha\}$, $V_{\mathcal{M}}(\mathbf{q}) = \eta^2$. Function $V_{\mathcal{M}}$ is positive definite on Ω with respect to \mathcal{M} , since $V_{\mathcal{M}}(\mathbf{q}) > 0$ for $\mathbf{q} \in \Omega \setminus \mathcal{M}$ and $V_{\mathcal{M}}(\mathbf{q}) = 0$ for $\mathbf{q} \in \mathcal{M}$.

The time derivative of function $V_{\mathcal{M}}$ is given by

$$\dot{V}_{\mathcal{M}} = \langle \nabla V_{\mathcal{M}}(\mathbf{q}), \dot{\mathbf{q}} \rangle. \quad (3.7)$$

From the definition of $V_{\mathcal{M}}$, $\nabla V_{\mathcal{M}}(\mathbf{q}) = (2\eta, \mathbf{0})$ and the time derivative of the attitude is given by

$$\dot{\mathbf{q}} = \frac{1}{2} \mathbf{q} \circ (0, \boldsymbol{\omega}(\mathbf{q} + \mathbf{e})), \quad (3.8)$$

$$\dot{\mathbf{q}} = \frac{1}{2} (\text{sgn}(\eta_m) \boldsymbol{\epsilon}^T \boldsymbol{\epsilon}_m, -\eta \text{sgn}(\eta_m) \boldsymbol{\epsilon}_m - \text{sgn}(\eta_m) \boldsymbol{\epsilon} \times \boldsymbol{\epsilon}_m), \quad (3.9)$$

where $\eta_m = \eta + \eta_r$ and $\boldsymbol{\epsilon}_m = \boldsymbol{\epsilon} + \boldsymbol{\epsilon}_r$. Hence,

$$\dot{V}_{\mathcal{M}} = \eta \text{sgn}(\eta + \eta_r) \boldsymbol{\epsilon}^T (\boldsymbol{\epsilon} + \boldsymbol{\epsilon}_r) \quad (3.10)$$

$$= \eta (-\text{sgn}(\eta)) \left(\sqrt{\frac{1 - (\beta(\eta - \text{sgn}(\eta)m))^2}{1 - \eta^2}} \boldsymbol{\epsilon}^T \boldsymbol{\epsilon} \right) \quad (3.11)$$

$$= -|\eta| \sqrt{1 - \beta^2(m - |\eta|)^2} \sqrt{1 - \eta^2}, \quad (3.12)$$

where (3.5) was used in (3.11) and $\boldsymbol{\epsilon}^T \boldsymbol{\epsilon} = 1 - \eta^2$ was used in (3.12).

Function $\dot{V}_{\mathcal{M}}$ is negative definite on Ω with respect to \mathcal{M} .

Since Ω compact, function $V_{\mathcal{M}}$ is continuously differentiable and positive definite, and function $\dot{V}_{\mathcal{M}}$ is negative definite, it is possible to affirm that every solution starting in Ω remains in Ω for all future time.

As $\mathcal{M}^* \subset \Omega$, $\mathbf{q}(t) \in \mathcal{M}^*$ for all $t \in [0, \infty)$. \square

^aThe upper limit can be deduced from (B.19) for $\eta = \pm 1$. The theorem is senseless for $\alpha > \sqrt{2}$ because $\max_{\mathbf{q}} d(\mathbf{q}, \mathcal{M}) = \sqrt{2}$ as shown in Lemma B.4.

The following sections refer to the dynamical system (2.10), described in Section 2.4.

3.4 DISCONTINUOUS ATTITUDE CONTROL

In order to achieve global attitude control, some authors, such as Fjellstad and Fossen [6], Fragopoulos and Innocenti [7] and Wie and Barba [8], proposed a discontinuous feedback law like the following

$$\boldsymbol{\tau}_1(y, \mathbf{q}_d) = -\bar{c}\bar{h}\boldsymbol{\epsilon}_e - \boldsymbol{\omega}, \quad (3.13)$$

where y is defined in (2.11), $\bar{c} > 0$ is the gain of the ‘‘proportional’’ term $-\bar{c}\bar{h}\boldsymbol{\epsilon}_e$ and $\bar{h} = \text{sgn}(\eta_e)$. The sgn function is defined as in (3.2).

The value of \bar{h} determines the direction of the ‘‘proportional’’ term so \mathbf{q}_e is regulated either to $\mathbf{1} = (1, \mathbf{0})$ or $-\mathbf{1} = (-1, \mathbf{0})$, as shown in Figure 3.2.

The closed-loop (2.10), (2.11) and $\boldsymbol{\tau} = \boldsymbol{\tau}_1$, with $\boldsymbol{\tau}_1$ given by (3.13) had been proved to be globally asymptotically stable [7]. However, when the initial condition of the system is near the discontinuity – i.e., near $\eta_e = 0$, a region near 180° away from the reference attitude –, measurement noise can cause chattering, which consists of multiple jumps (of states) occurring at the same time and keep the state near the discontinuity indefinitely [10]. This way, the discontinuous controller is not robust to measurement noise.

Figure 3.3 illustrates the difference in behavior when the output is corrupted by noise² for initial conditions $\eta_e(0) = 0$, $\boldsymbol{\epsilon}_e(0) = [1 \ 2 \ 3]^T / \sqrt{14}$ and $\boldsymbol{\omega}(0) = \mathbf{0}$. The chattering occurred during the first 6 seconds and

²The measured value of \mathbf{q} included noise generated in the same way as described in Section 4.3.

can be observed in the graph of $\bar{h}\eta_e$. During the chattering behavior, the controller “believes” the sign of η_e continually changes and, as a consequence, the system has its response lagged.

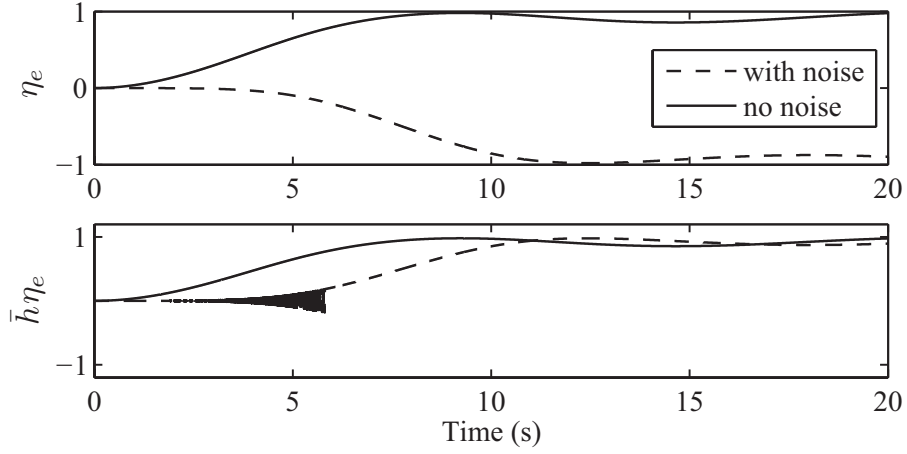


Figure 3.3: System behavior for the discontinuous controller when no noise is present in the output y and when the output is corrupted by noise.

3.5 HYSTERETIC HYBRID ATTITUDE CONTROL

In order to solve the robustness problem of the discontinuous controller, Mayhew *et al.* [10] proposed a hybrid control with hysteretic feedback by using the same torque feedback (3.13), but having \bar{h} determined in a different way. The idea of this controller is, instead of changing the dynamics (the value of \bar{h}) just after the sign of η_e changes, the value of \bar{h} is kept unchanged until a safe distance from the discontinuity is achieved. According to the definitions at the end of last section (Section 3.4), a safe distance means a distance so the sign of $\eta_e + \eta_r$ and η_e can not be different. As this behavior is more complex, a hybrid dynamic controller is considered.

The hysteretic controller of [10] has only one state variable $\bar{h} \in X_c \triangleq \{-1, 1\}$. The state of the overall system is represented by $\bar{x}_1 = (\bar{x}, \bar{h}) \in X_1 \triangleq X \times X_c$ and evolves according to (2.10), (2.11), the following dynamics of the controller³

$$\begin{aligned} \dot{\bar{h}} &= 0 & \bar{x}_1 \in C_1 &\triangleq \{\bar{x}_1 \in X_1 : \bar{h}\eta_e \geq -\delta\}, \\ \bar{h}^+ &\in \overline{\text{sgn}}(u_1) & \bar{x}_1 \in D_1 &\triangleq \{\bar{x}_1 \in X_1 : \bar{h}\eta_e \leq -\delta\}, \end{aligned} \quad (3.14)$$

where \bar{h}^+ is the value associated to \bar{h} just after the state transition⁴ and

$$\overline{\text{sgn}}(u_1) \triangleq \begin{cases} \{1\}, & u_1 > 0, \\ \{-1\}, & u_1 < 0, \\ \{-1, 1\}. & u_1 = 0. \end{cases}$$

The vector of inputs is $U_1 = (\tau, u_1)$ and the closed-loop law is achieved by setting

$$U_1 = \mathcal{K}_1(y, \bar{h}, \mathbf{q}_d) \triangleq (-\bar{c}\bar{h}\epsilon_e - \boldsymbol{\omega}, \eta_e). \quad (3.15)$$

The parameter $\delta \in (0, 1)$ represents the hysteresis half-width and provides robustness against chattering caused by output measurement. According to [10, Theorem 5.5], δ must be higher than 2α , where α is the maximum noise magnitude of the output measurement.

³Along the text, the dynamics representations follow the hybrid systems framework of Goebel *et al.* [48], summarized in Section 2.7.

⁴Note that for the closed-loop approach $u_1 = \eta_e$.

The closed system is globally asymptotically stable with respect to the set

$$A_1 = \{ \bar{x}_1 \in X_1 : \mathbf{q}_e = \bar{h}\mathbf{1} \text{ and } \boldsymbol{\omega} = \mathbf{0} \}. \quad (3.16)$$

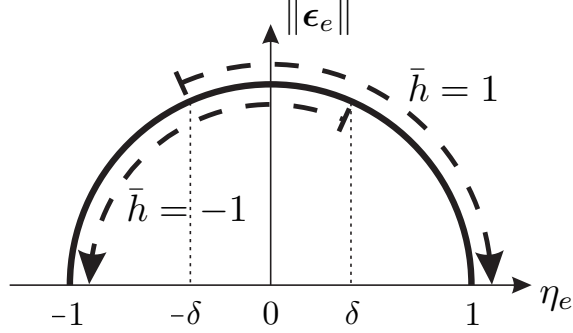


Figure 3.4: State space representation of the hysteretic controller (with one state variable \bar{h}). Arrows indicate the direction of the “proportional” term of the torque (dependent on \bar{h}) so the attitude is regulated to $\mathbf{1}$ or $-\mathbf{1}$. The parameter δ represents the hysteresis half-width of the on-off control for state \bar{h} .

Figure 3.4 shows the behavior of the hysteretic controller for a hysteresis width of 2δ . The state variable \bar{h} determines the “proportional” term direction of the torque feedback in order to move \mathbf{q}_e either to $\mathbf{1}$ or $-\mathbf{1}$.

In the sequel, it is presented some examples of system evolution for some distinct initial conditions and compares it when the controller is the discontinuous one. For the simulations below, the initial controller state for the hysteretic controller was $\bar{h}(0) = 1$ and the hysteresis parameter was set to $\delta = 0.4$. The simulations included measurement noise⁵ of maximum magnitude $\alpha = 0.2$.

For the scenario of Figure 3.3, with initial conditions $\eta_e(0) = 0$, $\boldsymbol{\epsilon}_e(0) = [1 \ 2 \ 3]^T/\sqrt{14}$ and $\boldsymbol{\omega}(0) = \mathbf{0}$, while the discontinuous controller presents chattering, the hysteretic controller behaves as the discontinuous controller when no noise is present. The hysteretic controller keeps the state variable $\bar{h} = 1$ along all the way.

Figure 3.5 exemplifies the problem mentioned in [10]. It is affirmed that there is a price to pay for robust global asymptotic stabilization with the hysteretic controller – a region in the state space where the hybrid control law pulls the rigid body in the direction of a longer rotation. In fact, the proportional term of the torque feedback pulls the body in the shorter rotation direction while $\bar{h}\eta_e \geq 0$. But, when $\bar{h}\eta_e$ gets negative, it still pulls in the same direction (the longer rotation direction now) until a safe distance (given by δ) is achieved to prevent chattering, i.e., until $\bar{h}\eta_e \leq -\delta$. In this simulation, the initial conditions $\eta_e(0) = -0.2$, $\boldsymbol{\epsilon}_e(0) = \sqrt{(1-0.2^2)}[1 \ 2 \ 3]^T/\sqrt{14}$ and $\boldsymbol{\omega}(0) = \mathbf{0}$ were chosen to contrast the longer rotation direction determined by the hysteretic controller and the shorter direction taken when the controller is the discontinuous one. The hysteretic controller keeps the state variable $\bar{h} = 1$ along all the way whereas the discontinuous one keeps \bar{h} at -1 .

The following scenario (Figure 3.6) illustrates an example with initial angular velocity different than zero. The initial conditions were $\eta_e(0) = -0.2$, $\boldsymbol{\epsilon}_e(0) = \sqrt{(1-0.2^2)}[1 \ 2 \ 3]^T/\sqrt{14}$ and $\boldsymbol{\omega}(0) = 0.5[1 \ 2 \ 3]^T/\sqrt{14}$. The control law of the discontinuous controller pulls the body toward $\eta_e = -1$ along all the way as \bar{h} keeps at -1 . Differently, the hysteretic controller is initiated with $\bar{h} = 1$ and the control law pulls the body to the opposite direction. Due to inertia, it rotates toward $\eta_e = -1$, however the angular velocity norm decreases until η_e crosses the hysteresis threshold ($\bar{h}\eta_e \leq -\delta$) – see the graph of the angular velocity. After that, the controller changes state \bar{h} to -1 and the body continues rotating toward $\eta_e = -1$. The moment the controller changes state \bar{h} can be seen on the graph of $\bar{h}\eta_e$.

⁵The measured value of \mathbf{q} included noise generated in the same way as described in Section 4.3.

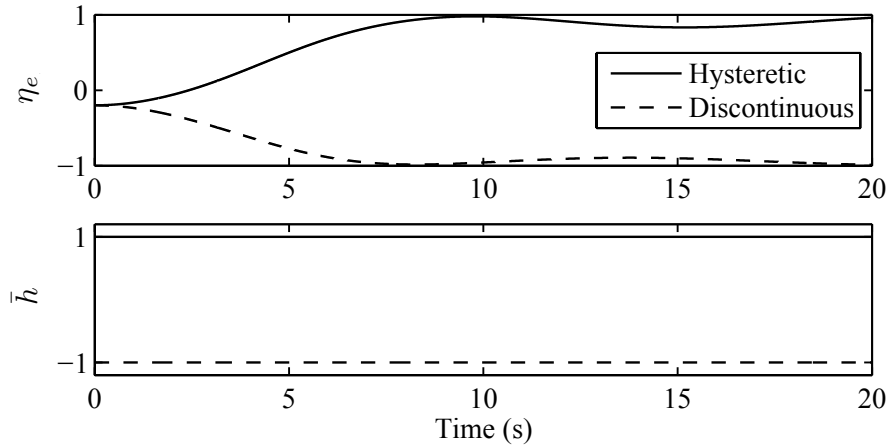


Figure 3.5: Comparison of the system behavior when the discontinuous controller and the hysteretic controller are applied to highlight the longer rotation direction determined by the hysteretic controller.

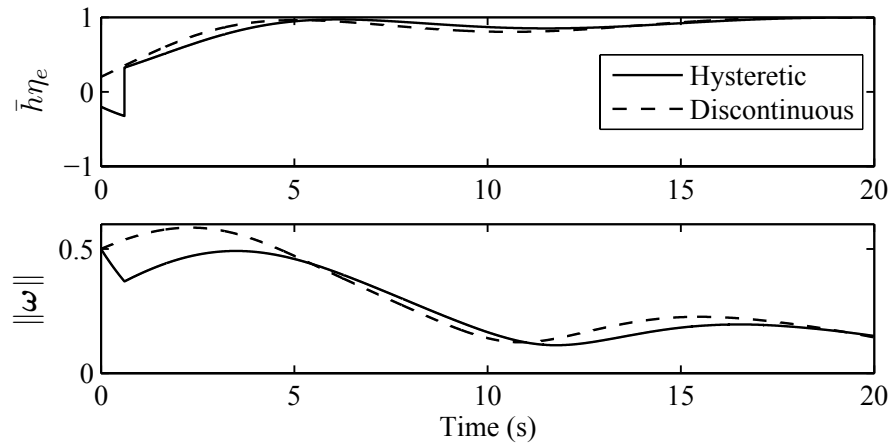


Figure 3.6: Comparison of the system behavior when the discontinuous controller and the hysteretic controller are applied to highlight the behavior when the initial condition of the system is not at rest.

3.6 PROBLEM DEFINITION

The problem of robust and global attitude stabilization for rigid body has been solved. However the choice of the best rotation direction to stabilize in order to spend less energy is not trivial. Mayhew et al. [10] affirm that there is a price to pay with the hysteretic controller – a region in the state space where the hybrid control law pulls the rigid body in the direction of a longer rotation. The problem that this thesis work solves is

PROBLEM

Find a controller with a better performance between settling time and energy consumption than the hysteretic controller suggested by [10] that keeps the robustness and global control stability.

In order to solve this problem, it is proposed two hybrid solutions by the introduction of one new mode that is used to indicate if the system attitude is close to a critical region (the chattering prone region):

- In Chapter 4, the first proposed hybrid controller (HY controller) is capable of reducing the energy consumption of rest-to-rest applications when compared with the hysteretic hybrid controller. Being capable of detecting when the reference changes abruptly or when the current attitude is far from the reference on the initial instant, it has more opportunities to determine the shorter rotation direction (compared with the hysteretic controller). But this is not always true when the initial angular velocity direction and the shorter rotation direction are opposite.
- In Chapter 5, a middle term solution in terms of cost between the memoryless discontinuous and the hysteretic hybrid control is proposed by introducing a new mode which also have a hysteresis structure. This new controller, called bimodal controller, reduces the region for the longer direction mentioned above without compromising the robustness (the controller has the same capability of noise rejection of the hysteretic controller) and, differently from the HY controller, it does not impose any restrictions on flow and jumps priorities. It is oriented for the rest-to-rest control of attitude, however it spend less energy in average for other initial angular velocities.

The two proposed controllers determine the direction to stabilize based only on the attitude information. Certainly, the angular velocity should also be considered. This is still an open problem. The two articles in the literature that takes the angular velocity into account, to the best of the author's knowledge, is [54] and [55]. In [54], the authors concluded that hysteretic controller presents advantages. The controller suggested in [55] is an adapted version of the hysteretic controller. Direct comparisons was possible with an adapted version of the bimodal controller in this manuscript (Subsection 5.3.3). The conclusions are favorable to the adapted bimodal controller.

4

FIRST PROPOSED HYBRID ATTITUDE CONTROLLER (HY)

This chapter presents the first proposed hybrid controller (HY) capable of reducing the energy consumption of rest-to-rest applications when compared with the hysteretic hybrid controller suggested by Mayhew et al [10]. It has two state variables $(\bar{h}, m) \in X_c \times X_c$. The state space of the system is now represented by $\bar{x}_2 = (\bar{x}, \bar{h}, m) \in X_2 \triangleq X \times X_c \times X_c$.

The controller objective is to globally asymptotically stabilize the set

$$A_2 = \{ \bar{x}_2 \in X_2 : \mathbf{q}_e = \bar{h}\mathbf{1} \text{ and } m = 1 \text{ and } \boldsymbol{\omega} = \mathbf{0} \}. \quad (4.1)$$

Consider parameter $\delta \in (0, 1)$. The system is given by (2.10), (2.11) and the following dynamics of the controller:

$$\left. \begin{array}{l} \dot{\bar{h}} = 0 \\ \dot{m} = 0 \end{array} \right\} \bar{x}_2 \in C_2, \quad (4.2)$$

$$\left. \begin{array}{l} \bar{h}^+ \in \overline{\text{sgn}}(u_2) \\ m^+ \in \overline{\text{sgn}}(|u_2| - \delta) \end{array} \right\} \bar{x}_2 \in D_2,$$

$$C_2 \triangleq \{ \bar{x}_2 \in X_2 : \bar{h}\eta_e \geq -\delta \text{ and } m|\eta_e| \geq m\delta - \delta/2 \}, \quad (4.3)$$

$$D_2 \triangleq \{ \bar{x}_2 \in X_2 : \bar{h}\eta_e \leq -\delta \text{ or } m|\eta_e| \leq m\delta \}, \quad (4.4)$$

where m^+ and \bar{h}^+ are values associated to m and \bar{h} , respectively, just after state transition. The sets C_2 and D_2 are depicted in Figure 4.1.

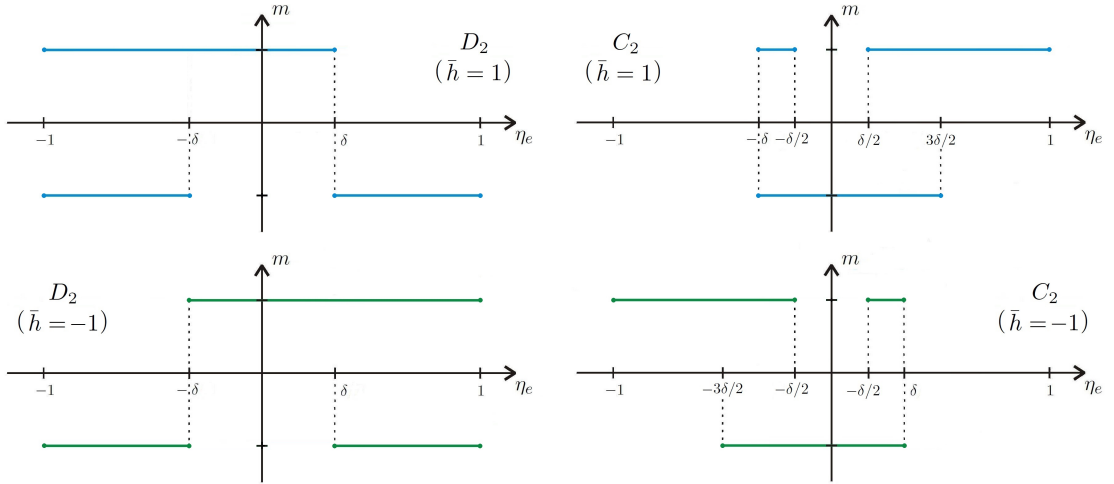


Figure 4.1: Graphical representation of sets C_2 and D_2 .

The vector of inputs is $U_2 = (\boldsymbol{\tau}, u_2, u_3)$ and the closed-loop system is achieved by setting

$$U_2 = \mathcal{K}_2(y, \mathbf{q}_d, \bar{h}, m) \triangleq (-\bar{c}\bar{h}\boldsymbol{\epsilon}_e - \boldsymbol{\omega}, \eta_e, \bar{h}). \quad (4.5)$$

As well as in the hysteretic controller, the state \bar{h} determines the “proportional” term direction of the torque feedback in order to move \mathbf{q}_e either to $\mathbf{1}$ or $-\mathbf{1}$. The state $m = 1$ indicates whether η_e is near ± 1 ($|\eta_e| \geq \delta$). Otherwise, $m = -1$. Figure 4.2 shows the proposed regulation.

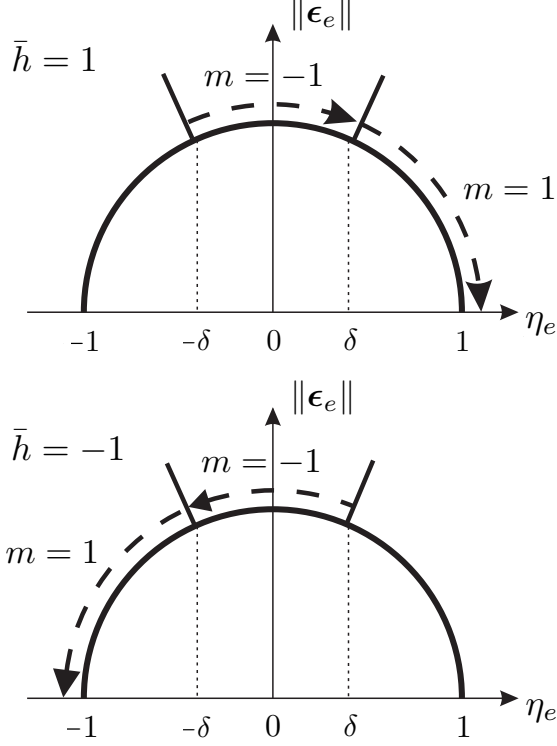


Figure 4.2: State space representation of η_e and $\|\epsilon_e\|$ and the proposed regulation with two state variables (\bar{h} and m). The parameter δ represents the hysteresis half-width of the on-off control for state \bar{h} .

The inclusion of a second discrete state variable (m) to the controller allows the state \bar{h} to be updated when m is about to be changed. For this reason, variable m was designed to be changed in two situations: whenever the reference attitude changes significantly (and system is near steady state) and on the initial instant in case the reference is far from the initial attitude (assuming that $m(0) = 1$). Apart from these two situations, the system evolves as if the controller were the hysteretic one, since the feedback law does not depend on m and the changes on m do not affect \bar{h} (see Section 4.2).

4.1 STABILITY ANALYSIS

Considering the proposed HY controller (4.2), the system can be written as a function of the vector of inputs, U_2 , as follows

$$\mathcal{H}(U_2) : \begin{cases} \dot{\bar{x}}_2 = F_2(\bar{x}_2, U_2), & \bar{x}_2 \in C_2, \\ \bar{x}_2^+ \in G_2(\bar{x}_2, U_2), & \bar{x}_2 \in D_2, \end{cases} \quad (4.6)$$

where $\bar{x}_2 = (\mathbf{q}_e, \boldsymbol{\omega}, \bar{h}, m)$, $U_2 = (\boldsymbol{\tau}, u_2, u_3)$,

$$F_2(\bar{x}_2, U_2) \triangleq \begin{bmatrix} \frac{1}{2} \mathbf{q}_e \circ (0, \boldsymbol{\omega}) \\ J^{-1}(S(J\boldsymbol{\omega})\boldsymbol{\omega} + \boldsymbol{\tau}) \\ 0 \\ 0 \end{bmatrix},$$

$$G_2(\bar{x}_2, U_2) \triangleq \begin{bmatrix} \mathbf{q}_e \\ \boldsymbol{\omega} \\ \overline{\text{sgn}}(u_2) \\ \overline{\text{sgn}}(|u_2| - \delta) \end{bmatrix}.$$

The system can also be written in the closed-loop form by substituting (4.5) into (4.6), denoted by $\bar{\mathcal{H}} \triangleq \mathcal{H}(\mathcal{K}_2)$. Let $\bar{F}_2(\bar{x}_2) \triangleq F_2(\bar{x}_2, \mathcal{K}_2)$ and $\bar{G}_2(\bar{x}_2) \triangleq G_2(\bar{x}_2, \mathcal{K}_2)$.

$$\bar{\mathcal{H}} : \begin{cases} \dot{\bar{x}}_2 = \bar{F}_2(\bar{x}_2), & \bar{x}_2 \in C_2, \\ \bar{x}_2^+ \in \bar{G}_2(\bar{x}_2), & \bar{x}_2 \in D_2, \end{cases} \quad (4.7)$$

$$\bar{F}_2(\bar{x}_2) = \begin{bmatrix} \frac{1}{2}\mathbf{q}_e \circ (0, \boldsymbol{\omega}) \\ J^{-1}(S(J\boldsymbol{\omega})\boldsymbol{\omega} - \bar{c}\bar{h}\boldsymbol{\epsilon}_e - \boldsymbol{\omega}) \\ 0 \\ 0 \end{bmatrix},$$

$$\bar{G}_2(\bar{x}_2) = \begin{bmatrix} \mathbf{q}_e \\ \boldsymbol{\omega} \\ \overline{\text{sgn}}(\eta_e) \\ \overline{\text{sgn}}(|\eta_e| - \delta) \end{bmatrix}.$$

Theorem 4.1

Let $\delta \in (0, 1)$ and $\bar{c} > 0$. Then, the compact set A_2 defined in (4.1) is globally asymptotically stable for the closed-loop hybrid system $\bar{\mathcal{H}}$.

Proof. The proof follows in the same way as that of Theorem 5.2 of [10]. Consider the Lyapunov function $V : X_2 \rightarrow \mathbb{R}$, defined as

$$V(\bar{x}_2) = 2\bar{c}(1 - \bar{h}\eta_e) + \frac{1}{2}\boldsymbol{\omega}^T J\boldsymbol{\omega}. \quad (4.8)$$

Let $V : X_2 \rightarrow \mathbb{R}$, $V(\bar{x}_2) = 2\bar{c}(1 - \bar{h}\eta_e) + \frac{1}{2}\boldsymbol{\omega}^T J\boldsymbol{\omega}$.

Function V is positive definite on X_2 with respect to A_2 , since $V(\bar{x}_2) > 0$ for $\bar{x}_2 \in X_2 \setminus A_2$ and $V(\bar{x}_2) = 0$ for $\bar{x}_2 \in A_2$.

The time derivative of V is given by

$$\begin{aligned} \dot{V}(\bar{x}_2) &= \langle \nabla V(\bar{x}_2), \bar{F}_2(\bar{x}_2) \rangle, \\ &= \left\langle \begin{bmatrix} \left[\begin{array}{cccc} (-2\bar{c}\bar{h}) & 0 & 0 & 0 \end{array} \right]^T \\ J\boldsymbol{\omega} \\ -2\bar{c}\eta_e \\ 0 \end{bmatrix}, \begin{bmatrix} \frac{1}{2} \left[\begin{array}{cc} -\boldsymbol{\epsilon}_e^T \boldsymbol{\omega} & (\eta_e \boldsymbol{\omega} + \boldsymbol{\epsilon}_e \times \boldsymbol{\omega})^T \end{array} \right]^T \\ J^{-1}(S(J\boldsymbol{\omega})\boldsymbol{\omega} - \bar{c}\bar{h}\boldsymbol{\epsilon}_e - \boldsymbol{\omega}) \\ 0 \\ 0 \end{bmatrix} \right\rangle, \\ &= -\boldsymbol{\omega}^T \boldsymbol{\omega} \leq 0. \end{aligned} \quad (4.9)$$

Thus, \dot{V} is negative semidefinite on X_2 .

Along jumps, when $\bar{x}_2 \in D_2$, the variation of V is given by $\Delta V(\bar{x}_2) = V(\bar{x}_2^+) - V(\bar{x}_2) = -2\bar{c}\eta_e(\bar{h}^+ - \bar{h})$.

Let $D_2 = D_{2a} \cup D_{2b}$, where $D_{2a} \triangleq \{\bar{x}_2 \in X_2 : \bar{h}\eta_e \leq -\delta\}$ and $D_{2b} \triangleq \{\bar{x}_2 \in X_2 : m|\eta_e| \leq m\delta\}$.

Hence,

$$\Delta V(\bar{x}_2) = \begin{cases} \leq -4\bar{c}\delta, & \bar{x}_2 \in D_{2a}, \\ \leq -4\bar{c}\delta, & \bar{x}_2 \in D_{2b} \cap D_{2a} \\ 0, & \bar{x}_2 \in D_{2b} \setminus D_{2a}. \end{cases} \quad (4.10)$$

As $\dot{V}(\bar{x}_2) \leq 0$ and $\Delta V(\bar{x}_2) \leq 0$ for all $\bar{x}_2 \in X_2$, it follows, from Theorem 7.6 of [56], that the compact set A_2 is stable.

The conclusion that the set A_2 is globally asymptotically stable comes when Theorem 4.7 of [56] is applied to prove that the set A_2 is the largest invariant set in $W = \{\bar{x}_2 \in C_2 : \dot{V}(\bar{x}_2) = 0\}$ or, equivalently, in

$$W = \{\bar{x}_2 \in X_2 : \omega = \mathbf{0} \text{ and } \bar{h}\eta_e \geq -\delta \text{ and } m|\eta_e| \geq m\delta - \delta/2\}.$$

On W , $\omega = \mathbf{0}$. From (4.7), the only way to keep $\omega \equiv \mathbf{0}$ is when $\epsilon_e \equiv \mathbf{0}$ ($\mathbf{q}_e = \pm \mathbf{1}$). Using restriction $\bar{h}\eta_e \geq -\delta$, it follows that $\mathbf{q}_e = \bar{h}\mathbf{1}$ and using the other restriction, $m = 1$. Thus, any solution $\bar{x}_2(t)$ approaches the largest invariant set A_2 .

According to Theorem 4.7, the largest invariant set should include states in $W_\Delta = \{\bar{x}_2 \in X_2 : \Delta V^{-1}(0) \cap \bar{G}_2(\Delta V^{-1}(0))\}$ but note that as it is demonstrated in Section 4.2, $W_\Delta \neq \emptyset$ refers to the chattering prone region (for variable m only). This is not the case for the strategy proposed in this chapter due to the following reasons:

1. The strategy considers that, during the controller program execution, jumps do not present higher priority than flows^a;
2. The control law does not depend on m , which is the state variable that changes (see Section 4.2);
3. Flow occurs as $W_\Delta \subset C_2 \cap D_2$.

□

^aExamples of how to implement priorities for jumps or flows in MATLAB can be found in [57].

Following is the proof that the number of jumps in variable \bar{h} is bounded for any solution trajectory to the closed loop system $\bar{\mathcal{H}}$ defined in (6.13).

Theorem 4.2

Given any compact set $K \subset X_2$, a solution trajectory^a to the hybrid system $\bar{\mathcal{H}}$, starting at $\bar{x}_2(0,0) \in K$ contains a finite number of jumps in variable \bar{h} .

^aThe domain of a solution trajectory to a hybrid system is called hybrid time domain. Further details are found in Section 2.7.

Proof. State \bar{h} changes when $\bar{h} = 1$ and $\eta_e \leq -\delta$ or when $\bar{h} = -1$ and $\eta_e \geq \delta$. In this case, $\bar{x}_2 \in D_{2a}$ and, from (4.10), the change in $V(\bar{x}_2)$ over the jump is at most $\Delta V_1 = -4\bar{c}\delta$.

Since $\dot{V}(\bar{x}_2) \leq 0$ along flows (see (4.9)), the maximum number of jumps is given by the maximum $n_j \in \{0, 1, 2, \dots\}$ that satisfies

$$n_j \leq \frac{V^*}{|\Delta V_1|} = \frac{V^*}{4\bar{c}\delta}$$

where $V^* = \max V(K)$.

After some time, no jumps occur any more and the system behaves as a continuous dynamical system. □

So far the stability analysis has not taken into account “outer perturbations” that includes both measurement and modeling errors [58, 10]. According to [58], a robustness analysis of $\bar{\mathcal{H}}$ should consider perturbed systems

$(\bar{F}_2^\alpha, \bar{G}_2^\alpha, C_2^\alpha, D_2^\alpha)$. A family of perturbed system, denoted $\bar{\mathcal{H}}^\alpha$, is defined below [58, 10].

$$\begin{aligned}\bar{F}_2^\alpha(\bar{x}_2) &= \bar{\text{co}} F_2(\bar{x}_2, \mathcal{K}_2(y + \alpha\mathbb{B}, \bar{h}, m, \mathbf{q}_d)) + \alpha\mathbb{B}, \\ \bar{G}_2^\alpha(\bar{x}_2) &= \{z \in X_2 : z \in G_2(\bar{x}_2, \mathcal{K}_2(y + \alpha\mathbb{B}, \bar{h}, m, \mathbf{q}_d))\},\end{aligned}\quad (4.11)$$

$$\begin{aligned}C_2^\alpha &= \{\bar{x}_2 \in X_2 : T(y + \alpha\mathbb{B}, \bar{h}, m, \mathbf{q}_d) \cap C_2 \neq \emptyset\}, \\ D_2^\alpha &= \{\bar{x}_2 \in X_2 : T(y + \alpha\mathbb{B}, \bar{h}, m, \mathbf{q}_d) \cap D_2 \neq \emptyset\}\end{aligned}\quad (4.12)$$

where $\bar{\text{co}}$ denotes the closed convex hull, function T is defined as $T : X_2 \times \mathbb{S}^3 \rightarrow X_2$, $T(y, \bar{h}, m, \mathbf{q}_d) = \bar{x}_2$, $\alpha > 0$ and \mathbb{B} is the closed unit ball.

Following the arguments used in [10], it is possible to affirm that there exists a maximum noise magnitude α such that the number of jumps in the perturbed system $\bar{\mathcal{H}}^\alpha$ gets bounded.

Theorem 4.3

Let $\delta \in (0, 1)$ and $\bar{c} > 0$. Then, given a compact set $K \subset X_2$, there exists $\alpha^{max} > 0$ such that for all $\alpha \in (0, \alpha^{max}]$, every solution trajectory to the hybrid system $\bar{\mathcal{H}}^\alpha$, starting at $\bar{x}_2^\alpha(0, 0) \in K$ contains a finite number of jumps in variable \bar{h} .

Proof. The proof of this theorem is similar to the proof of [10, Theorem 5.4].

Consider the Lyapunov function V defined in (4.8). According to Theorem 6.5 of [58], there exists $\beta \in \mathcal{KL}$ such that every solution trajectory to the hybrid system $\bar{\mathcal{H}}$ starting at $\bar{x}_2(0, 0) \in K$,

$$V(\bar{x}_2(t, j)) \leq \beta(V(\bar{x}_2(0, 0)), t + j) \quad \forall (t, j) \in \text{dom } \bar{x}_2 \quad (4.13)$$

Theorem 6.5 requires that the system $\bar{\mathcal{H}}$ satisfies the hybrid basic conditions and that there exists an open basin of attraction of the compact set A_2 . Both conditions are satisfied from Lemma B.3 (see Appendix B) and Theorem 4.1. Once (4.13) holds, according to Theorem 6.6 of [58], for each $\gamma > 0$ there exists $\alpha^{max} > 0$ such that for each $\alpha \in (0, \alpha^{max}]$, every trajectory solution of $\bar{\mathcal{H}}^\alpha$ starting at $\bar{x}_2^\alpha(0, 0) \in K$ satisfies

$$V(\bar{x}_2^\alpha(t, j)) \leq \beta(V(\bar{x}_2^\alpha(0, 0)), t + j) + \gamma \quad \forall (t, j) \in \text{dom } \bar{x}_2^\alpha \quad (4.14)$$

Theorem 6.6 requires that the system $\bar{\mathcal{H}}^\alpha$ have the convergence property. [58, Theorem 5.4] ensures that $\bar{\mathcal{H}}^\alpha$ has this property since it satisfies the hybrid basic conditions (Lemma B.3, Appendix B). Equation (4.14) affirms that $\lim_{t+j \rightarrow \infty} V(\bar{x}_2^\alpha(t, j)) \in [0, \gamma]$. From Theorem 4.4, it is known that jumps may occur if $V \geq 4\bar{c}\delta = |\Delta V_1|$. Hence, for $\gamma < 4\bar{c}\delta$, the number of jumps is bounded.

As $\bar{x}_2 = (\bar{x}, \bar{h}, m) \in X_2 \triangleq \mathbb{S}^3 \times \mathbb{R}^3 \times X_c \times X_e$, note that the set K can not include all the set X_2 , since the real set is not compact. However, it can include all initial attitudes of the body. \square

4.2 CHATTERING ANALYSIS

Due to noise present in measurements, chattering may occur when jumps map the state back into the jump set, i.e., when $G_2(D_2) \cap D_2 \neq \emptyset$. Considering that the output y is corrupted by noise of maximum magnitude α , the verification should be concentrated on intersection $\bar{G}_2^\alpha(D_2^\alpha) \cap D_2^\alpha$, where \bar{G}_2^α and D_2^α are defined in (4.11) e (4.12).

Theorem 4.4

Let $\alpha > 0$, $\delta > 2\alpha$, $\delta \in (0, 1)$. Then, $\overline{G}_2^\alpha(D_2^\alpha) \cap D_2^\alpha \neq \emptyset$ and, in this set, only state variable m can change.

Proof. It can be shown that $D_2^\alpha = D_{2a}^\alpha \cup D_{2b}^\alpha$, where

$$\begin{aligned} D_{2a}^\alpha &\triangleq \{\bar{x}_2 \in X_2 : \bar{h}\eta_e \leq -\delta + \alpha\}, \\ D_{2b}^\alpha &\triangleq \{\bar{x}_2 \in X_2 : m|\eta_e| \leq m\delta + \alpha\}. \end{aligned}$$

The jump maps for states \bar{h} and m , when measurement noise is taken into account, are given by

$$\bar{h}^+ \in \overline{\text{sgn}}(\eta_e + \alpha\mathbb{B}) \quad m^+ \in \overline{\text{sgn}}(|\eta_e + \alpha\mathbb{B}| - \delta)$$

or, equivalently, by $\bar{h}^+\eta_e \geq -\alpha$ and $m^+|\eta_e| \geq m^+\delta - \alpha$. Their graphical representations are shown in Figure 4.3.

When the state $\bar{x}_2 \in D_{2a}^\alpha$, it jumps into the set

$$\overline{G}_2^\alpha(D_{2a}^\alpha) = \{\bar{x}_2 \in X_2 : |\eta_e - \bar{h}\delta| \leq \alpha\} \cup \{\bar{x}_2 \in X_2 : \bar{h}\eta_e > \delta + \alpha \text{ and } m = 1\}.$$

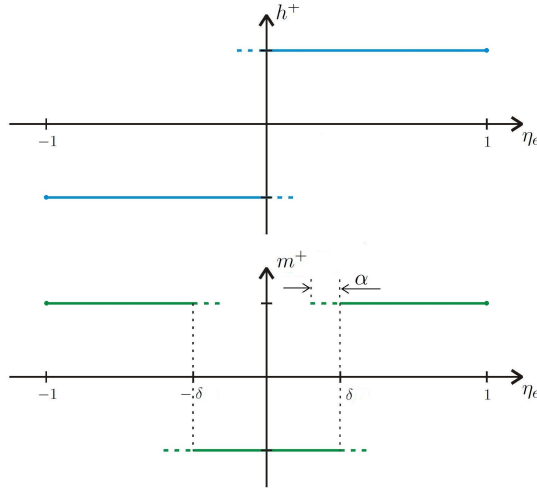


Figure 4.3: Graphical representation of the jump map for h^+ and m^+ .

When $\bar{x}_2 \in D_{2b}^\alpha$, it jumps into the set

$$\begin{aligned} \overline{G}_2^\alpha(D_{2b}^\alpha) &= \{\bar{x}_2 \in X_2 : |\eta_e - \bar{h}\delta| \leq \alpha\} \cup \{\bar{x}_2 \in X_2 : \bar{h}\eta_e > \delta + \alpha \text{ and } m = 1\} \cup \\ &\quad \{\bar{x}_2 \in X_2 : |\eta_e| < \delta - \alpha \text{ and } m = -1\}. \end{aligned}$$

As $\overline{G}_2^\alpha(D_{2a}^\alpha) \subset \overline{G}_2^\alpha(D_{2b}^\alpha)$, it follows that $\overline{G}_2^\alpha(D_2^\alpha) = \overline{G}_2^\alpha(D_{2a}^\alpha) \cup \overline{G}_2^\alpha(D_{2b}^\alpha) = \overline{G}_2^\alpha(D_{2b}^\alpha)$. Note that $\overline{G}_2^\alpha(D_{2b}^\alpha) \cap D_{2a}^\alpha = \emptyset$, but

$$\begin{aligned} \overline{G}_2^\alpha(D_{2b}^\alpha) \cap D_{2b}^\alpha &= \{\bar{x}_2 \in X_2 : |\eta_e - \bar{h}\delta| \leq \alpha\}, \\ &= \{\bar{x}_2 \in X_2 : \bar{h} = 1 \text{ and } \delta - \alpha \leq \eta_e \leq \delta + \alpha\} \cup \{\bar{x}_2 \in X_2 : \bar{h} = -1 \text{ and } -\delta - \alpha \leq \eta_e \leq -\delta + \alpha\}. \end{aligned}$$

Hence, $\overline{G}_2^\alpha(D_2^\alpha) \cap D_2^\alpha = \overline{G}_2^\alpha(D_{2b}^\alpha) \cap (D_{2a}^\alpha \cup D_{2b}^\alpha) = (\overline{G}_2^\alpha(D_{2b}^\alpha) \cap D_{2a}^\alpha) \cup (\overline{G}_2^\alpha(D_{2b}^\alpha) \cap D_{2b}^\alpha) = \overline{G}_2^\alpha(D_{2b}^\alpha) \cap D_{2b}^\alpha \neq \emptyset$. Thus, chattering can occur when $\bar{x}_2 \in \overline{G}_2^\alpha(D_2^\alpha) \cap D_2^\alpha$. Note also that only state variable m can change in this set. \square

The HY controller can be considered robust to measurement noise due to the following reasons:

1. The feedback law (3.13) depends on \mathbf{q}_e , $\boldsymbol{\omega}$ and \bar{h} ;
2. \mathbf{q}_e and $\boldsymbol{\omega}$ do not change via jumps and chattering does not occur in variable \bar{h} (only in m);
3. The proposed strategy considers that, during the controller program execution, jumps do not present higher priority than flows;
4. The region of chattering (in variable m) is a subset of $C_2 \cap D_2$.

Usually chattering is undesirable and causes unwanted effects as is illustrated for the discontinuous controller in the next section.

4.3 SIMULATION RESULTS

This section presents simulation results to compare performance of the proposed controller (HY), the discontinuous controller and the hysteretic controller.

In each simulation, all parameters considered were the same as those used for simulations in [10] to facilitate comparisons. The inertia matrix used was $J = \text{diag}(10\hat{\mathbf{v}})$, $\hat{\mathbf{v}} = [1 \ 2 \ 3]^T/\sqrt{14}$, the control gain $\bar{c} = 1$ and parameter $\delta = 0.4$. The initial state of the hysteretic controller was $\bar{h}(0) = 1$ and the ones of the proposed controller (HY) were $\bar{h}(0) = 1$, $m(0) = 1$. The desired reference was $\mathbf{q}_d = \mathbf{1}$ with $\boldsymbol{\omega}_d = \mathbf{0}$. The simulations were performed in MATLAB ambient, using ordinary differential equation solver with variable integration step (ode45) restricted to a maximum step of 1 ms.

The measured value of \mathbf{q} (\mathbf{q}_m) included noise and was calculated as follows: $\mathbf{q}_m = (\mathbf{q} + b\hat{\mathbf{e}}) / \|\mathbf{q} + b\hat{\mathbf{e}}\|_2$, $\hat{\mathbf{e}} = \mathbf{e} / \|\mathbf{e}\|_2$, where each element e was chosen from a gaussian distribution of zero mean and unitary standard deviation and b was chosen from a uniform distribution on the interval $[0, 0.2]$.

Figure 4.4 e 4.5 present five graphs each. The first graph, of η_e , shows the attitude evolution either to $\mathbf{q}_e = \mathbf{1}$ or $\mathbf{q}_e = -\mathbf{1}$. The second graph, of $\bar{h}\eta_e$, shows not only the evolution to 1 but also the jumps in \bar{h} . The third one presents the variable state m of the HY controller and its jumps. The fourth one shows the evolution of the angular velocity norm $\|\boldsymbol{\omega}\|$ and the last one, the energy spent by the applied control feedback strategy $\sqrt{\int_0^t \boldsymbol{\tau}^T \boldsymbol{\tau} dt}$.

The first scenario (Figure 4.4) illustrates the *chattering* effect on the discontinuous and the HY controllers. The initial conditions were $\mathbf{q}(0) = (0, \hat{\mathbf{v}})$ and $\boldsymbol{\omega}(0) = \mathbf{0}$. The *chattering* effect on the discontinuous controller can be observed in the $\bar{h}\eta_e$ graph. It induces a lag in response and higher energy consumption. In HY, this effect is observed in the m graph, however the system evolution is not affected. Due to the m variable, HY controller had a chance to update the discrete variables on the initial moment ($\bar{h} = 1$, $m = -1$). Consequently, it determined a movement toward $\eta_e = 1$. Note that depending on the noise on the initial moment, HY could have updated \bar{h} to -1 and determined a movement toward $\eta_e = -1$. The system evolution for the hysteretic controller is not shown as it coincides with the evolution for HY.

The second scenario (Figure 4.5) compares the evolution of the states for the hysteretic and the HY controllers when the initial angular velocity direction coincides with the shorter rotation direction. The initial conditions were $\mathbf{q}(0) = (-0.2, \sqrt{1 - 0.2^2}\hat{\mathbf{v}})$ and $\boldsymbol{\omega}(0) = 0.3\hat{\mathbf{v}}$. This simulation shows that as the initial state of \bar{h} for the hysteretic controller is 1, the control law pulls the attitude toward the longer rotation direction ($\eta_e = 1$). Thus, the angular velocity decreases, but before the movement is reversed, η_e crosses over the hysteresis threshold ($\eta_e \leq -\delta$). At this moment, \bar{h} changes to -1 and the control law pulls the attitude toward

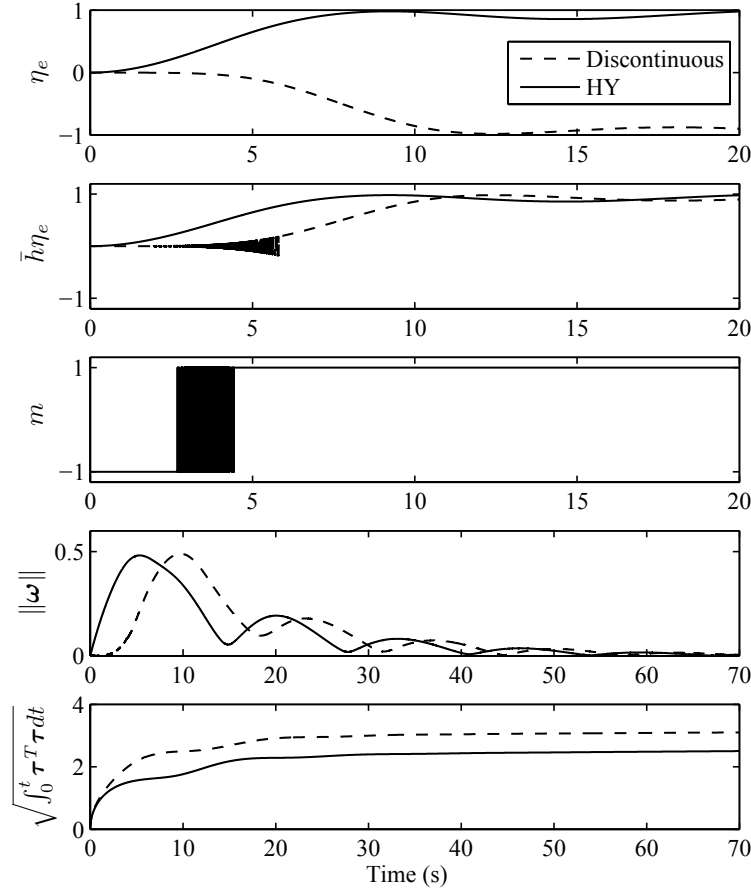


Figure 4.4: Comparison between the discontinuous controller and the proposed HY controller.

the shorter rotation direction ($\eta_e = -1$). On the other hand, HY controller decides, in the initial moments, to change \bar{h} to -1 and the feedback pulls the attitude toward the shorter direction ($\eta_e = -1$). Consequently, the system energy consumption is higher when the hysteretic controller is applied. The system evolution for the discontinuous controller is not shown as it coincides with the evolution for HY.

4.4 CHAPTER CONCLUSIONS

The proposed hybrid control globally asymptotically stabilizes the attitude of a rigid body and is robust against noise measurement. It also preserves the good characteristics of the hysteretic controller by avoiding the undesirable effects of unwinding and chattering due to measurement noise. Given that, during the controller program execution, jumps do not present higher priority than flows, the chattering that occurs in the second state variable m does not disturb the evolution of the system.

With one more state variable than the hysteretic controller, the HY controller is able to detect when the reference changes abruptly or when the current attitude is far from the reference on the initial instant. This way, it has more opportunities to determine the new state of variable \bar{h} , is more likely to take the shorter rotation direction and spend less energy.

This study was presented at the XII Simpósio Brasileiro de Automação Inteligente - SBAI 2015 and an online publication of the respective article is available at <http://swge.inf.br/SBAI2015/anais/413.pdf>.

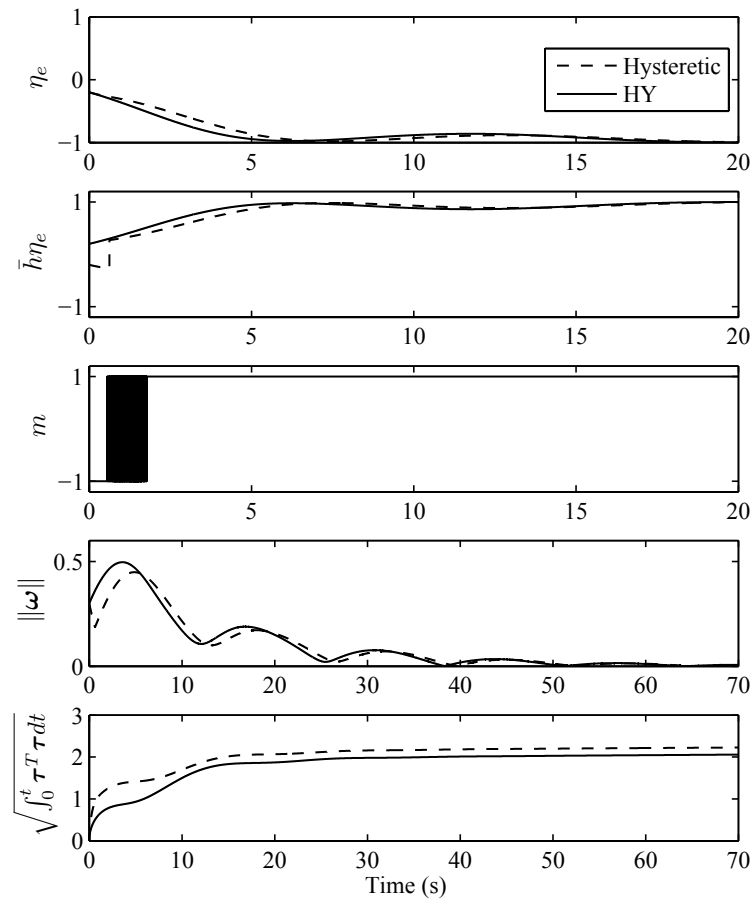


Figure 4.5: Comparison between the hysteretic controller and the proposed HY controller.

5

PROPOSED BIMODAL HYBRID ATTITUDE CONTROLLER

In Chapter 4 it was shown that the introduction of a new mode m allows less expensive solutions. However, it presents the disadvantage of having restriction in the software implementation and the chattering phenomenon in variable m . In order to avoid chattering (and also the restriction on the software implementation), it is proposed in this chapter that both controller states, \bar{h} and also m , should have a hysteresis structure, such that, the hysteresis half-width of the on-off control for state m is δ (a lower value would induce chattering) and the one for state \bar{h} is $\delta_a \in \{\delta/2, \delta\}$, adapted according to the state of m . The shorter width being set when state m indicates that body has moved away from the chattering prone region.

The proposed hybrid controller, called bimodal controller, has two state variables $(\bar{h}, m) \in X_c \times X_c$, $X_c \triangleq \{-1, 1\}$. As in the hysteretic controller, the state \bar{h} determines the “proportional” term direction of the torque feedback in order to move q_e either to 1 or -1 . The state m is introduced in order to adapt the hysteresis width δ_a of the on-off control for state \bar{h} .

In the bimodal controller, it is considered the same torque feedback suggested by [54], given by

$$\tau_2 = -\bar{c}\bar{h}\epsilon_e - K_\omega\omega, \quad (5.1)$$

where $K_\omega = K_\omega^T > 0$. Adding matrix K_ω to (3.13) gives more freedom to tune the control torque. For practical purposes, this extra torque parameter K_ω allows, for instance, the design of a bounded torque and to take into account the constraints of the angular velocity sensors, i.e., the slew rate limits [59] (see example in Section 5.3.2).

Let the state of the system plant + controller be represented by $\bar{x}_2 = (\bar{x}, \bar{h}, m) \in X_2 \triangleq X \times X_c \times X_c$. The complete system is given by (2.10), (2.11) and the following dynamics of the controller:

$$\left. \begin{array}{l} \dot{\bar{h}} = 0 \\ \dot{m} = 0 \end{array} \right\} \bar{x}_2 \in C_2, \quad (5.2)$$

$$\left. \begin{array}{l} \bar{h}^+ \in \overline{\text{sgn}}(u_2 - u_3\delta/2) \\ m^+ \in u_3 \overline{\text{sgn}}(u_2 - u_3\delta/2) \end{array} \right\} \bar{x}_2 \in D_2,$$

$$C_2 \triangleq \{\bar{x}_2 \in X_2 : (\bar{h}\eta_e \geq -\delta) \text{ and } (m = -1 \text{ or } \bar{h}\eta_e \geq -\delta/2) \text{ and } (m = 1 \text{ or } \bar{h}\eta_e \leq 3\delta/2)\}, \quad (5.3)$$

$$D_2 \triangleq \{\bar{x}_2 \in X_2 : (\bar{h}\eta_e \leq -\delta) \text{ or } (m = 1 \text{ and } \bar{h}\eta_e \leq -\delta/2) \text{ or } (m = -1 \text{ and } \bar{h}\eta_e \geq 3\delta/2)\}, \quad (5.4)$$

where m^+ and \bar{h}^+ are values associated to m and \bar{h} , respectively, just after state transition. Note that $C_2 = \overline{X_2 \setminus D_2}$. The sets C_2 and D_2 are depicted in Figure 5.1.

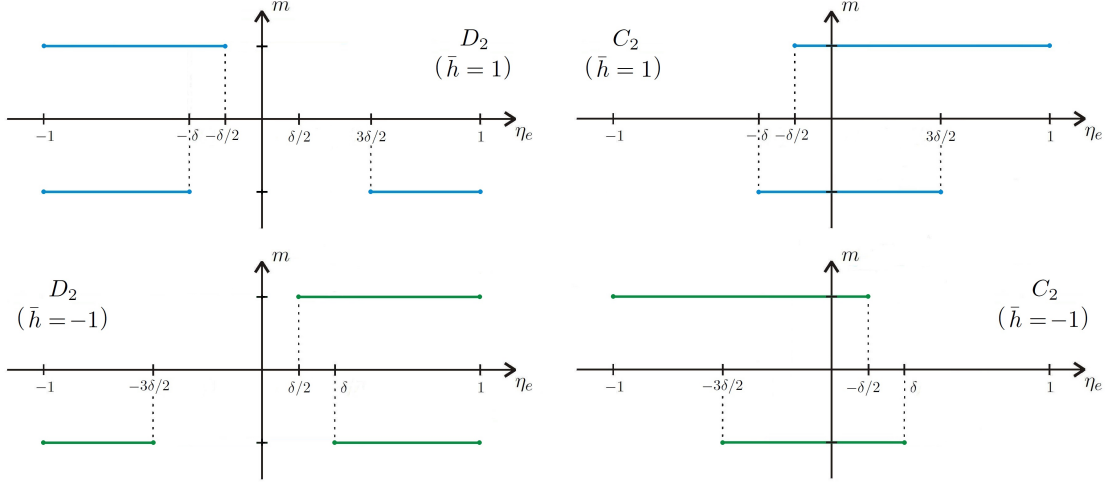


Figure 5.1: Graphical representation of sets C_2 and D_2 .

The vector of inputs of the controller is $U_2 = (\tau, u_2, u_3)$ and the closed-loop is achieved by setting

$$U_2 = \mathcal{K}_2(y, \bar{h}, m, \mathbf{q}_d) \triangleq (-\bar{c}\bar{h}\epsilon_e - K_\omega \boldsymbol{\omega}, \eta_e, \bar{h}). \quad (5.5)$$

The behavior of the controller can be seen in Figure 5.2.

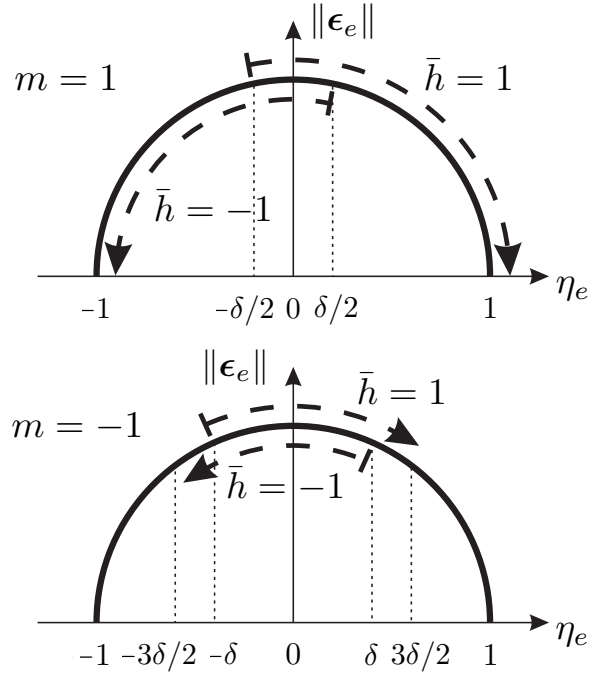


Figure 5.2: State space representation and the proposed regulation with two state variables (\bar{h} and m). Arrows indicate the direction of the “proportional” term of the torque (dependent on \bar{h}) so the attitude is regulated to 1 or -1 . The hysteresis half-width of the on-off control for state \bar{h} is $\delta/2$ when $m = 1$ and δ when $m = -1$.

The parameter $\delta \in (0, 1)$ is used to define the basic hysteresis width. The state m has the effect of adapting the hysteresis width δ_a of the on-off control for state \bar{h} . For $m = -1$, $\delta_a = \delta$ and the controller behaves as the hysteretic controller (\bar{h} changes when $\bar{h}\eta_e \leq -\delta$). For $m = 1$, $\delta_a = \delta/2$ and \bar{h} changes when $\bar{h}\eta_e \leq -\delta/2$. This distinct behavior is what differentiates the proposed controller from the hysteretic controller by allowing the change of state \bar{h} to be anticipated and, consequently, the change of direction of the “proportional” term of

the torque contribution towards the shorter rotation direction. The controller switches m from -1 to 1 when $\bar{h}\eta_e \geq 3\delta/2$, that is, when the attitude is far from the chattering prone region and switches m from 1 to -1 when $\bar{h}\eta_e \leq -\delta/2$. Note that the controller was designed so that m switches from 1 to -1 together with the change of \bar{h} .

It will be shown in the next section that the controller globally asymptotically stabilizes the set

$$A_2 = \{\bar{x}_2 \in X_2 : \mathbf{q}_e = \bar{h}\mathbf{1}, m = 1 \text{ and } \boldsymbol{\omega} = \mathbf{0}\}. \quad (5.6)$$

The following sections will enable us to compare performance of the bimodal controller with the hysteretic controller. In this comparison, if both controllers use the same value of δ , say, $\delta = \bar{\delta}$, then simulation experiments show that the bimodal controller spends less energy on average (see Section 5.3). If the hysteretic controller uses $\delta = \bar{\delta}/2$ and the bimodal controller uses $\delta = \bar{\delta}$ then, from Theorem 5.1 below, the bimodal controller avoids chattering for measurement noise of magnitude $\alpha < \bar{\delta}/2$ while the hysteretic controller avoids chattering only for $\alpha < \bar{\delta}/4$. That is, the bimodal controller is not just the hysteretic controller with half hysteresis width, but it is indeed a middle term solution which spends less energy in average while keeping robustness.

5.1 STABILITY ANALYSIS

Considering the proposed bimodal controller (5.2), the system can be written as a function of the vector of inputs, U_2 , as follows

$$\mathcal{H}(U_2) : \begin{cases} \dot{\bar{x}}_2 = F_2(\bar{x}_2, U_2), & \bar{x}_2 \in C_2, \\ \bar{x}_2^+ \in G_2(\bar{x}_2, U_2), & \bar{x}_2 \in D_2, \end{cases} \quad (5.7)$$

where $\bar{x}_2 = (\mathbf{q}_e, \boldsymbol{\omega}, \bar{h}, m)$, $U_2 = (\boldsymbol{\tau}, u_2, u_3)$,

$$F_2(\bar{x}_2, U_2) \triangleq \begin{bmatrix} \frac{1}{2}\mathbf{q}_e \circ (0, \boldsymbol{\omega}) \\ J^{-1}(S(J\boldsymbol{\omega})\boldsymbol{\omega} + \boldsymbol{\tau}) \\ 0 \\ 0 \end{bmatrix},$$

$$G_2(\bar{x}_2, U_2) \triangleq \begin{bmatrix} \mathbf{q}_e \\ \boldsymbol{\omega} \\ \overline{\text{sgn}}(u_2 - u_3\delta/2) \\ u_3 \overline{\text{sgn}}(u_2 - u_3\delta/2) \end{bmatrix}.$$

By substituting (5.5) in (5.7), it can be written in the closed-loop form, denoted as $\bar{\mathcal{H}} \triangleq \mathcal{H}(\mathcal{K}_2)$. Let $\bar{F}_2(\bar{x}_2) \triangleq F_2(\bar{x}_2, \mathcal{K}_2)$ and $\bar{G}_2(\bar{x}_2) \triangleq G_2(\bar{x}_2, \mathcal{K}_2)$.

$$\bar{\mathcal{H}} : \begin{cases} \dot{\bar{x}}_2 = \bar{F}_2(\bar{x}_2), & \bar{x}_2 \in C_2, \\ \bar{x}_2^+ \in \bar{G}_2(\bar{x}_2), & \bar{x}_2 \in D_2, \end{cases} \quad (5.8)$$

$$\bar{F}_2(\bar{x}_2) = \begin{bmatrix} \frac{1}{2}\mathbf{q}_e \circ (0, \boldsymbol{\omega}) \\ J^{-1}(S(J\boldsymbol{\omega})\boldsymbol{\omega} - \bar{c}\bar{h}\boldsymbol{\epsilon}_e - K_\omega\boldsymbol{\omega}) \\ 0 \\ 0 \end{bmatrix}, \quad (5.9)$$

$$\bar{G}_2(\bar{x}_2) = \begin{bmatrix} \mathbf{q}_e \\ \boldsymbol{\omega} \\ \overline{\text{sgn}}(\eta_e - \bar{h}\delta/2) \\ \bar{h} \overline{\text{sgn}}(\eta_e - \bar{h}\delta/2) \end{bmatrix}. \quad (5.10)$$

Theorem 5.1

Let $\delta \in (0, 1)$ and $\bar{c} > 0$. Then, the compact set A_2 defined in 5.6 is globally asymptotically stable for the closed-loop hybrid system $\bar{\mathcal{H}}$.

Proof. The proof follows in the same way as that of Theorem 5.2 in [10]. For easy presentation, let us first consider $\delta \in (0, 2/3]$ and the Lyapunov function $V : X_2 \rightarrow \mathbb{R}$, defined as

$$V(\bar{x}_2) = 2\bar{c}(1 - \bar{h}\eta_e) + \frac{1}{2}\omega^T J\omega. \quad (5.11)$$

Function V is positive definite on X_2 with respect to A_2 , since $V(\bar{x}_2) > 0$ for $\bar{x}_2 \in X_2 \setminus A_2$ and $V(\bar{x}_2) = 0$ for $\bar{x}_2 \in A_2$.

The time derivative of V , \dot{V} , is given by

$$\begin{aligned} \dot{V}(\bar{x}_2) &= \langle \nabla V(\bar{x}_2), \bar{F}_2(\bar{x}_2) \rangle, \\ &= \left\langle \begin{bmatrix} \left[\begin{array}{cccc} (-2\bar{c}\bar{h}) & 0 & 0 & 0 \end{array} \right]^T \\ J\omega \\ -2\bar{c}\eta_e \\ 0 \end{bmatrix}, \begin{bmatrix} \frac{1}{2} \left[\begin{array}{cc} -\epsilon_e^T \omega & (\eta_e \omega + \epsilon_e \times \omega)^T \end{array} \right]^T \\ J^{-1} (S(J\omega)\omega - \bar{c}\bar{h}\epsilon_e - K_\omega \omega) \\ 0 \\ 0 \end{bmatrix} \right\rangle, \\ &= -\omega^T K_\omega \omega \leq 0. \end{aligned} \quad (5.12)$$

Thus, \dot{V} is negative semidefinite on X_2 .

Along jumps, when $\bar{x}_2 \in D_2$,

$$\Delta V(\bar{x}_2) = V(\bar{x}_2^+) - V(\bar{x}_2) = -2\bar{c}\eta_e(\bar{h}^+ - \bar{h}).$$

Let $D_2 = D_{2a} \cup D_{2b} \cup D_{2c}$, where

$$D_{2a} \triangleq \{\bar{x}_2 \in X_2 : \bar{h}\eta_e \leq -\delta\}, \quad (5.13)$$

$$D_{2b} \triangleq \{\bar{x}_2 \in X_2 : m = 1 \text{ and } \bar{h}\eta_e \leq -\delta/2\}, \quad (5.14)$$

$$D_{2c} \triangleq \{\bar{x}_2 \in X_2 : m = -1 \text{ and } \bar{h}\eta_e \geq 3\delta/2\}. \quad (5.15)$$

From (5.10), note that $\bar{h}^+ = \bar{h}$ when $\bar{x}_2 \in D_{2c}$ and $\bar{h}^+ = -\bar{h}$ ($\Delta V(\bar{x}_2) = 4\bar{c}\bar{h}\eta_e$) when $\bar{x}_2 \in D_{2a} \cup D_{2b}$. Hence,

$$\Delta V(\bar{x}_2) = \begin{cases} \leq -4\bar{c}\delta_a, & \bar{x}_2 \in D_{2a} \cup D_{2b}, \\ 0, & \bar{x}_2 \in D_{2c}, \end{cases} \quad (5.16)$$

where $\delta_a = \delta$ for $\bar{x}_2 \in D_{2a} \setminus D_{2b}$ and $\delta_a = \delta/2$ for $\bar{x}_2 \in D_{2b}$.

From Theorem 7.6 of [56], it follows that the compact set A_2 is stable since $\Delta V(\bar{x}_2) \leq 0$ and $\dot{V}(\bar{x}_2) \leq 0$ for all $\bar{x}_2 \in X_2$. The conclusion that the set A_2 is globally asymptotically stable comes when Theorem 4.7 of [56] is applied to prove that the set A_2 is the largest invariant set in $W = W_1 \cup W_2$, where $W_1 \triangleq \{\bar{x}_2 \in C_2 : \dot{V}(\bar{x}_2) = 0\}$ and $W_2 \triangleq \Delta V^{-1}(0) \cap G_2(\Delta V^{-1}(0))$. It follows that $\Delta V^{-1}(0) = D_{2c}$ and $G_2(\Delta V^{-1}(0)) = \{\bar{x}_2 \in X_2 : m = 1 \text{ and } \bar{h}\eta_e \geq 3\delta/2\}$. Thus, $W_2 = \emptyset$ and

$$\begin{aligned} W &= W_1 = \{\bar{x}_2 \in X_2 : \omega = \mathbf{0} \text{ and } \bar{h}\eta_e \geq -\delta \text{ and} \\ &\quad (m = -1 \text{ or } \bar{h}\eta_e \geq -\delta/2) \text{ and } (m = 1 \text{ or } \bar{h}\eta_e \leq 3\delta/2)\}. \end{aligned}$$

Let W be the largest invariant set. On W , $\omega = \mathbf{0}$. From (5.9), the only way to keep $\omega \equiv \mathbf{0}$ is when $\epsilon_e \equiv \mathbf{0}$. This means $\mathbf{q}_e = \pm \mathbf{1}$. Using restriction $\bar{h}\eta_e \geq -\delta$, it follows that $\mathbf{q}_e = \bar{h}\mathbf{1}$ and using the other two restrictions, $m = 1$. Thus, any solution $\bar{x}_2(t)$ approaches the largest invariant set A_2 .

This controller restricts parameter δ to a value lower than or equal to $\delta^* = 2/3$, $\delta \in (0, \delta^*]$. For the case $\delta \in (2/3, 1)$, the system still behaves as proposed until state m changes to -1 (i.e. until the first jump, in case $m(0) = 1$). Afterwards, the controller works as the hysteretic controller, since m will not change any more. The proof of stability for this case follows by similar arguments used to prove the case $\delta \in (0, 2/3]$. \square

Following is the proof that the number of jumps is bounded for any solution trajectory to the closed loop system $\bar{\mathcal{H}}$ defined in (6.13). In other words, no Zeno solutions (infinite number of jumps in a finite amount of time [49, Definition 2.5] occur using the bimodal controller.

Theorem 5.2

Given any compact set $K \subset X_2$, a solution trajectory^a to the hybrid system $\bar{\mathcal{H}}$, starting at $\bar{x}_2(0, 0) \in K$ contains a finite number of jumps.

^aThe domain of a solution trajectory to a hybrid system is called hybrid time domain. Further details are found in Section 2.7.

Proof. There are three types of controller state changes. The first one is when state $m = -1$ and only state \bar{h} changes. It happens when $\bar{h} = 1$ and $\eta_e \leq -\delta$ or when $\bar{h} = -1$ and $\eta_e \geq \delta$. In this case, $\bar{x}_2 \in D_{2a} \setminus D_{2b}$ and, from (5.16), the change in $V(\bar{x}_2)$ over the jump is at most $\Delta V_1 = -4\bar{c}\delta$.

The second one is when state $m = -1$ and only state m changes to 1. It happens when $\bar{h} = 1$ and $\eta_e \geq 3\delta/2$ or when $\bar{h} = -1$ and $\eta_e \leq -3\delta/2$. In this case, $\bar{x}_2 \in D_{2c}$ and $\Delta V_2 = 0$ since $V(\bar{x}_2)$ does not depend on state m .

The last one is when state $m = 1$ and both states, \bar{h} and m , change. It happens when $\bar{h} = 1$ and $\eta_e \leq -\delta/2$ or when $\bar{h} = -1$ and $\eta_e \geq \delta/2$. In this case, $\bar{x}_2 \in D_{2b}$ and, from (5.16), the change in $V(\bar{x}_2)$ is at most $\Delta V_3 = -2\bar{c}\delta$. Note that this third controller state change is only possible if the second one has happened previously.

Summing up, $V(\bar{x}_2)$ varies at most $\Delta V_1 = -4\bar{c}\delta$ each time the controller state change occurs according to the first type of change and at most $\Delta V_2 + \Delta V_3 = -2\bar{c}\delta$ each time a sequence of two jumps occurs (second type followed by the third type). Since $\dot{V}(\bar{x}_2) \leq 0$ along flows (see (5.12)), the maximum number of jumps is given by the maximum $n_j \in \{0, 1, 2, \dots\}$ that satisfies

$$n_j \leq \frac{2V^*}{|\Delta V_2 + \Delta V_3|} + 1 = \frac{2V^*}{2\bar{c}\delta} + 1 = \frac{V^*}{\bar{c}\delta} + 1$$

where $V^* = \max V(K)$. The unit added on the amount of jumps refers to the case when the initial state of m is -1 and its final state is 1.

After some time, no jumps occur any more and the system behaves as a continuous dynamical system. \square

So far the stability analysis has not taken into account “outer perturbations” that includes both measurement and modeling errors [58, 10]. According to [58], a robustness analysis of $\bar{\mathcal{H}}$ should consider perturbed systems $(\bar{F}_2^\alpha, \bar{G}_2^\alpha, C_2^\alpha, D_2^\alpha)$. A family of perturbed system, denoted $\bar{\mathcal{H}}^\alpha$, is defined below [58, 10].

$$\begin{aligned} \bar{F}_2^\alpha(\bar{x}_2) &= \bar{\text{co}} F_2(\bar{x}_2, \mathcal{K}_2(y + \alpha\mathbb{B}, \bar{h}, m, \mathbf{q}_d)) + \alpha\mathbb{B}, \\ \bar{G}_2^\alpha(\bar{x}_2) &= \{z \in X_2 : z \in G_2(\bar{x}_2, \mathcal{K}_2(y + \alpha\mathbb{B}, \bar{h}, m, \mathbf{q}_d))\}, \end{aligned} \quad (5.17)$$

$$\begin{aligned} C_2^\alpha &= \{\bar{x}_2 \in X_2 : T(y + \alpha\mathbb{B}, \bar{h}, m, \mathbf{q}_d) \cap C_2 \neq \emptyset\}, \\ D_2^\alpha &= \{\bar{x}_2 \in X_2 : T(y + \alpha\mathbb{B}, \bar{h}, m, \mathbf{q}_d) \cap D_2 \neq \emptyset\} \end{aligned} \quad (5.18)$$

where $\bar{\text{co}}$ denotes the closed convex hull, function T is defined as $T : X_2 \times \mathbb{S}^3 \rightarrow X_2$, $T(y, \bar{h}, m, \mathbf{q}_d) = \bar{x}_2$, $\alpha > 0$ and \mathbb{B} is the closed unit ball.

Following the arguments used in [10], it is possible to affirm that there exists a maximum noise magnitude α such that the number of jumps in the perturbed system $\overline{\mathcal{H}}^\alpha$ gets bounded.

Theorem 5.3

Let $\delta \in (0, 1)$ and $\bar{c} > 0$. Then, given a compact set $K \subset X_2$, there exists $\alpha^{max} > 0$ such that for all $\alpha \in (0, \alpha^{max}]$, every solution trajectory to the hybrid system $\overline{\mathcal{H}}^\alpha$, starting at $\bar{x}_2^\alpha(0, 0) \in K$ contains a finite number of jumps.

Proof. The proof of this theorem is analogous to the proof of [10, Theorem 5.4].

Consider the Lyapunov function V defined in (5.11). According to Theorem 6.5 of [58], there exists $\beta \in \mathcal{KL}$ such that every solution trajectory to the hybrid system $\overline{\mathcal{H}}$ starting at $\bar{x}_2(0, 0) \in K$,

$$V(\bar{x}_2(t, j)) \leq \beta(V(\bar{x}_2(0, 0)), t + j) \quad \forall (t, j) \in \text{dom } \bar{x}_2 \quad (5.19)$$

Theorem 6.5 requires that the system $\overline{\mathcal{H}}$ satisfies the hybrid basic conditions and that there exists an open basin of attraction of the compact set A_2 . Both conditions are satisfied from Lemma B.3 (see Appendix B) and Theorem 5.1. Once (5.19) holds, according to Theorem 6.6 of [58], for each $\gamma > 0$ there exists $\alpha^{max} > 0$ such that for each $\alpha \in (0, \alpha^{max}]$, every trajectory solution of $\overline{\mathcal{H}}^\alpha$ starting at $\bar{x}_2^\alpha(0, 0) \in K$ satisfies

$$V(\bar{x}_2^\alpha(t, j)) \leq \beta(V(\bar{x}_2^\alpha(0, 0)), t + j) + \gamma \quad \forall (t, j) \in \text{dom } \bar{x}_2^\alpha \quad (5.20)$$

Theorem 6.6 requires that the system $\overline{\mathcal{H}}^\alpha$ have the convergence property. [58, Theorem 5.4] ensures that $\overline{\mathcal{H}}^\alpha$ has this property since it satisfies the hybrid basic conditions (Lemma B.3, Appendix B). Equation (5.20) affirms that $\lim_{t+j \rightarrow \infty} V(\bar{x}_2^\alpha(t, j)) \in [0, \gamma]$. From Theorem 5.2, it is known that jumps may occur if $V \geq 2\bar{c}\delta = |\Delta V_2 + \Delta V_3|$. Hence, for $\gamma < 2\bar{c}\delta$, the number of jumps is bounded.

As $\bar{x}_2 = (\bar{x}, \bar{h}, m) \in X_2 \triangleq \mathbb{S}^3 \times \mathbb{R}^3 \times X_c \times X_c$, note that the set K can not include all the set X_2 , since the real set is not compact. However, it can include all initial attitudes of the body. \square

5.2 CHATTERING ANALYSIS

Due to noise present in measurements, chattering is possible to occur when jumps map the state back into the jump set, i.e., when $G_2(D_2) \cap D_2 \neq \emptyset$. When this condition is met, the immediate consecutive jumps must also be analyzed to make sure a loop occurs and the following states are mapped to the jump set continuously. Considering that the output y is corrupted by noise of maximum magnitude α , the verification should be concentrated on intersections $\overline{G}_2^\alpha(D_2^\alpha) \cap D_2^\alpha$, $\overline{G}_2^\alpha(\overline{G}_2^\alpha(D_2^\alpha) \cap D_2^\alpha) \cap D_2^\alpha$, and so on until a loop or an empty set is achieved, where \overline{G}_2^α and D_2^α are defined in (5.17) and (5.18).

Theorem 5.4

Let $\alpha \in [0, 0.5)$ be the maximum noise magnitude and $\delta \in (2\alpha, 1)$. Either $\overline{G}_2^\alpha(D_2^\alpha) \cap D_2^\alpha = \emptyset$ or $\overline{G}_2^\alpha(\overline{G}_2^\alpha(D_2^\alpha) \cap D_2^\alpha) \cap D_2^\alpha = \emptyset$ for the closed-loop hybrid system $\overline{\mathcal{H}}$.

Proof. Firstly consider $\delta \in (0, 2/3]$ and let $D_2 = D_{2a} \cup D_{2b} \cup D_{2c}$, where D_{2a} , D_{2b} and D_{2c} are defined

in (5.13), (5.14) and (5.15), respectively. It can be shown that $D_2^\alpha = D_{2a}^\alpha \cup D_{2b}^\alpha \cup D_{2c}^\alpha$, where

$$\begin{aligned} D_{2a}^\alpha &\triangleq \{ \bar{x}_2 \in X_2 : \bar{h}\eta_e \leq -\delta + \alpha \}, \\ D_{2b}^\alpha &\triangleq \{ \bar{x}_2 \in X_2 : m = 1 \text{ and } \bar{h}\eta_e \leq -\delta/2 + \alpha \}, \\ D_{2c}^\alpha &\triangleq \{ \bar{x}_2 \in X_2 : m = -1 \text{ and } \bar{h}\eta_e \geq 3\delta/2 - \alpha \}. \end{aligned}$$

The jump maps for states \bar{h} and m , when measurement noise is taken into account, are given by

$$\bar{h}^+ \in \overline{\text{sgn}}(\eta_e + \alpha\mathbb{B} - \bar{h}\delta/2) \quad m^+ \in \bar{h} \overline{\text{sgn}}(\eta_e + \alpha\mathbb{B} - \bar{h}\delta/2)$$

and their graphical representations are shown in Figure 5.3.

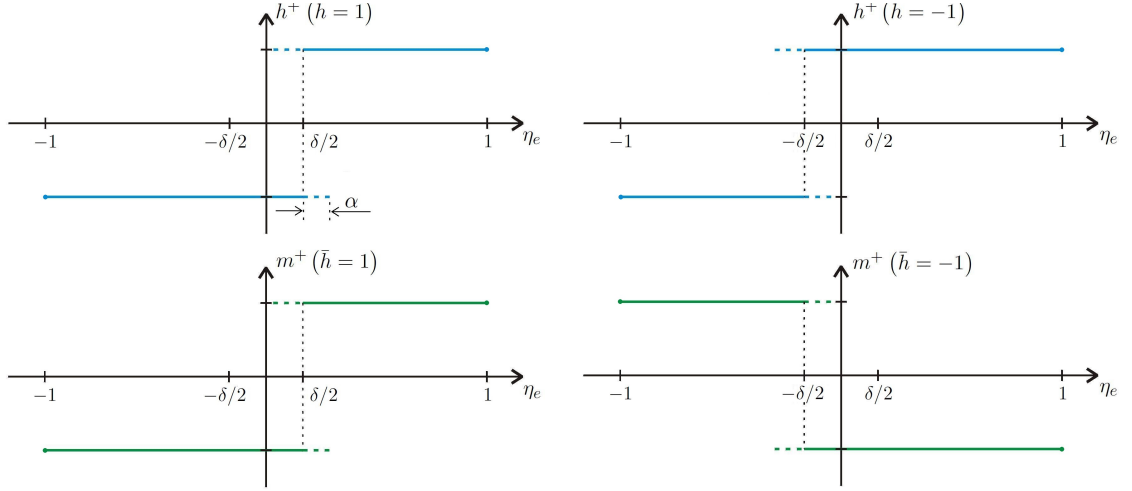


Figure 5.3: Graphical representation of the jump map for h^+ and m^+ .

In the sequel, the evolution of state \bar{x}_2 is analyzed after it enters the jump set D_2^α .

When the state $\bar{x}_2 \in D_{2a}^\alpha$, it jumps into the set

$$\overline{G}_2^\alpha(D_{2a}^\alpha) = \{ \bar{x}_2 \in X_2 : m = -1 \text{ and } \bar{h}\eta_e \geq \delta - \alpha \}.$$

A further jump may occur if $\overline{G}_2^\alpha(D_{2a}^\alpha) \cap D_2^\alpha \neq \emptyset$, i.e.,

$$\left(\overline{G}_2^\alpha(D_{2a}^\alpha) \cap D_{2a}^\alpha \right) \cup \left(\overline{G}_2^\alpha(D_{2a}^\alpha) \cap D_{2b}^\alpha \right) \cup \left(\overline{G}_2^\alpha(D_{2a}^\alpha) \cap D_{2c}^\alpha \right) \neq \emptyset.$$

As $\overline{G}_2^\alpha(D_{2a}^\alpha) \cap D_{2a}^\alpha = \emptyset$ and $\overline{G}_2^\alpha(D_{2a}^\alpha) \cap D_{2b}^\alpha = \emptyset$,

$$\overline{G}_2^\alpha(D_{2a}^\alpha) \cap D_2^\alpha = \overline{G}_2^\alpha(D_{2a}^\alpha) \cap D_{2c}^\alpha = \{ \bar{x}_2 \in X_2 : m = -1 \text{ and } \bar{h}\eta_e \geq 3\delta/2 - \alpha \}. \quad (5.21)$$

Proceeding with the following jump,

$$\overline{G}_2^\alpha \left(\overline{G}_2^\alpha(D_{2a}^\alpha) \cap D_{2c}^\alpha \right) = \{ \bar{x}_2 \in X_2 : m = 1 \text{ and } \bar{h}\eta_e \geq 3\delta/2 - \alpha \}.$$

As $\overline{G}_2^\alpha \left(\overline{G}_2^\alpha(D_{2a}^\alpha) \cap D_{2c}^\alpha \right) \cap D_2^\alpha = \emptyset$, the state \bar{x}_2 is mapped outside D_2^α .

When the state $\bar{x}_2 \in D_{2b}^\alpha$, it jumps into the set

$$\overline{G}_2^\alpha(D_{2b}^\alpha) = \{ \bar{x}_2 \in X_2 : m = -1 \text{ and } \bar{h}\eta_e \geq \delta/2 - \alpha \}.$$

Note that $\overline{G}_2^\alpha(D_{2b}^\alpha) \cap D_{2b}^\alpha = \emptyset$ and $\overline{G}_2^\alpha(D_{2b}^\alpha) \cap D_{2a}^\alpha = \emptyset$, but

$$\overline{G}_2^\alpha(D_{2b}^\alpha) \cap D_{2c}^\alpha = \{ \bar{x}_2 \in X_2 : m = -1 \text{ and } \bar{h}\eta_e \geq 3\delta/2 - \alpha \}.$$

This is the same set as (5.21). As already analyzed, states in this set are mapped outside D_2^α . And finally, when the state $\bar{x}_2 \in D_{2c}^\alpha$, it jumps into the set

$$\bar{G}_2^\alpha(D_{2c}^\alpha) = \{\bar{x}_2 \in X_2 : m = 1 \text{ and } \bar{h}\eta_e \geq 3\delta/2 - \alpha\}.$$

But $\bar{G}_2^\alpha(D_{2c}^\alpha) \cap D_2^\alpha = \emptyset$.

Hence, no chattering can occur using the bimodal controller strategy. The same conclusion is obtained for the case $\delta \in (2/3, 1)$ by following the same arguments and noting that $D_{2c} = \emptyset$ and, as a consequence, $D_{2c}^\alpha = \emptyset$. \square

Note that, from Theorem 5.4, the condition on parameter δ which avoids chattering, given a measurement noise of maximum magnitude α^{max} , is $\delta > 2\alpha^{max}$. This is the same condition for the hysteretic controller [10, Theorem 5.5].

5.3 SIMULATION RESULTS

This section presents simulation results to compare performance of the bimodal, the hysteretic and the discontinuous controller in three distinct scenarios: one using an arbitrary rigid body model and the other two using realistic models of a quadrotor mini-helicopter and a spacecraft reported in literature.

The simulations were performed in MATLAB ambient, using ordinary differential equation solver with variable integration step (ode45) restricted to a maximum step of 1 ms.

The measured value \mathbf{q}_m of the attitude quaternion \mathbf{q} included noise and was calculated¹ as follows: $\mathbf{q}_m = (\mathbf{q} + b\hat{\mathbf{e}}) / \|\mathbf{q} + b\hat{\mathbf{e}}\|_2$, $\hat{\mathbf{e}} = \mathbf{e} / \|\mathbf{e}\|_2$, where each element $\mathbf{e} \in \mathbb{R}^4$ was chosen from a gaussian distribution of zero mean and unitary covariance matrix and $b \in \mathbb{R}$ was chosen from a uniform distribution on either the interval $[0, 0.2]$ (for Sections 5.3.1 and 5.3.2) or interval $[0, 0.1]$ (for Section 5.3.3). In both cases, b is independent of \mathbf{e} . The initial controller state for the hysteretic controller was $\bar{h}(0) = 1$ and for the bimodal controller, $\bar{h}(0) = 1$ and $m(0) = 1$. The desired reference was $\mathbf{q}_d = \mathbf{1}$ with $\boldsymbol{\omega}_d = \mathbf{0}$.

5.3.1 Rigid body

This scenario refers to an arbitrary rigid body whose motion is described by (2.10) with inertia matrix $J = \text{diag}(10\hat{\mathbf{v}})$, $\hat{\mathbf{v}} = [1 \ 2 \ 3]^T / \sqrt{14}$. It is compared the evolution of the system for the hysteretic controller, given by (3.14) and (3.15), and for the proposed bimodal controller, given by (5.2) and (5.5). For tuning of the controller parameters, \bar{c} and K_ω , it may be better to start by the derivative gain K_ω . According to the time derivative of the Lyapunov function (5.12), the higher the derivative gain, the faster the convergence. Clearly, high derivative gain may not be possible due to measurement noise influence (the control performance can be degraded) or physical constraints (bounds on control action, slew rate limits etc). In the latter case, refer to [59] for a strategy of tuning. Afterwards, the proportional gain \bar{c} may be chosen so that the system gets underdamped, if possible. This way the system reaches near the reference faster (and oscillates) and moves away from the discontinuous region ($-\delta \leq \eta_e \leq \delta$). The advantage is that the final value of \bar{h} may be determined faster as well as the quaternion representation of the reference attitude $\mathbf{1}$ or $-\mathbf{1}$. Here, for easy comparison, the control parameters used, for both controllers, were the same as those used in [10]: $\bar{c} = 1$, $K_\omega = I_3$, I_3 is the identity matrix of dimension 3, and the hysteresis parameter $\delta = 0.4$.

Firstly it is presented an overview of the difference of energy spent when the controllers are applied as a

¹The formula used equals the one used in [10] to facilitate comparisons.

function of the initial state on a contour graph to illustrate the regions where each controller is advantageous.

Let $\mathcal{E}(t) = \sqrt{\int_0^t \boldsymbol{\tau}^T \boldsymbol{\tau} dt}$ represent the energy spent by the applied feedback control and $\mathcal{E}_h(40)$ and $\mathcal{E}_b(40)$ represent the energy spent when the hysteretic and the bimodal controller is applied, respectively, up to 40 s. Figure 5.4 shows a contour graph of the difference between the energy spent when the bimodal and the hysteretic controller is applied ($\Delta\mathcal{E} = \mathcal{E}_b(40) - \mathcal{E}_h(40)$) as a function of $\eta_e(0)$ and Ω that represent the initial conditions $\mathbf{q}(0) = (\eta_e(0), \sqrt{1 - \eta_e(0)^2} \hat{\mathbf{v}})$ and $\boldsymbol{\omega}(0) = \Omega \hat{\mathbf{v}}$. Ω and $\eta_e(0)$ ranges from -2 to 2 and -1 to 1 , respectively, in steps of 0.05 . The simulations were performed up to 40 s, supposed to be enough for the system to reach near steady state.

$\Delta\mathcal{E}$ ranges from -0.8 to 0.8 units. Negative values mean that less energy is spent when the bimodal controller is applied and positive values when the hysteretic controller is applied. Areas of the graph in lighter colors represent negative values whereas the ones in darker colors represent positive values. For reference, the higher values of $\mathcal{E}_h(40)$ and $\mathcal{E}_b(40)$ were about 5 units, located at $(\Omega, \eta_e(0))$ around $(-2, -1)$, $(-2, 1)$, $(2, -1)$, $(2, 1)$. Difference in the energy spent ($\Delta\mathcal{E}$) between -0.06 and 0.06 was considered irrelevant due to the noise included in the simulation.

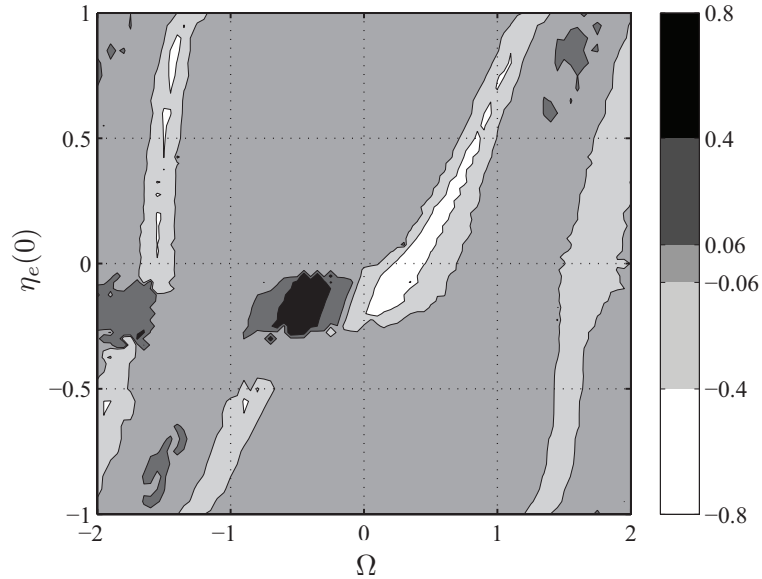


Figure 5.4: Difference between the energy spent when the bimodal and the hysteretic controller is applied ($\Delta\mathcal{E}$) as a function of the initial conditions, represented by $\eta_e(0)$ and Ω .

The proposed bimodal controller aimed to improve performance for the rest-to-rest case ($\Omega = 0$). Figure 5.4 confirms the bimodal controller is advantageous even when the initial angular velocity norm (Ω) is near zero. Regarding the other initial conditions, note that the areas in lighter colors are larger than the ones in darker colors. So, in a context of arbitrary initial condition, the bimodal controller would be more advantageous on average.

The area in black, where the hysteretic controller spends less energy, refers to a region of the state space where the control law pulls the rigid body in the direction of the longer rotation and the initial angular velocity is favorable, i.e., in the same direction. This condition illustrates that the choice of state $\bar{\mathbf{h}}$ is not trivial and should also depend on the angular velocity. This improvement is left for future research.

Figure 5.5 exemplifies a condition that presents a distinctive initial condition where the body presents a relatively high initial angular velocity to show that the bimodal controller may be viable in such conditions. The initial conditions were $\mathbf{q}(0) = (0.5, \sqrt{1 - 0.5^2} \hat{\mathbf{v}})$ and $\boldsymbol{\omega}(0) = -1.5 \hat{\mathbf{v}}$.

This simulation shows that the movement of both controllers coincided during the first seconds (state $\bar{\mathbf{h}}$ did

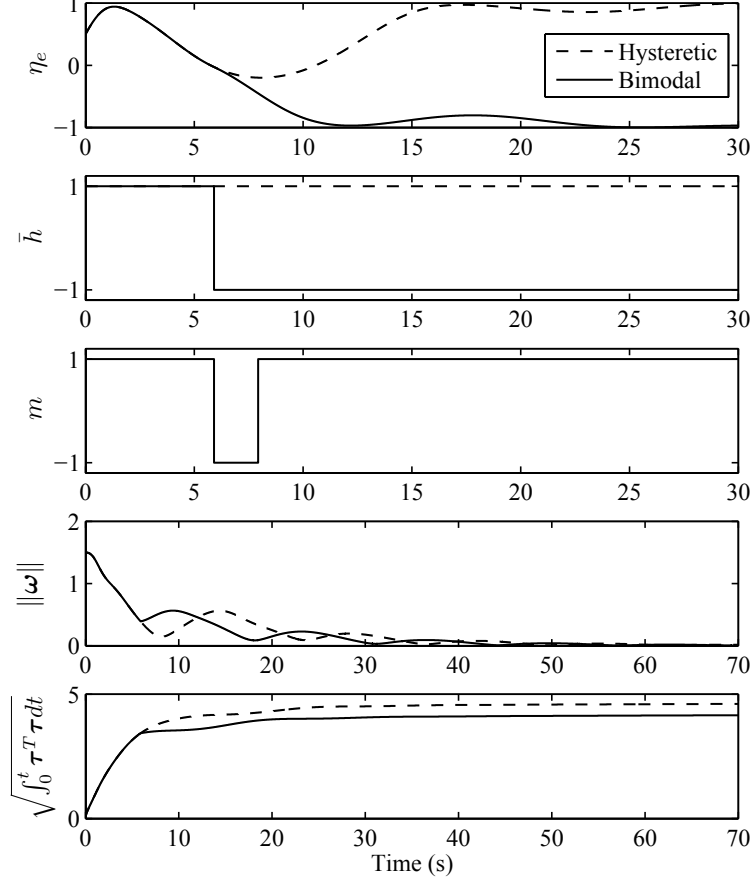


Figure 5.5: Comparison between the hysteretic and the proposed bimodal controller for a relatively high initial angular velocity norm.

not change). After having completed almost one revolution, the bimodal controller changed state \bar{h} when η_e crossed over its hysteresis threshold ($\eta_e \leq -\delta/2$). Then, it continued rotating towards $\eta_e = -1$. On the other hand, the hysteretic controller kept state \bar{h} unchanged. As a result, the body returned to $\eta_e = 1$, the direction of the longer rotation, and spent more energy.²

5.3.2 Quadrotor mini-helicopter

This scenario compares the state evolution of a quadrotor mini-helicopter from a rest position (hovering) for the three controllers. The model of the plant and the control parameters used were the same as those used by [59]. The kinematic and dynamic equations are

$$\begin{bmatrix} \dot{\mathbf{q}}_e \\ \dot{\boldsymbol{\omega}} \end{bmatrix} = \begin{bmatrix} \frac{1}{2} \mathbf{q}_e \circ (0, \boldsymbol{\omega}) \\ J_h^{-1} (S(J_h \boldsymbol{\omega}) \boldsymbol{\omega} - \boldsymbol{\tau}_G + \boldsymbol{\tau}) \end{bmatrix}, \quad (5.22)$$

where $J_h = 10^{-3} \text{diag}([8.28 \ 8.28 \ 15.7])$ kg m² is the inertia matrix of the quadrotor. The vector $\vec{\tau}_G$ is the gyroscopic effect that appears in lightweight constructions and is given by

$$\boldsymbol{\tau}_G = \sum_{i=1}^4 J_r (\boldsymbol{\omega} \times \hat{\mathbf{z}}_b) (-1)^{i+1} s_i, \quad (5.23)$$

²This simulation exemplifies a contrasting feature between the bimodal and the HY controller (Chapter 4). The reference remained fixed, the bimodal and the hysteretic controller determined the same value for the variable \bar{h} during the initial instants and different values afterwards. HY controller would have determined the same value for \bar{h} as the hysteretic controller.

where $J_r = 3.4 \times 10^{-5} \text{ kg m}^2$ is the inertia of the rotor, \hat{z}_b is the unit vector in the direction of the body-frame z-axis and s_i represents the rotational speed of rotor i . The relationship between the rotor speed and the torque τ is given by

$$\begin{bmatrix} \tau \\ t_z \end{bmatrix} = \begin{bmatrix} 0 & db & 0 & -db \\ db & 0 & -db & 0 \\ k & -k & k & -k \\ b & b & b & b \end{bmatrix} \begin{bmatrix} s_1^2 \\ s_2^2 \\ s_3^2 \\ s_4^2 \end{bmatrix}, \quad (5.24)$$

where $d = 0.225 \text{ m}$, $b = 29.1 \times 10^{-5} \text{ kg m rad}^{-2}$, $k = 1.14 \times 10^{-6} \text{ kg m}^2 \text{ rad}^{-2}$ and t_z is a component of the total thrust $\mathbf{t} = [0 \ 0 \ t_z]^T$ expressed in the body frame. The position equations are omitted as they are beyond the scope of this work.

The plant model is different from (2.10) due to the presence of the gyroscopic effect τ_G . The contribution of this effect in (5.22) is minimum as the inertia of the rotor is very small. The control law does not need modifications and the stability analysis is almost the same from that of Section 5.1 since the extra term τ_G is canceled during the time derivative \dot{V} calculation (5.12).

To make a fair comparison, the torque feedback (5.1) was applied to all the controllers. The control parameters used were $\bar{c} = 0.075$ and $K_\omega = \text{diag}([\bar{c}/\rho_1 \ \bar{c}/\rho_2 \ \bar{c}/\rho_3])$, $\rho_1 = \rho_2 = 4.2$ and $\rho_3 = 1.74$. As commented in [59], these parameters were chosen so the stability is not affected by the limits of the angular velocity sensors. The hysteresis parameter was set to $\delta = 0.4$ for the hysteretic and bimodal controller.

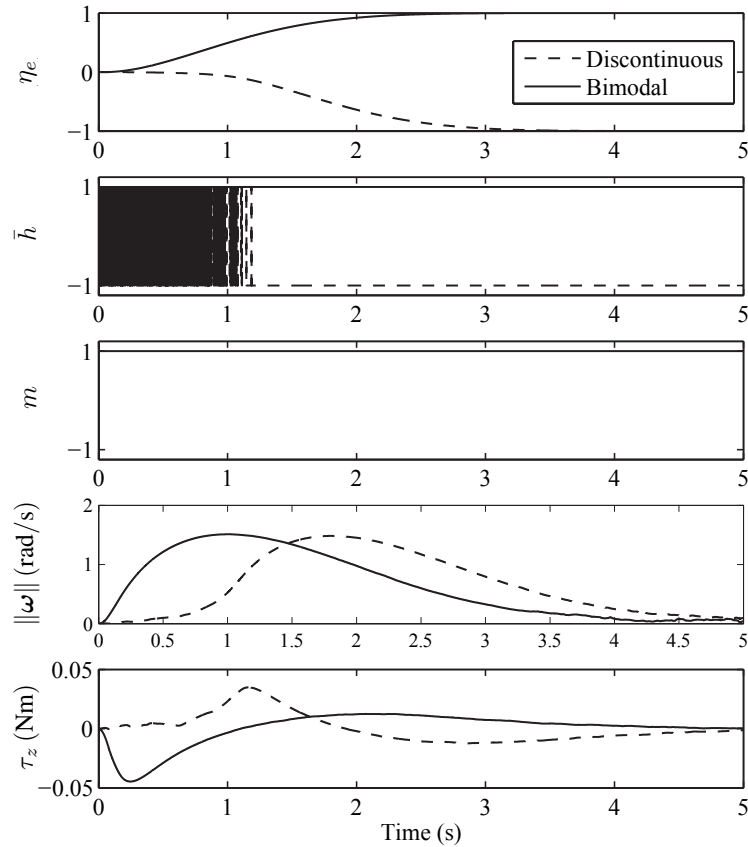


Figure 5.6: Comparison between the discontinuous and the proposed bimodal controller for the quadrotor.

Figure 5.6 illustrates the chattering behavior when the discontinuous controller is applied and compares it with the bimodal controller. The hysteretic controller is not shown as it behaves as the bimodal one. The initial conditions were $\mathbf{q}(0) = (0, [0 \ 0 \ 1]^T)$ and $\boldsymbol{\omega}(0) = \mathbf{0}$, i.e., the yaw angle was 180° from the reference. The desired thrust was $t_z > 4.59 \text{ N}$ to compensate the quadrotor weight. The graphs of η_e and the angular

velocity norm $\|\omega\|$ show that the discontinuous system had its response lagged due to the chattering on variable \bar{h} (caused by measurement noise) for over than 1 s. Recall that, as mentioned in Section 3.4, there exists a noise that keeps the state near the discontinuity ($\eta_e = 0$) indefinitely. On the other hand, the bimodal controller kept state \bar{h} unchanged at 1 (as well as state m) and the body moved toward 1. The last graph, of τ_z , shows only the τ_z component of the torque $\tau = (\tau_x, \tau_y, \tau_z)$ for both controllers as the other components stayed near 0.

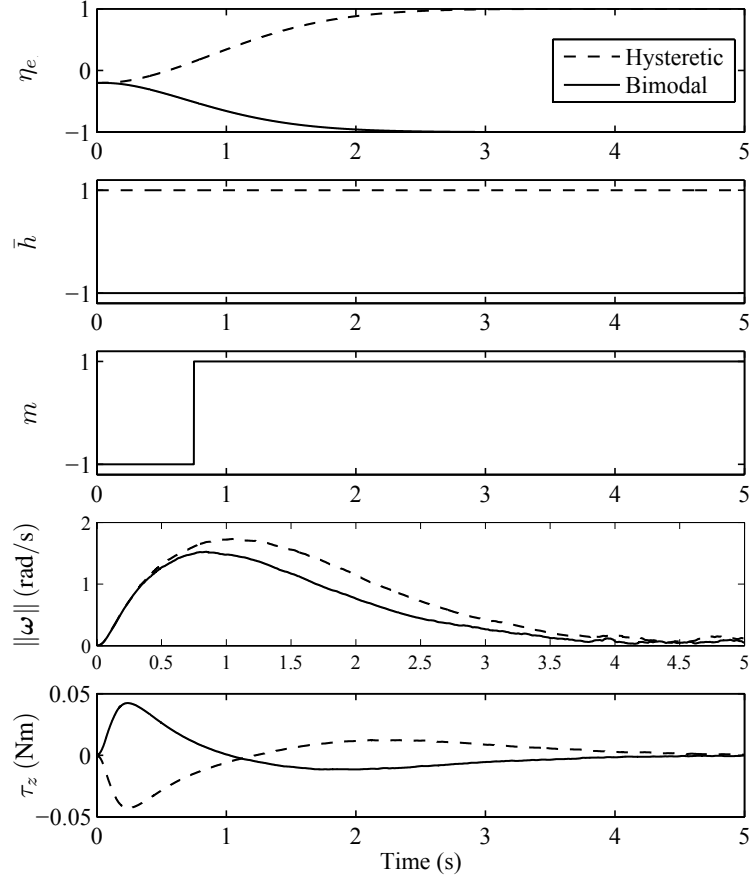


Figure 5.7: Comparison between the hysteretic and the proposed bimodal controller for the quadrotor.

Figure 5.7 presents the behavior of the bimodal and the hysteretic controllers. The initial conditions were $q(0) = (-0.2, \sqrt{1-0.2^2} [0 \ 0 \ 1]^T)$ and $\omega(0) = \mathbf{0}$. For the hysteretic controller only, this initial condition belongs to that region of the state space where the control law pulls the rigid body in the direction of the longer rotation. Consequently, hysteretic and bimodal controllers made the rigid body take a different direction of rotation from the beginning. Note in the graph of the angular velocity norm $\|\omega\|$ that the system with the bimodal controller converges faster.

5.3.3 Spacecraft

Here, it is intended to show that for controllers with analogous structure of the hysteretic controller (3.14) and (3.15), the bimodal philosophy can be easily adapted to obtain a new controller with expected advantages similar to that of the bimodal controller (5.2) and (6.10). Consider the scenario of a spacecraft attitude control studied by [55]. The plant model is given by (2.10) and the torque feedback is given by

$$\tau_s = J\dot{\omega}_r - S(J\omega)\omega_r - k_q T_h^T e_{hq} - k_w(\omega - \omega_r), \quad (5.25)$$

where $\boldsymbol{\omega}_r = \boldsymbol{\omega}_d - \gamma T_h^T e_{hq}$; $e_{hq} = [(1 - \bar{h}\eta_e) \quad \boldsymbol{\epsilon}_e^T]^T$; $k_q, k_w, \gamma > 0$ and

$$T_h = \begin{bmatrix} \bar{h}\boldsymbol{\epsilon}_e^T \\ \eta_e I + S(\boldsymbol{\epsilon}_e) \end{bmatrix}.$$

The hysteretic controller for this plant is given by

$$\begin{aligned} \dot{\bar{h}} &= 0 & \bar{x}_1 &\in C_{s1} \triangleq \{ \bar{x}_1 \in X_1 : \bar{h}\eta_\sigma \geq -\delta \}, \\ \bar{h}^+ &\in \overline{\text{sgn}}(u_{s1}) & \bar{x}_1 &\in D_{s1} \triangleq \{ \bar{x}_1 \in X_1 : \bar{h}\eta_\sigma \leq -\delta \} \end{aligned} \quad (5.26)$$

where

$$\eta_\sigma \triangleq k_q \eta_e - \gamma \boldsymbol{\epsilon}_e^T J(\boldsymbol{\omega} - \boldsymbol{\omega}_d)/2 \quad (5.27)$$

and the vector of inputs $U_{s1} = (\boldsymbol{\tau}, u_{s1})$ set to $\mathcal{K}_{s1}(y, \bar{h}, \mathbf{q}_d) \triangleq (\boldsymbol{\tau}_s, \eta_\sigma)$.

Note that (3.14) turns to (5.26) by changing η_e to η_σ and the vector of inputs U_1 (3.15) turns to U_{s1} by changing $\boldsymbol{\tau}_1$ (3.13) to $\boldsymbol{\tau}_s$ (5.25) and η_e to η_σ . The same analogy was applied to obtain the adapted bimodal controller for this plant, given by

$$\begin{aligned} \left. \begin{aligned} \dot{\bar{h}} &= 0 \\ \dot{m} &= 0 \end{aligned} \right\} & \bar{x}_2 \in C_{s2}, \\ \left. \begin{aligned} \bar{h}^+ &\in \overline{\text{sgn}}(u_{s2} - u_{s3}\delta/2) \\ m^+ &\in u_{s3} \overline{\text{sgn}}(u_{s2} - u_{s3}\delta/2) \end{aligned} \right\} & \bar{x}_2 \in D_{s2}, \end{aligned} \quad (5.28)$$

$$\begin{aligned} C_{s2} &\triangleq \{ \bar{x}_2 \in X_2 : (\bar{h}\eta_\sigma \geq -\delta) \text{ and} \\ &(m = -1 \text{ or } \bar{h}\eta_\sigma \geq -\delta/2) \text{ and } (m = 1 \text{ or } \bar{h}\eta_\sigma \leq 3\delta/2) \}, \\ D_{s2} &\triangleq \{ \bar{x}_2 \in X_2 : (\bar{h}\eta_\sigma \leq -\delta) \text{ or} \\ &(m = 1 \text{ and } \bar{h}\eta_\sigma \leq -\delta/2) \text{ or } (m = -1 \text{ and } \bar{h}\eta_\sigma \geq 3\delta/2) \} \end{aligned}$$

and the vector of inputs $U_{s2} = (\boldsymbol{\tau}, u_{s2}, u_{s3})$ set to $\mathcal{K}_{s2}(y, \bar{h}, m, \mathbf{q}_d) \triangleq (\boldsymbol{\tau}_s, \eta_\sigma, \bar{h})$.

Note also that η_σ (5.27) depends on both the attitude and the angular velocity. For the rest-to-rest case, when $\boldsymbol{\omega}(0) = \mathbf{0}$, $\eta_\sigma(0) = \eta_e(0)$ and, in the beginning, jump sets $D_{s1} = D_1$ (3.14) and $D_{s2} = D_2$ (5.4). Hence, if the initial attitude is near $\eta_e(0) = -\delta/2$ as is the case illustrated in Figure 5.7, the same behavior of the controllers is expected, that is, each of them makes the rigid body take a different direction of rotation from the beginning, with the hysteretic controller determining a rotation to the longer direction.

Figures 5.8 and 5.9 show the evolution of the system for the hysteretic and the adapted bimodal controllers when η_σ is near $-\delta/2$ (so the controllers determine a different direction of rotation from the beginning) but $\boldsymbol{\omega} \neq \mathbf{0}$. Two symmetric initial attitudes were chosen and the average energy consumption was evaluated. The parameters used for the simulations for both controllers were the same: the inertia matrix of the spacecraft $J = \text{diag}([4.35 \quad 4.33 \quad 3.664]) \text{ kg m}^2$, $k_q = 1$, $k_w = 2$ and $\gamma = 1$. The hysteresis parameter was set to $\delta = 0.2$. The initial conditions for Figure 5.8 were $\mathbf{q}(0) = (-0.4, \sqrt{1-0.4^2}\hat{\mathbf{v}}_s)$, $\hat{\mathbf{v}}_s = [3 \quad -4 \quad 5]^T / \sqrt{50}$ and $\boldsymbol{\omega}(0) = -0.16\hat{\mathbf{v}}_s$ and for Figure 5.9, $\mathbf{q}(0) = (0.4, \sqrt{1-0.4^2}\hat{\mathbf{v}}_s)$ and $\boldsymbol{\omega}(0) = 0.275\hat{\mathbf{v}}_s$. The graph of η_e of Figure 5.8 shows that the adapted bimodal controller made the spacecraft rotate to the shorter direction and, according to the last graph, less energy was spent ($\mathcal{E}_b(15) = 4.5$ and $\mathcal{E}_h(15) = 6.4$). The opposite occurred for Figure 5.9 ($\mathcal{E}_b(15) = 6.1$ and $\mathcal{E}_h(15) = 5.1$). Based on the average of energy spent by the controllers in both simulations, it is possible to affirm the adapted bimodal controller spends less energy on average.

Finally it is presented an overview of the difference of energy spent when the controllers are applied as a function of the initial state on a contour graph to illustrate the regions where each controller is advantageous.

Let $\mathcal{E}(t) = \sqrt{\int_0^t \boldsymbol{\tau}^T \boldsymbol{\tau} dt}$ represent the energy spent by the applied feedback control and $\mathcal{E}_h(20)$ and $\mathcal{E}_b(20)$ represent the energy spent when the hysteretic and the bimodal controller is applied, respectively, up to 20

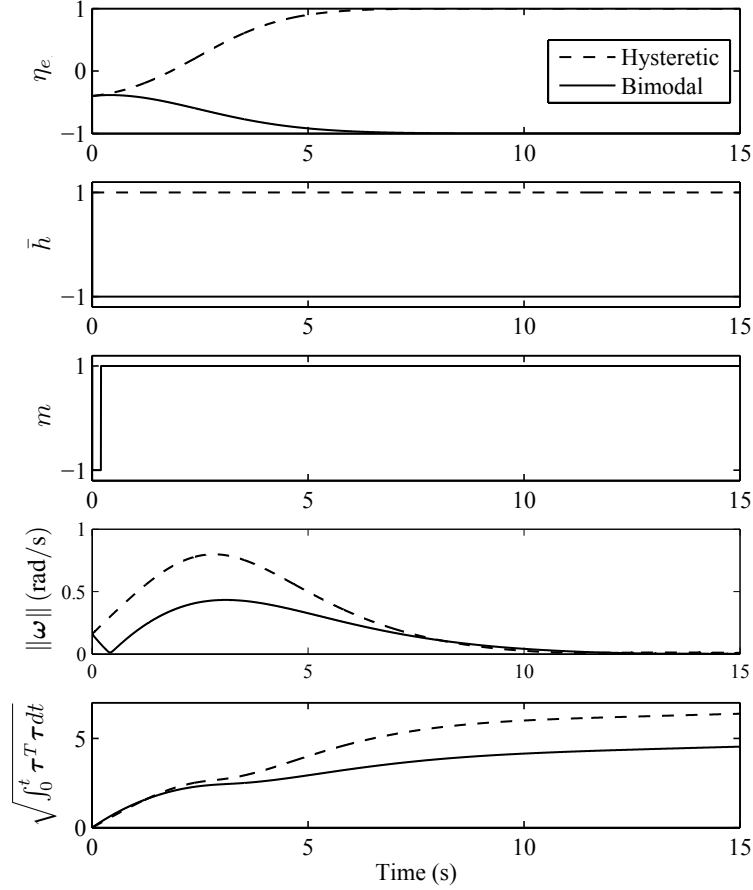


Figure 5.8: Comparison between the hysteretic and the proposed bimodal controller for the spacecraft. Initial condition $\eta_e = -0.4$ and η_σ near -0.1 .

s. Figure 5.10 shows a contour graph of the difference between the energy spent when the bimodal and the hysteretic controller is applied ($\Delta\mathcal{E} = \mathcal{E}_b(20) - \mathcal{E}_h(20)$) as a function of $\eta_e(0)$ and Ω that represent the initial conditions $\mathbf{q}(0) = (\eta_e(0), \sqrt{1 - \eta_e(0)^2}\hat{\mathbf{v}}_s)$ and $\boldsymbol{\omega}(0) = \Omega\hat{\mathbf{v}}_s$. Ω and $\eta_e(0)$ ranges from -2 to 2 and -1 to 1 , respectively, in steps of 0.1 . The simulations were performed up to 20 s, supposed to be enough for the system to reach near steady state. The hysteresis parameter was set to $\delta = 0.4$ to facilitate comparison with Figure 5.4.

$\Delta\mathcal{E}$ ranges from -0.8 to 0.8 units. Negative values mean that less energy is spent when the bimodal controller is applied and positive values when the hysteretic controller is applied. Areas of the graph in lighter colors represent negative values whereas the ones in darker colors represent positive values. For reference, the higher values of $\mathcal{E}_h(20)$ and $\mathcal{E}_b(20)$ were about 7 units, located at $(\Omega, \eta_e(0))$ around $(-2, -1)$, $(-2, 1)$, $(2, -1)$, $(2, 1)$. Difference in the energy spent ($\Delta\mathcal{E}$) between -0.06 and 0.06 was considered irrelevant due to the noise included in the simulation.

As well as it happened to the simulations of Subsection 5.3.1, Figure 5.10 confirms the bimodal controller is advantageous even when the initial angular velocity norm (Ω) is near zero. Regarding the other initial conditions, note that the areas in lighter colors are larger than the ones in darker colors. So, in a context of arbitrary initial condition, the bimodal controller would be more advantageous on average.

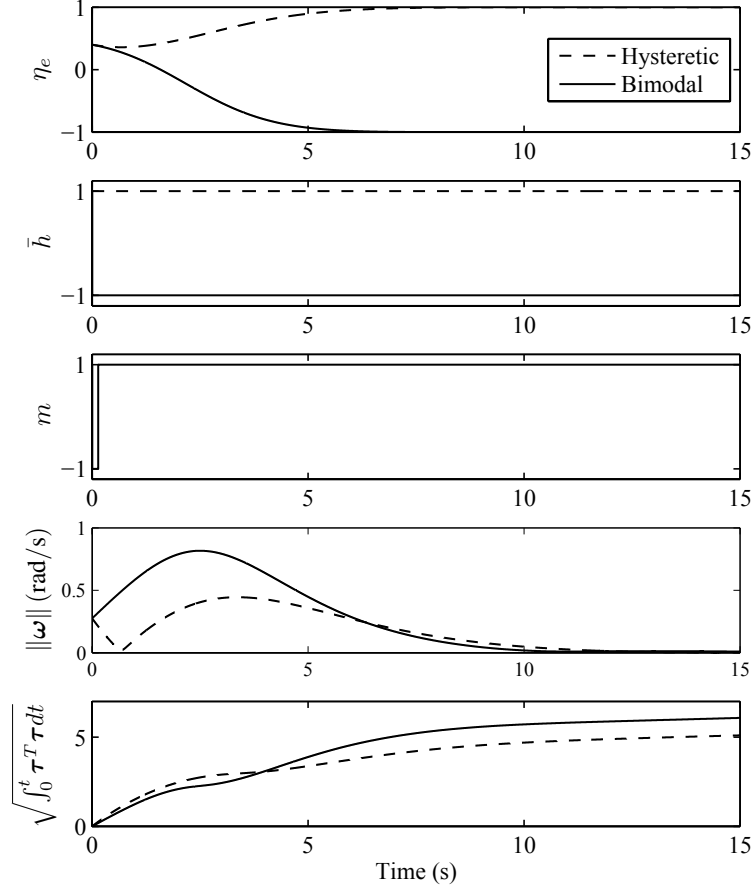


Figure 5.9: Comparison between the hysteretic and the proposed bimodal controller for the spacecraft. Initial condition $\eta_e = 0.4$ and η_σ near -0.1 .

5.4 CHAPTER CONCLUSIONS

In this chapter, the bimodal hybrid controller was proposed. It is well suited for the rest-to-rest attitude control of a rigid body with globally asymptotically stability property. The proposed controller can be seen as a middle term solution between the memoryless discontinuous and the hysteretic hybrid controller. Differently from the less costly discontinuous controller, the bimodal controller is robust in the sense of having capability of avoiding chattering due to measurement noise. Compared with the unimodal hysteretic hybrid controller, while both keep robustness and stability, the bimodal spends less energy in average.

It was also shown that the bimodal philosophy can be extended for other controllers which have one hysteretic mode. A bimodal controller is expected to be the most interesting choice when the attitude noise level may be expressive as for example when low cost components are used or when the system is under an electromagnetically noisy environment.

An article about the study of this chapter has already been published in the Journal of the Franklin Institute [33].

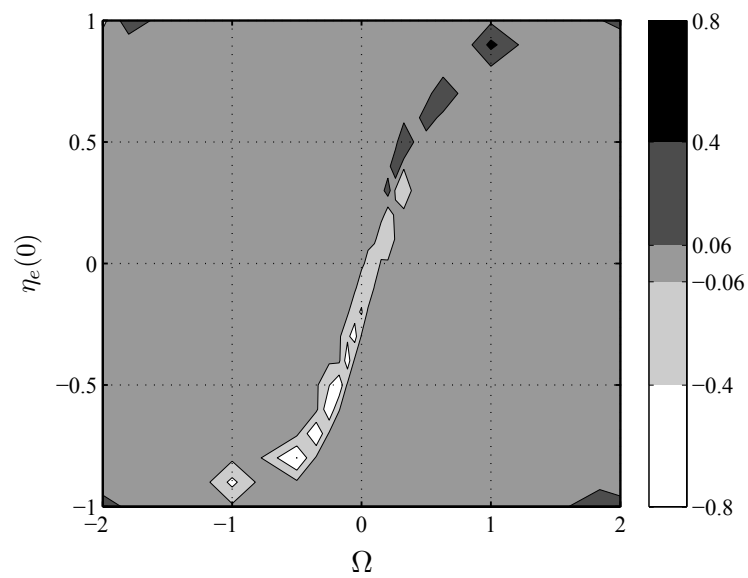


Figure 5.10: Difference between the energy spent when the bimodal and the hysteretic controller is applied ($\Delta\mathcal{E}$) as a function of the initial conditions, represented by $\eta_e(0)$ and Ω .

6

ROBUST GLOBAL DISTRIBUTED ATTITUDE CONTROL FOR MULTIPLE RIGID BODIES

Rigid-body attitude control applied to multi-agent systems in a cooperative control is an area that has also been studied for decades. In 1978, Labeyrie [60] proposed a stellar interferometer formation from free-flying telescopes. Research on multiple mobile robot (and multi-vehicle) systems initiated in the late 1980's [61] and increased in the 1990's thanks to the development of inexpensive and reliable wireless communications systems [62]. In the late 1990's and early 2000's, an area that became highly active was the cooperative control of multiple aircraft, especially unmanned aerial vehicles (UAVs) [62]. Much research has been developed on attitude coordination control in the last 10-15 years [15, 16, 17, 18, 19] but the great majority of them suggested continuous or discontinuous state-feedback laws that present known problems such as unstable states, unwinding phenomenon and chattering. In this chapter, it is proposed a distributed attitude synchronization control with globally asymptotically stability property and robustness against noise measurement for an undirected connected network (cyclic or acyclic) of rigid bodies (agents). The strategy uses a quaternion representation of the attitude and the hysteretic hybrid feedback with one binary logic variable, suggested by [10] (see Section 3.5), for each agent.¹

6.1 PRELIMINARIES

6.1.1 Attitude kinematics and dynamics of a group of n-agents

For a group of n-agents, in which it is associated an index $i = 1, 2, \dots, n$ for each agent, let \mathbf{q}_i and $\boldsymbol{\omega}_i$ represent, respectively, the attitude and the angular velocity of the agent i relative to each body frame and let \mathbf{q}_0 represent a fixed reference attitude with angular velocity $\boldsymbol{\omega}_0 = \mathbf{0}$ for all the agents.

The attitude error of agent i relative to the common reference attitude is given by

$$\mathbf{q}_{i0} = (\eta_{i0}, \boldsymbol{\epsilon}_{i0}) = \mathbf{q}_0^* \circ \mathbf{q}_i. \quad (6.1)$$

The relative attitude between agent i and j , $R_{ij} = R_j^T R_i = \mathcal{R}(\mathbf{q}_{ij})$, is represented by the relative quaternion

$$\mathbf{q}_{ij} = (\eta_{ij}, \boldsymbol{\epsilon}_{ij}) = \mathbf{q}_j^* \circ \mathbf{q}_i \quad (6.2)$$

which satisfies the following kinematic equation

$$\dot{\mathbf{q}}_{ij} = \frac{1}{2} \mathbf{q}_{ij} \circ (0, \boldsymbol{\omega}_{ij}), \quad (6.3)$$

where the relative angular velocity $\boldsymbol{\omega}_{ij}$ is

$$\boldsymbol{\omega}_{ij} = \boldsymbol{\omega}_i - R_{ij}^T \boldsymbol{\omega}_j. \quad (6.4)$$

Let $X = \mathbb{S}^3 \times \mathbb{R}^3$ and $x_i = (\mathbf{q}_{i0}, \boldsymbol{\omega}_i) \in X$. Since each physical attitude $R \in SO(3)$ is represented by a pair of antipodal unit quaternions $\pm \mathbf{q} \in \mathbb{S}^3$, the objective of the control, for each agent, becomes to stabilize the set

$$A_i = \{(\mathbf{1}, \mathbf{0}), (-\mathbf{1}, \mathbf{0})\} \subset X$$

¹The author informs that applying the hysteretic controller suggested by [10], instead of the bimodal controller proposed in Chapter 5, leads to better results due to restrictions arisen when using the Lyapunov function (6.20).

for the following agent equation

$$\dot{x}_i = \begin{bmatrix} \dot{\mathbf{q}}_{i0} \\ \dot{\boldsymbol{\omega}}_i \end{bmatrix} = F_i(x_i, \boldsymbol{\tau}_i) \triangleq \begin{bmatrix} \frac{1}{2} \mathbf{q}_{i0} \circ (0, \boldsymbol{\omega}_i) \\ J_i^{-1}(S(J_i \boldsymbol{\omega}_i) \boldsymbol{\omega}_i + \boldsymbol{\tau}_i) \end{bmatrix}, \quad (6.5)$$

by means of an appropriate choice of a feedback torque law $\boldsymbol{\tau}_i$. The output of the agent i is assumed to be

$$y_i = (\mathbf{q}_i, \boldsymbol{\omega}_i), \quad (6.6)$$

that is, \mathbf{q}_i and $\boldsymbol{\omega}_i$ are supposed to be measured. The output together with the desired fixed reference, \mathbf{q}_0 and the states $x_j = (\mathbf{q}_{j0}, \boldsymbol{\omega}_j)$ of its neighbors are assumed to be available for feedback.

6.1.2 Graph theory

The interaction topology among agents is usually modeled by a graph $\mathcal{G} = (\mathcal{V}, \mathcal{E}, G)$ where $\mathcal{V} = \{1, 2, \dots, n\}$ is the set of agents, $\mathcal{E} \subseteq \mathcal{V} \times \mathcal{V}$ is the set of directed edges and $G = [g_{ij}] \in \mathbb{R}^{n \times n}$ is the adjacency matrix. The adjacency element is defined as $g_{ii} = 0$ and for $i \neq j$, $g_{ij} = 1$ if $(i, j) \in \mathcal{E}$ and 0 otherwise. A directed edge from agent i to agent j , (i, j) , represents a unidirectional information exchange link from agent i to agent j , that is, agent j can receive or obtain information from agent i . An undirected graph is a graph where $(i, j) \in \mathcal{E} \Leftrightarrow (j, i) \in \mathcal{E}$, i.e., its adjacency matrix is symmetric. A path is a sequence of distinct agents (i_1, i_2, \dots, i_n) such that consecutive agents $(i_j, i_{j+1}) \in \mathcal{E}$. An undirected graph is connected if there is a path between every pair of distinct agents. Agent i communicates with agent j if j is a neighbor of i . The set of neighbors of agent i is denoted by $\mathcal{N}_i = \{j \in \mathcal{V} : (i, j) \in \mathcal{E}\}$ and $|\mathcal{N}_i|$ denotes the number of neighbors or the degree of agent i . Further details about Graph Theory can be found in [63]. In this study, it is assumed that if information flows between agents in one direction it also occurs in the opposite direction and the interaction topology is modeled by an undirected connected graph.

6.1.3 Multiple agents attitude coordination control

An example of continuous distributed control law for attitude synchronization of multiple agents is the one suggested by Ren [17], which brings the angular velocity to zero under an undirected communication graph. Ren's study assumed that the information available for each body i is \mathbf{q}_0 , $(\mathbf{q}_i, \boldsymbol{\omega}_i)$ and $(\mathbf{q}_j, \boldsymbol{\omega}_j)$, where $j \in \mathcal{N}_i$.

The strategy consists of applying the following torque feedback $\boldsymbol{\tau}_i$ to the i th agent.

$$\boldsymbol{\tau}_i = -k_G \boldsymbol{\epsilon}_{i0} - D_{Gi} \boldsymbol{\omega}_i - \sum_{j=1}^n g_{ij} [a_{ij} \boldsymbol{\epsilon}_{ij} + b_{ij} (\boldsymbol{\omega}_i - \boldsymbol{\omega}_j)], \quad (6.7)$$

where $k_G > 0$, $D_{Gi} = D_{Gi}^T > 0$, $a_{ij} = a_{ji} > 0$ and $b_{ij} = b_{ji} > 0$. Parameters k_G , D_{Gi} , a_{ij} and b_{ij} are the control gains.

Theorem 3.1 of [17] states that if the undirected graph \mathcal{G} is connected and if $k_G > \sum_{i=1}^n g_{ij} a_{ij}$, then $\mathbf{q}_i \rightarrow \mathbf{q}_j \rightarrow \mathbf{q}_0$ and $\boldsymbol{\omega}_i \rightarrow \boldsymbol{\omega}_j \rightarrow \mathbf{0}$ asymptotically, $\forall i \neq j$. The proof used the following Lyapunov function

$$V = k_G \sum_{i=1}^n \|\mathbf{q}_{i0} - \mathbf{1}\|^2 + \frac{1}{2} \sum_{i=1}^n \sum_{j=1}^n g_{ij} a_{ij} \|\mathbf{q}_{ij} - \mathbf{1}\|^2 + \frac{1}{2} \sum_{i=1}^n \boldsymbol{\omega}_i^T J_i \boldsymbol{\omega}_i. \quad (6.8)$$

Unfortunately the author did not draw attention to the fact that there are two equilibrium points: $(1, \mathbf{0})$ which is stable and $(-1, \mathbf{0})$ which is unstable. The fact that the feedback law (6.7) is continuous leads to the undesirable phenomenon known as *unwinding*, where the agent may start at rest arbitrarily close to the desired final attitude and yet rotate through large angles before coming to rest [5]. So, if, for some reason, the attitude

error of agent i is close to -1 , then the *unwinding* phenomenon may occur. Moreover, if the other agents are close to the reference, agent i may spend too much time to move away from the unstable equilibrium point region since the feedback torque of agent i depends on ϵ_{i0} and ϵ_{ij} which are close to $\mathbf{0}$. The problem gets worse if measurement noise is taken into account. In this case, the state of agent i may remain near the unstable equilibrium point for an indefinite period of time. This case is exemplified in Section 6.4.

In the next section, it is proposed a modification in the feedback law (6.7) to accommodate the hysteretic hybrid controller suggested by [10] in the multiple agents scenario. This way, both equilibrium points, $\mathbf{q}_{i0} = \mathbf{1}$ and $\mathbf{q}_{i0} = -\mathbf{1}$, for each agent i , become stable and the control becomes global and robust.

6.2 PROPOSED HYBRID ATTITUDE CONTROLLER

This study proposes a global and robust distributed control law for attitude synchronization of multiple agents. The strategy uses the hysteretic hybrid controller suggested by [10] with one state logic variable $h_i \in X_c = \{1, -1\}$ and vector of inputs $U_i = (\boldsymbol{\tau}_i, u_i)$ for each agent i .

The state of the subsystem plant + controller of agent i is represented by $\bar{x}_i = (\mathbf{q}_{i0}, \boldsymbol{\omega}_i, h_i) \in \bar{X} \triangleq \mathbb{S}^3 \times \mathbb{R}^3 \times X_c$, $i = 1, 2, \dots, n$. Each subsystem evolves according to (6.5), (6.6), the following dynamics of the controller²

$$\begin{aligned} \dot{h}_i &= 0 & \bar{x} \in C_i &\triangleq \{\bar{x} \in \bar{X}^n : h_i \eta_{i0} \geq -\delta_i\}, \\ h_i^+ &\in \overline{\text{sgn}}(u_i) & \bar{x} \in D_i &\triangleq \{\bar{x} \in \bar{X}^n : h_i \eta_{i0} \leq -\delta_i\}, \end{aligned} \quad (6.9)$$

where h_i^+ is the value associated to h_i just after state transition,

$$\overline{\text{sgn}}(u_i) = \begin{cases} \{1\}, & u_i > 0, \\ \{-1\}, & u_i < 0, \\ \{-1, 1\}, & u_i = 0 \end{cases}$$

and the closed-loop law

$$U_i = \mathcal{K}(y_i, \mathbf{q}_0, h_i, \mathbf{q}_j, \boldsymbol{\omega}_j) \triangleq (\boldsymbol{\tau}_i, \eta_{i0}), \quad j \in \mathcal{N}_i. \quad (6.10)$$

The parameter $\delta_i \in (0, 1)$ represents the hysteresis half-width and provides robustness against chattering caused by output measurement.

The feedback torque $\boldsymbol{\tau}_i$ is given by

$$\boldsymbol{\tau}_i = -k_{G_i} h_i \boldsymbol{\epsilon}_{i0} - D_{G_i} \boldsymbol{\omega}_i - \sum_{j=1}^n g_{ij} [a_{ij} h_i h_j \boldsymbol{\epsilon}_{ij} + b_{ij} (\boldsymbol{\omega}_i - R_{ij}^T \boldsymbol{\omega}_j)], \quad (6.11)$$

where the control gains $k_{G_i} > 0$, $D_{G_i} = D_{G_i}^T > 0$, $a_{ij} = a_{ji} > 0$ and $b_{ij} = b_{ji} > 0$. Note that, differently from (6.7), R_{ij}^T multiplies $\boldsymbol{\omega}_j$ in the torque equation because the coordinates of $\boldsymbol{\omega}_j$ refers to the agent- j frame.

Figure 6.1 shows the behavior of the subsystem for a hysteresis width of $2\delta_i$. The state variable h_i determines the torque feedback so the agent attitude \mathbf{q}_{i0} is regulated either to $\mathbf{1}$ or $-\mathbf{1}$.

Let the state of the whole system be represented by $\bar{x} = (\bar{x}_1, \bar{x}_2, \dots, \bar{x}_n) \in \bar{X}^n$. It will be shown in the next section that the controller globally asymptotically stabilizes the set

$$\bar{A} = \bigcap_{i=1}^n \bar{A}_i \quad \bar{A}_i \triangleq \{\bar{x} \in \bar{X}^n : \bar{x}_i = (\mathbf{1}, \mathbf{0}, 1) \text{ or } \bar{x}_i = (-\mathbf{1}, \mathbf{0}, -1)\}. \quad (6.12)$$

²Along the text, the dynamics representations follow the hybrid systems framework of Goebel et al. [48], summarized in Section 2.7.

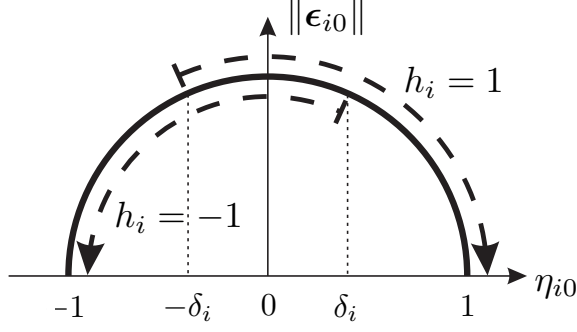


Figure 6.1: Agent i state space representation and the proposed regulation. The hysteresis half-width of the on-off control for state h_i is δ_i .

6.3 STABILITY ANALYSIS

Considering the proposed controller (6.9) the agent- i subsystem can be written in closed-loop form, denoted by $\overline{\mathcal{H}}_i$, as

$$\overline{\mathcal{H}}_i \begin{cases} \dot{\bar{x}}_i = \overline{F}_i(\bar{x}_i), & \bar{x}_i \in C_i, \\ \bar{x}_i^+ \in \overline{G}_i(\bar{x}_i), & \bar{x}_i \in D_i, \end{cases} \quad (6.13)$$

$$\overline{F}_i(\bar{x}_i) = \begin{bmatrix} \frac{1}{2} \mathbf{q}_{i0} \circ (0, \boldsymbol{\omega}_i) \\ J_i^{-1} (S(J_i \boldsymbol{\omega}_i) \boldsymbol{\omega}_i + \boldsymbol{\tau}_i) \\ 0 \end{bmatrix}, \quad (6.14)$$

$$\overline{G}_i(\bar{x}_i) = \begin{bmatrix} \mathbf{q}_{i0} \\ \boldsymbol{\omega}_i \\ \overline{\text{sgn}}(\eta_{i0}) \end{bmatrix}. \quad (6.15)$$

Before describing the complete system, by grouping all the agents, its necessary to define the flow and jump sets as $C \triangleq \bigcap_{i=1}^n C_i$ and $D \triangleq \bigcup_{i=1}^n D_i$, respectively. Note that more than one jump can occur simultaneously and the jump map is not straightforward. Let the set of agents whose state of h_i is about to change be defined as

$$\mathcal{T}(\bar{x}) \triangleq \{i \in \mathcal{V} : \bar{x}_i \in D_i\} \quad (6.16)$$

and $\overline{G}_0(\bar{x}_i) = [\mathbf{q}_{i0}^T \quad \boldsymbol{\omega}_i^T \quad h_i]^T$ represent a mapping that keeps the state variables of agent i unchanged. Motivated by the mapping suggested in [21], the jump map of \bar{x} is defined as

$$\Gamma(\bar{x}) = \bigcup_{i \in \mathcal{T}} \{\gamma_i(\bar{x})\}, \quad (6.17)$$

where $\gamma_i(\bar{x}) = [\gamma_{i1}^T \quad \dots \quad \gamma_{in}^T]^T$, $\gamma_{ij} = \overline{G}_0(\bar{x}_j)$, $j \neq i$ and $\gamma_{ii} = \overline{G}_i(\bar{x}_i)$.

The complete system, denoted as $\overline{\mathcal{H}}$, is given by

$$\overline{\mathcal{H}} : \begin{cases} \dot{\bar{x}} = \overline{F}(\bar{x}), & \bar{x} \in C, \\ \bar{x}^+ \in \overline{G}(\bar{x}), & \bar{x} \in D, \end{cases} \quad (6.18)$$

where $\overline{F}(\bar{x}) \triangleq [\overline{F}_1^T(\bar{x}_1) \quad \dots \quad \overline{F}_n^T(\bar{x}_n)]^T$ and $\overline{G}(\bar{x}) \triangleq \Gamma(\bar{x})$.

Theorem 6.1

Let $\alpha < 0.5$ be the maximum measurement noise magnitude. If the graph \mathcal{G} is connected, $k_{G_i} > 2 \sum_{j=1}^n g_{ij} a_{ij}$ and $\delta_i \in (\delta_i^*, 1)$,

$$\delta_i^* = \max \left\{ 2\alpha, \frac{\sum_{j=1}^n g_{ij} a_{ij}}{k_{G_i}} \right\}, \quad (6.19)$$

then the compact set \bar{A} defined in (6.12) is globally asymptotically stable for the closed-loop hybrid system $\bar{\mathcal{H}}$ and the control is robust to measurement noise.

Proof. Let $V : \bar{X}^n \rightarrow \mathbb{R}$,

$$V(\bar{x}) = \sum_{i=1}^n 2k_{G_i}(1 - h_i \eta_{i0}) + \sum_{i=1}^n \sum_{j=1}^n g_{ij} a_{ij} (1 - h_i h_j \eta_{ij}) + \frac{1}{2} \sum_{i=1}^n \omega_i^T J_i \omega_i. \quad (6.20)$$

Note that (6.8) is a special case of (6.20) when $k_{G_i} = k_G$ and $h_i = 1, i = 1, \dots, n$.

Function V is positive definite on \bar{X}^n with respect to \bar{A} , since $V(\bar{X}^n) \geq 0$ for $\bar{x} \in \bar{X}^n$ and $V(\bar{x}) = 0 \Leftrightarrow \bar{x} \in \bar{A}$ (Lemma B.10).

Along flows, $\bar{x} \in C$, the time derivative of function V is given by

$$\dot{V}(\bar{x}) = -2 \sum_{i=1}^n k_{G_i} h_i \dot{\eta}_{i0} - \sum_{i=1}^n \sum_{j=1}^n g_{ij} a_{ij} h_i h_j \dot{\eta}_{ij} + \sum_{i=1}^n \omega_i^T J_i \dot{\omega}_i \quad (6.21)$$

$$= \sum_{i=1}^n k_{G_i} h_i \omega_i^T \epsilon_{i0} + \frac{1}{2} \sum_{i=1}^n \sum_{j=1}^n g_{ij} a_{ij} h_i h_j (\omega_{ij}^T \epsilon_{ij}) + \sum_{i=1}^n \omega_i^T (S(J_i \omega_i) \omega_i + \tau_i), \quad (6.22)$$

$$= \sum_{i=1}^n k_{G_i} h_i \omega_i^T \epsilon_{i0} + \frac{1}{2} \sum_{i=1}^n \sum_{j=1}^n g_{ij} a_{ij} h_i h_j (\omega_i^T - \omega_j^T R_{ij}) \epsilon_{ij} + \sum_{i=1}^n \omega_i^T \tau_i. \quad (6.23)$$

In (6.22), it was used the fact that $\dot{\eta}_{ij} = -\frac{1}{2} \epsilon_{ij}^T \omega_{ij}$ and (6.14). In (6.23), it was applied (6.4) and that $\omega_i^T S(J_i \omega_i) \omega_i = 0$ since the matrix $S(J_i \omega_i)$ is skew-symmetric.

As $R_{ij} \epsilon_{ij} = \epsilon_{ij}$ (Lemma B.9), the second summation simplifies to

$$\frac{1}{2} \sum_{i=1}^n \sum_{j=1}^n g_{ij} a_{ij} h_i h_j (\omega_i^T - \omega_j^T R_{ij}) \epsilon_{ij} = \frac{1}{2} \sum_{i=1}^n \sum_{j=1}^n g_{ij} a_{ij} h_i h_j (\omega_i^T - \omega_j^T) \epsilon_{ij}. \quad (6.24)$$

Developing (6.24) as in [17, Theorem 3.1],

$$\frac{1}{2} \sum_{i=1}^n \sum_{j=1}^n g_{ij} a_{ij} h_i h_j (\omega_i^T - \omega_j^T) \epsilon_{ij} = \frac{1}{2} \sum_{i=1}^n \sum_{j=1}^n g_{ij} a_{ij} h_i h_j \omega_i^T \epsilon_{ij} - \frac{1}{2} \sum_{j=1}^n \sum_{i=1}^n g_{ji} a_{ji} h_j h_i \omega_i^T \epsilon_{ji}, \quad (6.25)$$

$$= \frac{1}{2} \sum_{i=1}^n \omega_i^T \sum_{j=1}^n g_{ij} a_{ij} h_i h_j \epsilon_{ij} + \frac{1}{2} \sum_{i=1}^n \omega_i^T \sum_{j=1}^n g_{ij} a_{ij} h_i h_j \epsilon_{ij}, \quad (6.26)$$

$$= \sum_{i=1}^n \omega_i^T \sum_{j=1}^n g_{ij} a_{ij} h_i h_j \epsilon_{ij}. \quad (6.27)$$

In (6.26), equalities $g_{ji} = g_{ij}$ and $a_{ji} = a_{ij}$ were used and that $\epsilon_{ji} = -\epsilon_{ij}$ (from $\mathbf{q}_{ji} = \mathbf{q}_{ij}^{-1} = \mathbf{q}_{ij}^*$).

Substituting (6.27) in (6.23),

$$\dot{V}(\bar{x}) = \sum_{i=1}^n \omega_i^T \left(k_{G_i} h_i \epsilon_{i0} + \sum_{j=1}^n g_{ij} a_{ij} h_i h_j \epsilon_{ij} + \tau_i \right) \quad (6.28)$$

and, finally, using the torque definition τ_i (6.11) in (6.28),

$$\dot{V}(\bar{x}) = - \sum_{i=1}^n \omega_i^T D_{G_i} \omega_i - \sum_{i=1}^n \sum_{j=1}^n g_{ij} b_{ij} \omega_i^T (\omega_i - R_{ij}^T \omega_j). \quad (6.29)$$

Developing the last term of (6.29),

$$\sum_{i=1}^n \sum_{j=1}^n g_{ij} b_{ij} \omega_i^T (\omega_i - R_{ij}^T \omega_j) = \frac{1}{2} \sum_{i=1}^n \sum_{j=1}^n g_{ij} b_{ij} \omega_i^T (\omega_i - R_{ij}^T \omega_j) + \frac{1}{2} \sum_{i=1}^n \sum_{j=1}^n g_{ij} b_{ij} \omega_i^T (\omega_i - R_{ij}^T \omega_j), \quad (6.30)$$

$$= \frac{1}{2} \sum_{i=1}^n \sum_{j=1}^n g_{ij} b_{ij} \omega_i^T (\omega_i - R_{ij}^T \omega_j) + \frac{1}{2} \sum_{i=1}^n \sum_{j=1}^n g_{ji} b_{ji} \omega_j^T (\omega_j - R_{ji}^T \omega_i), \quad (6.31)$$

$$= \frac{1}{2} \sum_{i=1}^n \sum_{j=1}^n g_{ij} b_{ij} [\omega_i^T (\omega_i - R_{ij}^T \omega_j) - \omega_j^T (R_{ij} \omega_i - \omega_j)], \quad (6.32)$$

$$= \frac{1}{2} \sum_{i=1}^n \sum_{j=1}^n g_{ij} b_{ij} [\omega_i^T (\omega_i - R_{ij}^T \omega_j) - \omega_j^T R_{ij} (\omega_i - R_{ij}^T \omega_j)], \quad (6.33)$$

$$= \frac{1}{2} \sum_{i=1}^n \sum_{j=1}^n g_{ij} b_{ij} [(\omega_i^T - \omega_j^T R_{ij}) (\omega_i - R_{ij}^T \omega_j)], \quad (6.34)$$

$$= \frac{1}{2} \sum_{i=1}^n \sum_{j=1}^n g_{ij} b_{ij} \|\omega_i - R_{ij}^T \omega_j\|^2. \quad (6.35)$$

In (6.32), equalities $g_{ji} = g_{ij}$, $b_{ji} = b_{ij}$ and $R_{ji}^T = R_{ij}$ were used. Now, substituting (6.35) into (6.29),

$$\dot{V}(\bar{x}) = - \sum_{i=1}^n \omega_i^T D_{G_i} \omega_i - \frac{1}{2} \sum_{i=1}^n \sum_{j=1}^n g_{ij} b_{ij} \|\omega_i - R_{ij}^T \omega_j\|^2. \quad (6.36)$$

Note that function \dot{V} is negative semidefinite on \bar{X}^n with respect to \bar{A} , since $\dot{V}(\bar{x}) \leq 0$ for all $\bar{x} \in \bar{X}^n$ and $\dot{V}(\bar{x}) = 0 \Leftrightarrow \omega_i = \mathbf{0}, i = 1, \dots, n$.

Along jumps, $\bar{x} \in D$,

$$\Delta V(\bar{x}) = V(\bar{x}^+) - V(\bar{x}), \quad (6.37)$$

where $\bar{x}^+ = (\bar{x}_1^+, \bar{x}_2^+, \dots, \bar{x}_n^+) \in \bar{X}^n$.

From (6.15), $\mathbf{q}_{i0}^+ = \mathbf{q}_{i0}$, $\omega_i^+ = \omega_i$ and $h_i^+ = -h_i$. It follows that

$$\Delta V(\bar{x}) = - \sum_{i=1}^n 2k_{G_i} (h_i^+ - h_i) \eta_{i0} - \sum_{i=1}^n \sum_{j=1}^n g_{ij} a_{ij} (h_i^+ h_j^+ - h_i h_j) \eta_{ij}. \quad (6.38)$$

In the first summation in (6.38), $h_i^+ \neq h_i$ whenever $\bar{x}_i \in D_i$, i.e., when $i \in \mathcal{T}$ (6.16). Regarding the second summation, $h_i^+ h_j^+ \neq h_i h_j$ when $i \in \mathcal{T}$ and $j \notin \mathcal{T}$ and vice-versa. Therefore,

$$\begin{aligned} \Delta V(\bar{x}) &= - \sum_{i \in \mathcal{T}} 2k_{G_i} (h_i^+ - h_i) \eta_{i0} - \sum_{i \in \mathcal{T}} \sum_{j \notin \mathcal{T}} g_{ij} a_{ij} (h_i^+ h_j^+ - h_i h_j) \eta_{ij} - \\ &\quad \sum_{i \notin \mathcal{T}} \sum_{j \in \mathcal{T}} g_{ij} a_{ij} (h_i^+ h_j^+ - h_i h_j) \eta_{ij} \\ &= 4 \sum_{i \in \mathcal{T}} k_{G_i} h_i \eta_{i0} + 2 \sum_{i \in \mathcal{T}} \sum_{j \notin \mathcal{T}} g_{ij} a_{ij} h_i h_j \eta_{ij} + 2 \sum_{i \notin \mathcal{T}} \sum_{j \in \mathcal{T}} g_{ij} a_{ij} h_i h_j \eta_{ij} \end{aligned} \quad (6.39)$$

As $a_{ij} = a_{ji}$, $g_{ij} = g_{ji}$ and $\eta_{ij} = \eta_{ji}$,

$$\sum_{i \in \mathcal{T}} \sum_{j \notin \mathcal{T}} g_{ij} a_{ij} h_i h_j \eta_{ij} = \sum_{j \notin \mathcal{T}} \sum_{i \in \mathcal{T}} g_{ji} a_{ji} h_j h_i \eta_{ji} = \sum_{i \notin \mathcal{T}} \sum_{j \in \mathcal{T}} g_{ij} a_{ij} h_i h_j \eta_{ij}. \quad (6.40)$$

Hence,

$$\Delta V(\bar{x}) = 4 \sum_{i \in \mathcal{T}} \left(k_{Gi} h_i \eta_{i0} + \sum_{j \notin \mathcal{T}} g_{ij} a_{ij} h_i h_j \eta_{ij} \right). \quad (6.41)$$

Since $\bar{x} \in D$, according to (6.9) $h_i \eta_{i0} \leq -\delta_i$ and given that $h_i h_j \eta_{ij} \leq 1$,

$$\Delta V(\bar{x}) \leq 4 \sum_{i \in \mathcal{T}} \left(-k_{Gi} \delta_i + \sum_{j \in \mathcal{N}_i \setminus \mathcal{T}} g_{ij} a_{ij} \right). \quad (6.42)$$

Suppose that the following restriction is considered,

$$\delta_i > \frac{\sum_{j \in \mathcal{N}_i} g_{ij} a_{ij}}{k_{Gi}} = \frac{\sum_{j=1}^n g_{ij} a_{ij}}{k_{Gi}}, \quad (6.43)$$

so that $\Delta V(\bar{x}) < 0, \forall \bar{x} \in \bar{X}^n$. Thus, from Theorem 7.6 of [56], it follows that the compact set \bar{A} is stable since $\Delta V(\bar{x}) < 0$ and $\dot{V}(\bar{x}) \leq 0$ for all $\bar{x} \in \bar{X}^n$. The conclusion that the set \bar{A} is globally asymptotically stable comes when Theorem 4.7 of [56] is applied to prove that the set \bar{A} is the largest invariant set in

$$W = \{\bar{x} \in C : \dot{V}(\bar{x}) = 0\}. \quad (6.44)$$

In the largest invariant set, $\dot{V} \equiv 0$. From (6.36), $\omega_i \equiv \mathbf{0}, i = 1, \dots, n$. Using (6.14) and then (6.11), it follows that $\tau_i \equiv \mathbf{0}$ and

$$k_{Gi} \epsilon_{i0} + \sum_{j=1}^n g_{ij} a_{ij} \epsilon_{ij} = \mathbf{0}. \quad (6.45)$$

Left multiplying both members in (6.45) by ϵ_{i0}^T and using the fact that $\epsilon_{ij} = \eta_{j0} \epsilon_{i0} - \eta_{i0} \epsilon_{j0} - \epsilon_{j0} \times \epsilon_{i0}$,

$$k_{Gi} \epsilon_{i0}^T \epsilon_{i0} + \sum_{j=1}^n g_{ij} a_{ij} \epsilon_{i0}^T (\eta_{j0} \epsilon_{i0} - \eta_{i0} \epsilon_{j0} - \epsilon_{j0} \times \epsilon_{i0}) = 0, \quad (6.46)$$

$$\epsilon_{i0}^T \left(k_{Gi} + \sum_{j=1}^n \eta_{j0} g_{ij} a_{ij} \right) \epsilon_{i0} - \epsilon_{i0}^T \left(\sum_{j=1}^n \eta_{i0} g_{ij} a_{ij} \right) \epsilon_{j0} = 0. \quad (6.47)$$

Since (6.47) is valid for all $i, i = 1, \dots, n$, the following equation holds.

$$\hat{q}_s^T (P \otimes I_3) \hat{q}_s = 0, \quad (6.48)$$

where \otimes is the Kronecker product, $\hat{q}_s = [\epsilon_{10}^T \quad \epsilon_{20}^T \quad \dots \quad \epsilon_{n0}^T]^T, P = [p_{ij}] \in \mathbb{R}^{n \times n}, p_{ii} = k_{Gi} + \sum_{j=1}^n \eta_{j0} g_{ij} a_{ij}$ and $p_{ij} = -\eta_{i0} g_{ij} a_{ij}$.

Applying Gerschgorin Theorem [64] and supposing that

$$k_{Gi} > 2 \sum_{j=1}^n g_{ij} a_{ij}, \quad (6.49)$$

matrix $P \otimes I_3$ gets strictly diagonally dominant and positive definite. Hence, $\hat{q}_s = \mathbf{0}$ is the only solution to (6.48). As a result, $\epsilon_{i0} = \mathbf{0}, i = 1, \dots, n$ and $\mathbf{q}_{i0} = \mathbf{1}$ or $\mathbf{q}_{i0} = -\mathbf{1}$ are candidates for the largest invariant set. Finally, using restriction $\bar{x} \in C$ from (6.44), it follows that $\mathbf{q}_{i0} = h_i \mathbf{1}$.

Summing up, any solution $\bar{x}(t)$ approaches the largest invariant set \bar{A} (6.12) as long as hypotheses (6.49) and (6.43) are satisfied. Regarding the robustness of the control, the proof is a direct application of Theorem 5.4 and 5.5 of [10] to the system $\bar{\mathcal{H}}$ where it is proved that the number of jumps is bounded and the chattering phenomenon is eliminated if $\alpha \in [0, 0.5)$ and $\delta_i \in (2\alpha, 1)$. Both restrictions on δ_i are satisfied if $\delta_i \in (\delta_i^*, 1)$, where

$$\delta_i^* = \max \left\{ 2\alpha, \frac{\sum_{j=1}^n g_{ij} a_{ij}}{k_{Gi}} \right\}.$$

□

The restriction $\delta_i < 1$ allows variable h_i to switch between 1 and -1 . If $\delta_i > 1$ and $h_i(0) = 1$ for all agents, the controller behaves as suggested by [17]. Note that if $a_{ij} \ll k_{Gi}$ and $b_{ij} \ll k_{Gi}$, the interactions among the agents become too weak according to the torque feedback expression (6.11). In the limit, when $a_{ij} = 0$ and $b_{ij} = 0$, subsystem $\bar{\mathcal{H}}_i$ gets independent from the other subsystems and behaves as a single agent using the controller suggested by [10].

Corollary 6.1

Let $\alpha < 0.25$ be the maximum measurement noise magnitude. Then if the graph \mathcal{G} is connected, $k_{Gi} > 2 \sum_{j=1}^n g_{ij} a_{ij}$ and $\delta_i \in [0.5, 1)$, the proposed controller (6.9) robustly globally asymptotically stabilize the set \bar{A} defined in (6.12).

Corollary 6.1 affirms that if $\alpha < 0.25$ and restriction (6.49) is satisfied, there exists δ_i and it is possible to make the system robustly globally asymptotically stable. This is an interesting conclusion since the stability does not depend on inertial matrices, initial attitudes and angular velocities, number of agents and so on. Note that when the dynamics of one subsystem depends on other subsystems dynamics, it is not obvious that the “potential” function of the system, V (6.20), decreases after every jump. Another important conclusion is that scalability is not a problem for the proposed controller. If the number of neighbors $|\mathcal{N}_i|$ is limited as well as parameters a_{ij} , then there is no need to increase k_{Gi} . Regarding the convergence time, it depends on parameters D_{Gi} and b_{ij} , according to (6.36). The only restrictions on these parameters are the physical bounds on the torque. Note also that the assumption that the graph \mathcal{G} should be connected is not necessary, however it is maintained so that in future works the reference attitude is made available to only a subset of agents as well as in the study of [18].

The next section contrasts performance of the continuous controller of literature, outlined in Subsection 6.1.3, and the proposed controller. Comparisons with the other hybrid controller of literature [21] was not possible as its goal is to stabilize a synchronized state and the goal of the proposed controller is to stabilize a reference attitude.

6.4 SIMULATION RESULTS

This section presents simulation results to compare performance of the proposed hysteretic hybrid controller (6.9)–(6.10)–(6.11) and the continuous controller suggested by [17] (6.7), hereafter referred as hybrid and continuous controllers, respectively. Two scenarios are considered, the first one illustrates some of the problems that may arise when the control strategy uses a continuous state feedback torque to stabilize disconnected reference points ($\mathbf{q}_{i0} = \pm 1$). The second one exemplifies a situation where the problems faced by the continuous controller in the previous scenario is not present to highlight the other advantages of the hybrid controller.

The topology of communication is shown in Figure 6.2. It is a simple cycle graph with nodes labeled from 1 to 6 referring to the agents.

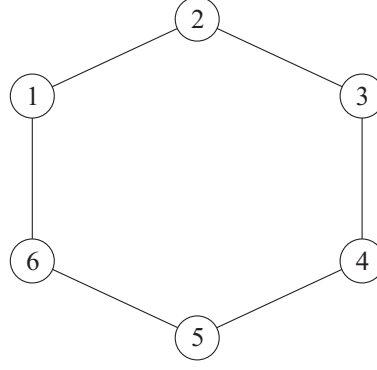


Figure 6.2: Topology of communication.

Table 6.1: Inertial matrices of the agents

J_1	[1 0.1 0.1; 0.1 0.1 0.1; 0.1 0.1 0.9] kg.m ²
J_2	[1.5 0.2 0.3; 0.2 0.9 0.4; 0.3 0.4 2.0] kg.m ²
J_3	[0.8 0.1 0.2; 0.1 0.7 0.3; 0.2 0.3 1.1] kg.m ²
J_4	[1.2 0.3 0.7; 0.3 0.9 0.2; 0.7 0.2 1.4] kg.m ²
J_5	[0.9 0.15 0.3; 0.15 1.2 0.4; 0.3 0.4 1.2] kg.m ²
J_6	[1.1 0.35 0.45; 0.35 1.0 0.5; 0.45 0.5 1.3] kg.m ²

The corresponding adjacency matrix is

$$G = \begin{bmatrix} 0 & 1 & 0 & 0 & 0 & 1 \\ 1 & 0 & 1 & 0 & 0 & 0 \\ 0 & 1 & 0 & 1 & 0 & 0 \\ 0 & 0 & 1 & 0 & 1 & 0 \\ 0 & 0 & 0 & 1 & 0 & 1 \\ 1 & 0 & 0 & 0 & 1 & 0 \end{bmatrix}. \quad (6.50)$$

In each simulation, the inertia matrices considered are shown in Table 6.1 (the same as in [17]) and the control parameters were $k_{Gi} = 1$, $D_{Gi} = I_3$, $a_{ij} = 0.24$ and $b_{ij} = 0.25$, $i = 1, \dots, 6$. The other parameters of the hybrid controller were chosen as $\delta_i = 0.5$ and $h_i(0) = 1$. The desired fixed reference was $\mathbf{q}_0 = (\sqrt{0.8475}, (-0.2, 0.15, -0.3))$ with $\boldsymbol{\omega}_0 = \mathbf{0}$.

The simulations were performed in MATLAB ambient, using ordinary differential equation solver with variable integration step (ode45) restricted to a maximum step of 1 ms.

The measured value of the attitude of each agent, $\mathbf{q}_{i_m} = (\eta_{i_m}, \boldsymbol{\epsilon}_{i_m})$, included noise and was calculated as follows: $\mathbf{q}_{i_m} = (\mathbf{q}_{i_m} + b\hat{\mathbf{e}}) / \|\mathbf{q}_{i_m} + b\hat{\mathbf{e}}\|_2$, $\hat{\mathbf{e}} = \mathbf{e} / \|\mathbf{e}\|$, where each element \mathbf{e} was chosen from a gaussian distribution of zero mean and unitary covariance matrix and b was chosen from a uniform distribution on the interval $[0, 0.2]$ (independently of \mathbf{e}).

The first scenario (Figure 6.3) compares the evolution of the attitude error scalar component (η_{i0}) of each agent i . The initial conditions are described in Table 6.2. To emphasize the problems arisen when an agent is near an unstable equilibrium point, agent 4 attitude was submitted to a specific measurement noise \mathbf{e}_4 , $\|\mathbf{e}_4\| < 0.2$, between 0.6 and 10 s. During this period of time, the measured value of its attitude was calculated as $\mathbf{q}_{4_m} = \mathbf{q}_4 + \mathbf{e}_4$, where \mathbf{e}_4 was such that the vector components of the measured attitude error, $\boldsymbol{\epsilon}_{40_m}$, had the opposite sign of the vector components of $\boldsymbol{\epsilon}_{40}$ when \mathbf{q}_{40} approached $-\mathbf{1}$. More precisely, \mathbf{e}_4 was calculated so

Table 6.2: Initial condition of the agents for the first scenario

i	$\mathbf{q}_i(0)$	$\boldsymbol{\omega}_i(0)$
1	$(\sin(-\pi/6), (\cos(-\pi/6), 0, 0))$	$(0, 0, 0)$
2	$(\sin(\pi/6), (0, 0, \cos(\pi/6)))$	$(0, 0, 0)$
3	$(\cos(\pi/6), (0, \sin(\pi/6), 0))$	$(0, 0, -\cos(\pi/6))$
4	$(-0.7181, (0.4943, -0.1144, 0.4763))$	$(0.7, 0.1\sqrt{2}, 0.7)$
5	$(\sin(\pi/4), (0, \cos(\pi/4), 0))$	$(0, -\cos(\pi/4), 0)$
6	$(\cos(\pi/4), (\sin(\pi/4), 0, 0))$	$(1, 0, 0)$

Table 6.3: Initial condition of the agents for the second scenario

i	$\mathbf{q}_i(0)$	$\boldsymbol{\omega}_i(0)$
1	$(\sin(-\pi/6), (\cos(-\pi/6), 0, 0))$	$(0, 0, 0)$
2	$(\cos(\pi/6), (0, \sin(\pi/6), 0))$	$(0, 0, 0)$
3	$(-\sin(\pi/4), (0, 0, -\cos(\pi/4)))$	$(0, 0, -\cos(\pi/6))$
4	$(\cos(\pi/4), (\sin(\pi/4), 0, 0))$	$(0.35, 0.05\sqrt{2}, 0.35)$
5	$(\sin(\pi/4), (0, \cos(\pi/4), 0))$	$(0, \cos(\pi/4), 0)$
6	$(\sin(-\pi/4), (0, 0, \cos(-\pi/4)))$	$(1, 0, 0)$

that $\epsilon_{40_m} = (1 - 0.199/\|\epsilon_{40}\|)\epsilon_{40}$. This example demonstrates that the continuous controller is not robust to arbitrary noise of small magnitude. After reaching an attitude near the unstable point, the resulting torque of agent 4 pulled its attitude toward the unstable point. Besides, after noise e_4 vanishes, it lasted too much time to move away from the unstable point region and come to rest at the stable point (*unwinding* phenomenon). On the other hand, the hybrid controller changed h_1 and h_4 to -1 from the beginning and determined the movement of the respective agents toward the shorter rotation direction.

The second scenario compares the attitude error of all the agents (Figure 6.4) and their respective angular velocities (Figure 6.5). The initial conditions are described in Table 6.3. The agents reached the reference faster when the hybrid controller was used since the control law pulls agents 1, 3 and 6 toward the shorter rotation direction. State of variables h_1 and h_6 was changed to -1 at the beginning. Agent 3 controller, however, kept h_3 unchanged at 1 for approximately 0.35 s and started moving toward $\eta_{30} = -1$ due to its initial angular velocity. As soon as η_{30_m} crossed over the hysteresis threshold ($\eta_{30_m} < -0.5$), h_3 was changed to -1 and the control law pulled its attitude error toward -1 . The change in h_3 is more noticeable in the ω_{3_z} graph.

6.5 CHAPTER CONCLUSIONS

In this chapter, it was proposed a hybrid distributed attitude synchronization control with globally asymptotically stability property and robustness against noise measurement for an undirected connected network (cyclic or acyclic) of agents. Application of a hybrid controller solution is much challenging due to the inherent inter-agent interactions. The strategy counted on the hysteretic hybrid controller suggested by Mayhew et al. [10] and the robust global stability was obtained at the cost of having one more restriction on the hysteresis half-width parameter δ_i .

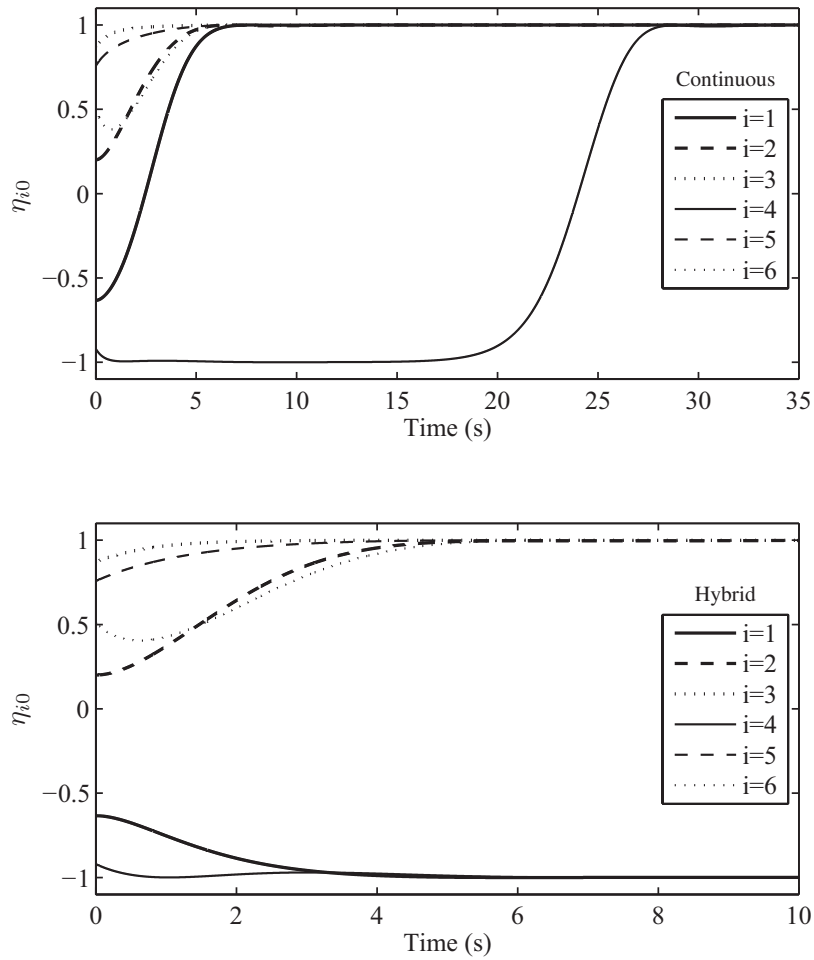


Figure 6.3: Evolution of the first component of the attitude of the agents in the first scenario. In the upper graphic (continuous controller), a specific noise of magnitude lower than 0.2 was applied to agent 4 between 0.6 and 10 s. The lower graphic refers to the hybrid controller.

Results from simulation contrast the continuous controller and the hybrid controller and show that the longer rotation direction is avoided in the hybrid scheme when the initial state is near an equilibrium point, decreasing the settling time. Results also emphasize some problems arisen when a continuous state-feedback law is applied such as the unwinding phenomenon and the lagged response when the state of an agent is near an unstable point of equilibrium.

An article about the study of this chapter has been submitted to the International Journal of Systems Science.

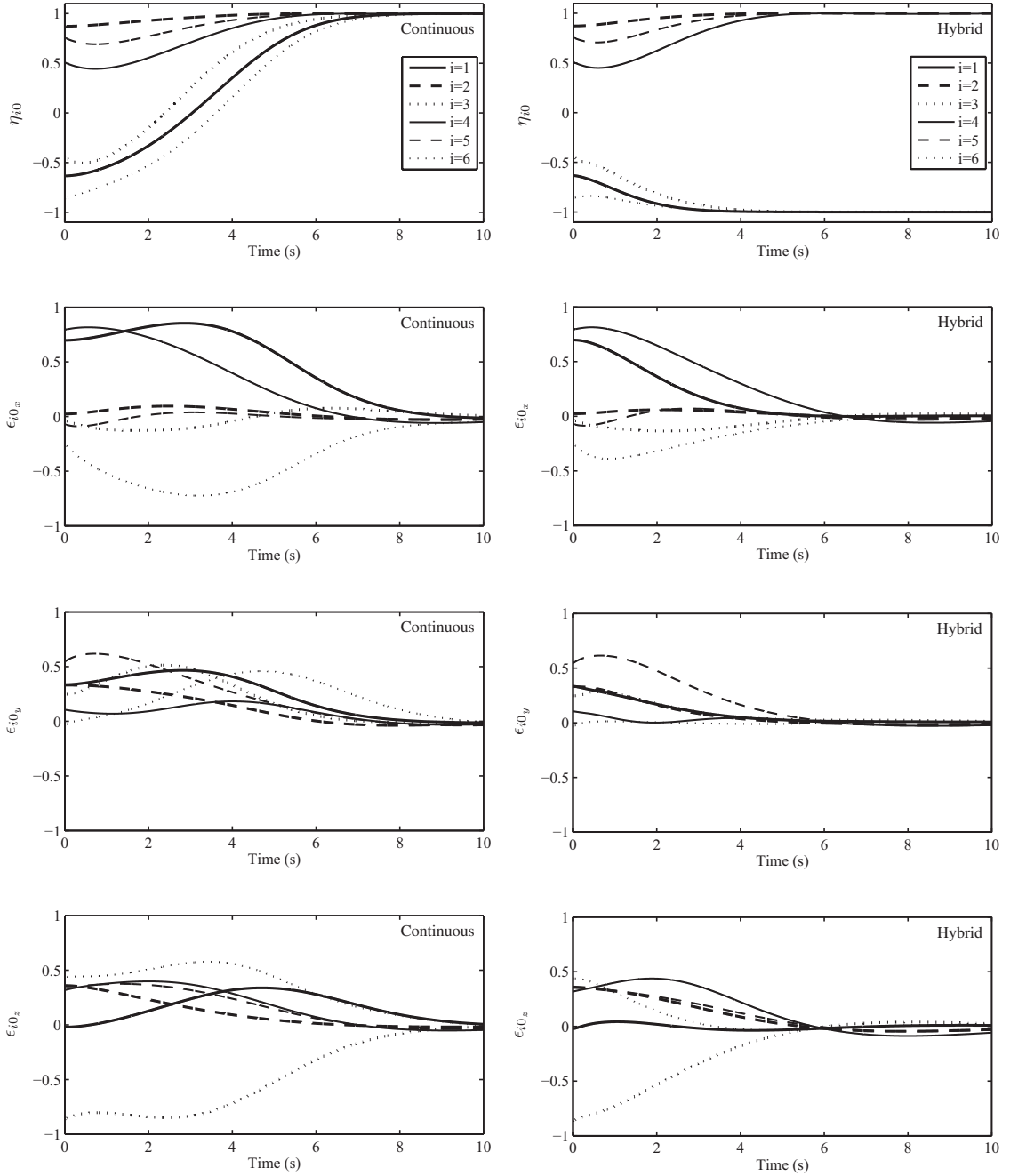


Figure 6.4: Evolution of the attitude $\mathbf{q}_{i0} = (\eta_{i0}, \boldsymbol{\epsilon}_{i0})$ of the agents in the second scenario, where $\boldsymbol{\epsilon}_{i0} = (\epsilon_{i0x}, \epsilon_{i0y}, \epsilon_{i0z})$. The graphics on the left refers to the continuous controller and the others on the right to the hybrid one.

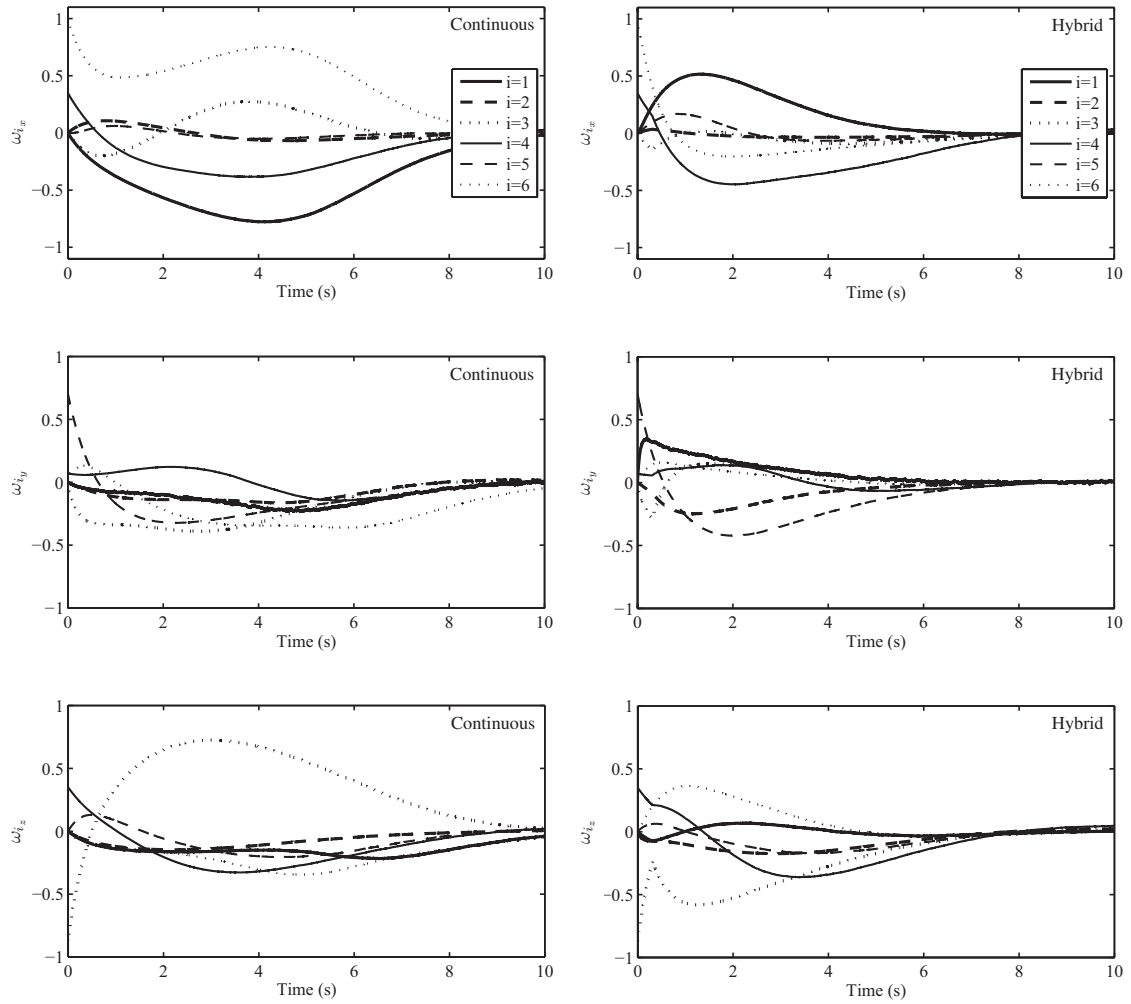


Figure 6.5: Evolution of the angular velocity $\omega_i = (\omega_{i_x}, \omega_{i_y}, \omega_{i_z})$ of the agents in the second scenario. The graphics on the left refers to the continuous controller and the others on the right to the hybrid one.

In this manuscript, two hybrid controllers were proposed in order to improve the solution in terms of cost when compared with the fixed width hysteresis control of literature. Both of them are well suited for the rest-to-rest attitude control of a rigid body with globally asymptotically stability property.

The first proposed controller (HY) offers more opportunities of updating the main logic variable that indicates which quaternion representation of the reference attitude should be followed, when compared with the hysteretic hybrid controller, and is more likely to take the shorter rotation direction and spend less energy. However, it presents the disadvantage of having restrictions on flow and jumps priorities. As long as jumps do not have higher priority than flows, robustness against noise measurements is achieved despite the chattering that may occur in the auxiliary variable.

The second proposed controller, called bimodal, supersedes the HY controller for not having the mentioned drawback and can be seen as a middle term solution between the memoryless discontinuous and the hysteretic hybrid controller. Differently from the less costly discontinuous controller, the bimodal controller is robust in the sense of having capability of avoiding chattering due to measurement noise. Compared with the unimodal hysteretic hybrid controller, while both keep robustness and stability, the bimodal spends less energy in average. It was also shown that the bimodal philosophy can be extended for other controllers which have one hysteretic mode. The bimodal controller is expected to be the most interesting choice when the attitude noise level may be expressive as for example when low cost components are used or when the system is under an electromagnetically noisy environment.

Two other studies were added as an extension of the studies described above.

The first study refers to the attitude synchronization control for a network of rigid bodies (agents). It was proposed a hybrid distributed control with globally asymptotically stability property and robustness against noise measurement for an undirected connected network (cyclic or acyclic) of agents. Application of a hybrid controller solution is much challenging due to the inherent inter-agent interactions. The strategy counted on the hysteretic hybrid controller of literature and the robust global stability was obtained at the cost of having one more restriction on the hysteresis half-width parameter δ_i . Results from simulation show that the longer rotation direction is avoided when the initial state is near an equilibrium point, decreasing the settling time. It is also emphasized that the great majority of the studies suggest a continuous state-feedback law strategy which are prone to problems such as the unwinding phenomenon and the lagged response when the state of an agent is near an unstable point of equilibrium.

The second one refers to the kinematic control for rigid-body pose within the group of unit norm dual-quaternions. It is presented a novel control strategy for robust global rigid body kinematic stabilization. To address the topological obstruction to global stability inherent to any rigid body representation—which renders the unwinding phenomenon in the case of unit quaternions and unit dual quaternions—it is exploited an hybrid control technique based on hysteresis, called bimodal, which ensures solution without chattering, with the introduction of two binary logic state memory variable that reduces the liability of having the solution trajectory travel to the farther antipodal equilibrium.

8.1 FUTURE WORK

As an extension to the present work, the author suggests:

1. A global hybrid control strategy for rigid-body pose problem that is robust against measurement noise, using the kinematic and dynamic equations to describe the pose motion;
2. A distributed pose synchronization control of agents with globally asymptotically stability property and robustness against noise measurement;
3. A global hybrid control strategy for rigid-body attitude problem that is robust against measurement noise, using a control law based on the attitude and the angular velocity;
4. Adapt the multi-agent distributed attitude control of Chapter 6 to the consensus problem (i.e. attitude synchronization problem only, as in [21]);
5. Extend the rest-to-rest attitude and pose control problem to allow tracking;
6. Extend the multi-agent cooperative pose control problem to allow scenarios where the agents are coupled and subject to holonomic constraints.

Bibliography

- [1] N. Chaturvedi, A. Sanyal, and N. McClamroch, “Rigid-body attitude control,” *IEEE Control Syst.*, vol. 31, no. 3, pp. 30–51, 2011.
- [2] G. Singh, P. Kabamba, and N. McClamroch, “Planar, time-optimal, rest-to-rest slewing maneuvers of flexible spacecraft,” *J. Guid. Control Dynam.*, vol. 12, no. 1, pp. 71–81, 1989.
- [3] J. Stuelpnagel, “On the parametrization of the three-dimensional rotation group,” *SIAM Rev.*, vol. 6, no. 4, pp. 422–430, 1964.
- [4] M. Spong, S. Hutchinson, and M. Vidyasagar, *Robot Modeling and Control*. John Wiley & Sons, Inc., 2005.
- [5] S. P. Bhat and D. S. Bernstein, “A topological obstruction to continuous global stabilization of rotational motion and the unwinding phenomenon,” *Syst. Control Lett.*, vol. 39, no. 1, pp. 63–70, 2000.
- [6] O. Fjellstad and T. Fossen, “Quaternion feedback regulation of underwater vehicles,” in *Proc. 3rd IEEE Conf. Control Appl.*, vol. 2, Aug. 1994, pp. 857–862.
- [7] D. Fragopoulos and M. Innocenti, “Stability considerations in quaternion attitude control using discontinuous Lyapunov functions,” *Inst. Elect. Eng. Proc., Control Theory Appl.*, vol. 151, no. 3, pp. 253–258, May 2004.
- [8] B. Wie and P. M. Barba, “Quaternion feedback for spacecraft large angle maneuvers,” *Journal of Guidance, Control, and Dynamics*, vol. 8, no. 3, pp. 360–365, 1985.
- [9] R. Sanfelice, M. Messina, S. Emre Tuna, and A. Teel, “Robust hybrid controllers for continuous-time systems with applications to obstacle avoidance and regulation to disconnected set of points,” in *Amer. Control Conf.*, 2006, pp. 3352–3357.
- [10] C. Mayhew, R. Sanfelice, and A. Teel, “Quaternion-based hybrid control for robust global attitude tracking,” *IEEE Trans. Autom. Control*, vol. 56, no. 11, pp. 2555–2566, Nov. 2011.
- [11] J. L. Crassidis, F. L. Markley, and Y. Cheng, “Survey of nonlinear attitude estimation methods,” *J. Guid. Control Dynam.*, vol. 30, no. 1, pp. 12 – 28, 2007.
- [12] D. Gebre-Egziabher, G. H. Elkaim, J. D. Powell, and B. W. Parkinson, “A gyro-free quaternion-based attitude determination system suitable for implementation using low cost sensors,” in *Position Location and Navigation Symposium, IEEE 2000*, 2000, pp. 185–192.
- [13] A. Cavallo, A. Cirillo, P. Cirillo, G. D. Maria, P. Falco, C. Natale, and S. Pirozzi, “Experimental comparison of sensor fusion algorithms for attitude estimation,” *{IFAC} Proceedings Volumes*, vol. 47, no. 3, pp. 7585 – 7591, 2014, 19th {IFAC} World Congress.
- [14] A. Fu, E. Modiano, and J. Tsitsiklis, “Optimal energy allocation and admission control for communications satellites,” *IEEE/ACM Trans. Netw.*, vol. 11, no. 3, pp. 488–500, Jun. 2003.
- [15] R. Kristiansen, A. Loría, A. Chaillet, and P. J. Nicklasson, “Spacecraft relative rotation tracking without angular velocity measurements,” *Automatica*, vol. 45, no. 3, pp. 750 – 756, 2009.
- [16] Z. Meng, Z. You, G. Li, and C. Fan, “Cooperative attitude control of multiple rigid bodies with multiple time-varying delays and dynamically changing topologies,” *Mathematical Problems in Engineering*, pp. 853–858, 2010.

- [17] W. Ren, "Distributed attitude alignment in spacecraft formation flying," *International Journal of Adaptive Control and Signal Processing*, vol. 21, pp. 95–113, 2007.
- [18] A. M. Zou, "Distributed attitude synchronization and tracking control for multiple rigid bodies," *IEEE Transactions on Control Systems Technology*, vol. 22, no. 2, pp. 478–490, 2014.
- [19] A. M. Zou and K. D. Kumar, "Distributed attitude coordination control for spacecraft formation flying," *IEEE Transactions on Aerospace and Electronic Systems*, vol. 48, no. 2, pp. 1329–1346, APRIL 2012.
- [20] L. Ma, H. Min, S. Wang, Y. Liu, and S. Liao, "An overview of research in distributed attitude coordination control," *IEEE/CAA Journal of Automatica Sinica*, vol. 2, no. 2, pp. 121–133, April 2015.
- [21] C. G. Mayhew, R. G. Sanfelice, J. Sheng, M. Arcak, and A. R. Teel, "Quaternion-based hybrid feedback for robust global attitude synchronization," *IEEE Transactions on Automatic Control*, vol. 57, no. 8, pp. 2122–2127, Aug 2012.
- [22] H. Bai, M. Arcak, and J. T. Wen, "Rigid body attitude coordination without inertial frame information," *Automatica*, vol. 44, no. 12, pp. 3170 – 3175, 2008.
- [23] R. W. Brockett, "System theory on group manifolds and coset spaces," *SIAM J. Control*, vol. 10, no. 2, pp. 265–284, 1972.
- [24] F. Bullo and R. M. Murray, "Proportional derivative (PD) control on the Euclidean group," California Institute of Technology, Technical Report Caltech/CDS 95–010, May 1995.
- [25] F. Bullo, R. M. Murray, and A. Sarti, "Control on the sphere and reduced attitude stabilization," California Institute of Technology, Technical Report Caltech/CDS 95–005, Jan. 1995.
- [26] J. Funda, R. H. Taylor, and R. P. Paul, "On homogeneous transforms, quaternions, and computational efficiency," vol. 6, no. 3, pp. 382–388, 1990.
- [27] J. M. Selig, *Geometric Fundamentals of Robotics*, 2nd ed., ser. Monographs in Computer Science. Springer, 2007.
- [28] H. T. M. Kussaba, L. F. C. Figueredo, J. Y. Ishihara, and B. V. Adorno, "Hybrid kinematic control for rigid body pose stabilization using dual quaternions," *J. Franklin Inst.*, vol. 354, no. 7, pp. 2769–2787, 2017.
- [29] D.-P. Han, Q. Wei, and Z.-X. Li, "Kinematic control of free rigid bodies using dual quaternions," *Int. J. Autom. Comput.*, vol. 5, no. 3, pp. 319–324, 2008.
- [30] D. Han, Q. Wei, and Z. Li, "A dual-quaternion method for control of spatial rigid body," in *Proc. 2008 IEEE Int. Conf. Networking, Sensing and Control*, 2008, pp. 1–6.
- [31] D. Han, Q. Wei, Z. Li, and W. Sun, "Control of oriented mechanical systems: A method based on dual quaternion," in *Proc. 17th IFAC World Congr.*, 2008, pp. 3836–3841.
- [32] X. Wang and C. Yu, "Unit dual quaternion-based feedback linearization tracking problem for attitude and position dynamics," *Syst. Contr. Letts.*, vol. 62, no. 3, pp. 225–233, 2013.
- [33] P. P. M. Magro, J. Y. Ishihara, and H. C. Ferreira, "Robust global bimodal rest-to-rest attitude control of rigid body using unit quaternion," *J. Franklin Inst.*, vol. 354, no. 8, pp. 3554–3573, 2017.
- [34] P. P. M. Magro, H. T. M. Kussaba, L. F. C. Figueredo, and J. Y. Ishihara, "Dual quaternion-based bimodal global control for robust rigid body pose kinematic stabilization," in *2017 American Control Conference (ACC)*, May 2017, pp. 1205–1210.

- [35] J. Wertz, *Spacecraft Attitude Determination and Control*. Kluwer Academic Publishers, 1978.
- [36] Wikipedia, “Orientation (geometry) — Wikipedia, the free encyclopedia,” 2004, [Online; accessed 10-November-2016]. [Online]. Available: [https://en.wikipedia.org/wiki/Orientation_\(geometry\)](https://en.wikipedia.org/wiki/Orientation_(geometry))
- [37] R. Murray, Z. Li, and S. Sastry, *A Mathematical Introduction to Robotic Manipulation*. CRC Press, 1994.
- [38] R. E. S. Cabette, “Estabilidade do movimento rotacional de satélites artificiais,” Ph.D. dissertation, INPE, 2006.
- [39] W. R. Hamilton, “On quaternions, or on a new system of imaginaries in algebra: Copy of a letter from Sir William R. Hamilton to John T. Graves, esq. on quaternions,” *Philos. Mag.*, vol. 25, no. 3, pp. 489–495, 1844.
- [40] J. Solà, “Quaternion kinematics for the error-state kf,” p. 73, 2016. [Online]. Available: <https://hal.archives-ouvertes.fr/hal-01122406v4/document>
- [41] O. Bottema and B. Roth, *Theoretical Kinematics*. Dover Publications, Inc., 1990.
- [42] M. Shuster, “A survey of attitude representations,” *J. Astronaut. Sci.*, vol. 41, no. 4, pp. 439–517, 1993.
- [43] W. K. Clifford, “A preliminary sketch of biquaternions,” in *Proc. London Math. Soc.*, 1871, pp. 381–395.
- [44] E. Study, “Von den bewegungen und umlegungen,” *Mathematische Annalen*, vol. 39, no. 4, pp. 441–565, 1891.
- [45] X. Wang, D. Han, C. Yu, and Z. Zheng, “The geometric structure of unit dual quaternion with application in kinematic control,” *J. Math. Anal. Appl.*, vol. 389, no. 2, pp. 1352–1364, 2012.
- [46] Y. Wu, X. Hu, D. Hu, T. Li, and J. Lian, “Strapdown inertial navigation system algorithms based on dual quaternions,” vol. 41, no. 1, pp. 110–132, 2005.
- [47] D. P. Chevallier, “On the transference principle in kinematics: its various forms and limitations,” *Mech. Mach. Theory*, vol. 31, no. 1, pp. 57–76, 1996.
- [48] R. Goebel, R. Sanfelice, and A. Teel, “Hybrid dynamical systems,” *IEEE Control Syst.*, vol. 29, no. 2, pp. 28–93, Apr. 2009.
- [49] ———, *Hybrid dynamical systems*. Princeton University Press, 2012.
- [50] R. E. Mortensen, “Quarternion feedback regulator for spacecraft eigenaxis rotations,” *International Journal of Control*, vol. 8, no. 3, pp. 297–302, 1968.
- [51] R. E. Roberson, “Two decades of spacecraft attitude control,” *Journal of Guidance, Control, and Dynamics*, vol. 2, no. 1, pp. 3–8, 1979.
- [52] J. Hrastar, “Attitude control of a spacecraft with a strapdown inertial reference system and onboard computer,” NASA, Technical Report Tn D–5959, Sep. 1970.
- [53] H. Khalil, *Nonlinear Systems*. Macmillan Publishing Company, 1992.
- [54] C. Mayhew, R. Sanfelice, and A. Teel, “Robust global asymptotic attitude stabilization of a rigid body by quaternion-based hybrid feedback,” in *Proc. 48th IEEE Conf. Decision Control.*, Dec. 2009, pp. 2522–2527.
- [55] R. Schlanbusch, A. Loria, and P. J. Nicklasson, “On the stability and stabilization of quaternion equilibria of rigid bodies,” *Automatica*, vol. 48, no. 12, pp. 3135 – 3141, 2012.

- [56] R. Sanfelice, R. Goebel, and A. Teel, “Invariance principles for hybrid systems with connections to detectability and asymptotic stability,” *IEEE Trans. Autom. Control*, vol. 52, no. 12, pp. 2282–2297, Dec. 2007.
- [57] R. Sanfelice, D. Copp, and P. Nanez, “A toolbox for simulation of hybrid systems in matlab/simulink,” in *2013 Hybrid Systems: Computation and Control (HSCC)*, Apr. 2013, pp. 101–106.
- [58] R. Goebel and A. Teel, “Solutions to hybrid inclusions via set and graphical convergence with stability theory applications,” *Automatica*, vol. 42, no. 4, pp. 573–587, 2006.
- [59] J. Guerrero-Castellanos, N. Marchand, A. Hably, S. Lesecq, and J. Delamare, “Bounded attitude control of rigid bodies: Real-time experimentation to a quadrotor mini-helicopter,” *Control Engineering Practice*, vol. 19, no. 8, pp. 790 – 797, 2011.
- [60] L. Labeyrie, “Stellar interferometry methods,” *Ann. Rev. Astron. Astrophys.*, vol. 16, pp. 77–102, 1978.
- [61] L. Parker, “Current state of the art in distributed autonomous mobile robotics,” in *Proc. 5th International Symposium on Distributed Autonomous Robotic Systems (DARS)*, 2000.
- [62] R. M. Murray, “Two decades of spacecraft attitude control,” *J. Dyn. Sys., Meas., Control*, vol. 129, no. 5, pp. 571–583, 2007.
- [63] R. Wilson, *Introduction to Graph Theory*. Pearson, 2012.
- [64] C. D. Meyer, *Matrix Analysis and Applied Linear Algebra*. SIAM, 2001.
- [65] J. L. Meriam and L. G. Kraige, *Engineering Mechanics: Dynamics*. Wiley, 2009.
- [66] E. L. Lima, *Análise Real Funções de n variáveis - volume 2*. IMPA, 2013.
- [67] A. Izmailov and M. Solodov, *Otimização - volume 1*. IMPA, 2009.

APPENDICES

A

RESUMO ESTENDIDO EM LÍNGUA PORTUGUESA

O controle de atitude de um corpo rígido é um quesito importante em projetos de veículos aeroespaciais (aeronaves e naves espaciais) assim como em projetos de veículos submarinos, terrestres e em aplicações de sistemas robóticos, dentre outros [1]. Em uma gama de aplicações, mudanças no ponto de operação são necessárias e consequentemente resolver o problema de regulação a partir do estado inicial em repouso é um objetivo comum desejado [2]. Em particular, quando excursões arbitrárias na atitude são desejadas ou permitidas, surge o problema de se projetar um sistema de controle globalmente estável [1].

O controle global de atitude é um problema desafiante a começar pela escolha apropriada de uma representação para a atitude. É sabido que da gama existente de representações de atitude, nenhuma representação em três parâmetros do $SO(3)$ – como é o caso dos frequentemente utilizados ângulos de Euler – é globalmente não singular e isso é um obstáculo para se conseguir a estabilidade global [3]. Neste contexto, o quatérnio unitário se torna interessante por representar a atitude com o menor número de parâmetros possível sem singularidades.

O espaço de estados do quatérnio unitário é uma dupla cobertura do $SO(3)$ – um par de quatérnios unitários antipodais correspondem à mesma atitude em $SO(3)$ – que leva, quando um controlador contínuo baseado em quatérnio unitário é usado, a um fenômeno indesejado conhecido como *unwinding*, em que o corpo pode estar em repouso arbitrariamente próximo à atitude final desejada e, ainda assim, rotacionar grandes ângulos antes de chegar ao repouso [5]. Esse efeito pode ser evitado usando-se uma realimentação de estado descontínua (sem memória), tal como as sugeridas por Fjellstad and Fossen [6], Fragopoulos and Innocenti [7] ou Wie and Barba [8]. Apesar da estabilização global assintótica ser alcançada, a natureza descontínua do controlador introduz o fenômeno *chattering*, que consiste em múltiplos saltos (de estado) ocorrendo ao mesmo tempo, e que pode ocorrer na presença de ruído de medição quando o sistema está em uma região próxima de 180° da atitude de referência [9].

Um controle de atitude com a propriedade de estabilidade assintótica e global e robustez contra ruídos de medição (ou seja, estes ruídos não levam a fenômenos de *chattering*) foi obtido com o controlador híbrido de comportamento histerético sugerido por Mayhew et al. [10]. denominado controlador histerético, usando uma variável lógica binária. O tamanho da banda de histerese que cobre a região propensa a *chattering* pode ser projetado para um determinado nível máximo de ruído. Comparado com o controlador descontínuo (sem memória), o controlador histerético consegue eliminar o *chattering* ao custo de impor trajetórias de rotação mais longas para algumas condições iniciais de atitude levando a um maior tempo médio de estabilização ou consumo de energia.

Para reduzir o consumo de energia para o controlador histerético, uma alternativa seria reduzir o nível de ruído recebido no controlador utilizando-se sensores de alta precisão de preços elevados e/ou estimadores de atitude baseados na filtragem de Kalman ou de Partículas. Apesar dessas soluções serem efetivas em determinadas situações, há outras em que um ruído expressivo já é esperado. De um lado, tem-se a demanda crescente por soluções baratas com componentes baixo custo. Como filtros – especialmente o Filtro de Partículas, são computacionalmente “caros” [11] – para processadores embedded com pouca memória e recursos computacionais, geralmente um estimador simplificado e pouco efetivo é usado, resultando em um ruído de estimação de atitude alto. Por outro lado, sensores de baixo custo resultam em um nível maior de ruído. Por exemplo, no experimento de Gebre-Egziabher et al. [12], é possível observar ruídos de amplitude em torno de 10 graus. Se, além disso, o sistema estiver imerso em um ambiente com excesso de ruído eletromagnético ou se a velocidade angular for alta, o nível de ruído é ainda maior [13].

Neste estudo, procurou-se um controlador com a propriedade de estabilidade global e robusta que representasse uma melhor solução em termos de custo quando comparado com o controlador de banda de histerese fixa. Redução de custo representada por tempo médio de estabilização ou consumo de energia é importante, por exemplo, em satélites ou sistemas operados por bateria [14]. Propõe-se dois controladores distintos, ambos com duas variáveis de estado lógicas binárias (uma a mais que o controlador histerético) para o controle de atitude representado por quatérnio. O primeiro controlador, denominado HY, tem a variável principal determinada por um controle on-off com histerese para indicar qual representação em quatérnio da atitude de referência deve ser seguida e uma outra variável auxiliar determinada por um controle on-off sem histerese para indicar a proximidade à região crítica sujeita a *chattering*. Esse esquema oferece mais oportunidades de atualização da variável principal que o controlador híbrido histerético, por exemplo quando há uma variação abrupta na atitude de referência ou no momento inicial quando a atitude de referência está longe da atitude inicial. Isso reduz as chances do corpo seguir na direção da rotação mais longa. Contudo, essa estratégia impõe restrições na forma como o controlador é implementado. Prova-se que o sistema pode apresentar *chattering* na variável auxiliar e que esse *chattering* não afeta a robustez do sistema se “jumps” não tiverem prioridade sobre “flows”.

No segundo controlador proposto, denominado bimodal, ambas as variáveis são determinadas por um controle on-off com histerese. A variável principal indica qual representação em quatérnio da atitude de referência deve ser seguida e a outra variável indica a proximidade à região crítica sujeita a *chattering*. Essa estratégia elimina as restrições sobre a forma de implementação do controlador, porém torna a dinâmica dessas variáveis mais complexas, dado que uma variável interfere no comportamento da outra. O efeito resultante é que a banda de histerese do controle on-off referente à variável principal, se adapta de acordo com o estado da outra variável, sendo ora igual, ora a metade do valor do parâmetro banda de histerese. Esse controlador é uma solução intermediária entre o controlador descontínuo e o controlador híbrido histerético.

São apresentadas provas formais de que ambos os controladores deixam o sistema com as seguintes propriedades:

- estabilidade assintótica e global;
- sem *unwinding*;
- robustez contra ruídos de medição (sem *chattering*).

A eficácia dos controladores é mostrada por meio de simulações. Em alguns casos foram utilizados modelos realistas reportados em literatura. Embora os resultados indiquem que o desempenho dos controladores propostos apresentam vantagens para a configuração rest-to-rest, os controladores continuam apresentando bom desempenho mesmo quando a velocidade angular inicial e final não são nulas, desde que relativamente baixas. No caso do controlador bimodal, mesmo para outras velocidades angulares iniciais, o consumo de energia do sistema é, em média, inferior ao consumo do controlador híbrido histerético. Melhores desempenhos ocorrem quando a banda de histerese é maior como no caso em que são usados sensores mais baratos ou em ambientes onde há muito ruído eletromagnético.

Como extensão dos resultados descritos acima, duas outras contribuições foram propostas: uma sobre controle de sincronização de atitude de uma rede de corpos rígidos (agentes) e outra sobre controle cinemático de pose de corpo rígido dentro do grupo de quatérnios duais de norma unitária.

Com relação à primeira contribuição, muita pesquisa tem sido desenvolvida em controle de coordenação de atitude nos últimos 10-15 anos [15, 16, 17, 18, 19]. Comparado com o sistema com um só agente, os sistemas multiagentes têm vantagens interessantes como viabilidade de ser implementado, produção de resultados mais exatos, robustos, menor custo etc., além de ter uma gama de aplicações como monitoramento de ambientes, procura e resgate, interferômetros espaciais, manuseio de materiais dentre outras [20].

Como mencionado acima, o problema de estabilização global e robusta de atitude, para um único corpo

rígido, foi resolvido há poucos anos [10], mas a estabilização em um cenário de uma rede de agentes traz muito mais desafios devido às interações existentes entre os agentes. Até o momento, a maioria dos estudos sobre estratégias de sincronização de atitude são capazes de promover uma estabilização quase global como em [18, 17] e quando é global, não é robusta a ruídos de medição.

O único estudo em sincronização de atitude de múltiplos agentes, que o autor tem conhecimento, e que realiza uma sincronização global e robusta é o de Mayhew et al. (2012) [21]. Assume-se que cada agente tem acesso somente à atitude relativa entre seus vizinhos e à sua velocidade angular em relação ao sistema de coordenadas do corpo. Seu objetivo é alcançar a estabilidade de um estado sincronizado (que não é uma atitude de referência absoluta específica) usando um esquema de realimentação híbrida. A vantagem de não requerer sensores para medições de atitude inercial tem o custo de se obter a sincronização apenas para redes conexas e acíclicas [22], pois existe um obstáculo físico para a convergência global quando o grafo contém ciclos [22, Theorem 1].

Neste estudo, propõe-se um controle de sincronização de atitude distribuído com a propriedade de estabilidade assintótica e global e robustez contra ruídos de medição para uma rede de agentes representada por um grafo não direcionado e conexo (cíclico ou acíclico). A estratégia usa o quatérnio como representação da atitude inercial e uma realimentação híbrida histerética com uma variável lógica binária, sugerida por Mayhew et al. [10], para cada agente, a fim de resolver os conhecidos problemas que surgem quando uma lei de realimentação de estados, contínua ou descontínua, é empregada como presença de estados instáveis, fenômeno “unwinding” e “chattering”. O custo de se utilizar esta estratégia é o surgimento de mais uma restrição no parâmetro da banda de histerese δ_i no controlador de cada agente.

Os resultados das simulações contrastam o controlador contínuo com o controlador híbrido proposto e mostram que a direção de rotação mais longa é evitada no caso do esquema híbrido quando o estado inicial está próximo a um ponto de equilíbrio, reduzindo o tempo de estabilização. Além disso, eles enfatizam alguns dos problemas provenientes da lei de realimentação contínua como o atraso na resposta quando o estado de um agente está muito próximo a um ponto de equilíbrio instável.

Com relação à segunda contribuição, o grupo de Lie do deslocamento de um corpo rígido aparece naturalmente no estudo de sistemas aeroespaciais e robóticos. A partir do trabalho inicial de Brockett [23] sobre teoria de controle em grupos de Lie gerais, grande parte da literatura foi dedicada ao controle de sistemas definidos no $SE(3)$. Embora seja usual projetar controladores para este sistema usando matrizes para representar elementos deste grupo de Lie [24, 25], alguns autores observaram que os controladores projetados usando-se um outro tipo de representação, a saber, o quatérnio dual unitário para $SE(3)$, podem apresentar vantagens em relação ao tempo computacional e aos requisitos de armazenamento [26, 27].

É importante observar que, como neste caso o espaço de estado de um sistema dinâmico é uma variedade genérica, algumas dificuldades são esperadas para se projetar um controlador capaz de estabilizar o sistema. Na verdade, o problema da estabilização robusta e global de pose de um corpo rígido não é simples, mas é, de certa forma, análogo ao problema de atitude.

Em primeiro lugar, não existe um controlador com realimentação contínua capaz de estabilizar assintoticamente e globalmente um ponto de equilíbrio na variedade do grupo quatérnio dual unitário [28].

Em segundo lugar, como o grupo de Lie de quatérnio dual unitário é uma cobertura dupla do grupo de Lie de deslocamento de corpo rígido $SE(3)$ [29, 28], induz-se, quando um controlador contínuo baseado em quatérnio dual é usado, um fenômeno similar ao de “unwinding” em $SO(3)$ [5]: o corpo rígido pode iniciar do repouso em uma pose arbitrariamente perto da final desejada e, ainda, ser conduzido para o ponto de equilíbrio estável e mais afastado antes retornar ao repouso.

Por fim, mesmo usando uma realimentação de estado descontínua (sem memória), é impossível obter uma estabilização global e robusta de um conjunto de pontos não conexos, provenientes da cobertura dupla do $SE(3)$

[10, 9].

Há poucos estudos em que se tenta eliminar o problema de “unwinding” no contexto de estabilização de pose usando quatérnio dual unitário [29, 30, 31, 32]. Todos sugerem realimentação descontínua e são propensos a “chattering” para condições iniciais arbitrariamente próximas da descontinuidade.

Inspirado no controle híbrido baseado em histerese de Mayhew et al. [10] desenvolvido apenas para estabilização do controle de atitude, Kussaba et al. [28] projetou uma extensão desse controlador para obter a estabilidade da atitude e translação de forma acoplada. No entanto, este controlador de pose sugerido por Kussaba et al. [28] herda o mesmo custo do controlador histerético de atitude, mencionado anteriormente, de impor trajetórias de rotação mais longas para determinadas atitudes iniciais, fazendo com que o tempo de estabilização ou consumo de energia seja maior. Além disso, o problema do consumo de energia também se agrava neste contexto, pois os movimentos casados de translação e rotação consomem mais energia. [28].

Para reduzir esse custo, propõe-se uma lei de controle bimodal híbrido que combine o controlador bimodal de atitude proposto acima e o controle sugerido por Kussaba et al. [28] de modo que ele represente uma solução intermediária em termos de custo entre o controlador descontínuo e o histerético.

Os resultados de simulação comparam a evolução do sistema quando o controlador utilizado é o bimodal com os controladores descontínuo e o histerético. Uma ideia do consumo de energia pode ser obtida a partir da área embaixo da curva do gráfico do módulo da velocidade angular quando cada controlador é utilizado.

As contribuições desta tese são:

1. Enuncia-se um teorema sobre um problema que ocorre com o controlador de atitude descontínuo na presença de ruídos de medição no espaço do quatérnio unitário (veja Teorema 3.4, página 15). Este resultado é uma correção em um teorema de [10] em que o sistema está corrompido por ruído, porém a variável medida não pertence ao espaço do quatérnio unitário. Consequentemente, o modelo do sistema perde o sentido físico.
2. Apresenta-se um controle de atitude (representada por quatérnios) de um corpo rígido, que é híbrido e global, além de ser robusto a ruídos de medição, voltado para casos em que a velocidade angular inicial e final é zero (veja Capítulo 4). O controlador proposto estende um controlador híbrido histerético da literatura introduzindo uma nova variável de estado lógica e binária. O controlador é capaz de detectar quando a atitude de referência muda abruptamente ou quando a atitude inicial está distante da atitude de referência. Desta forma, ele tem mais oportunidades de determinar qual representação em quatérnio da atitude de referência deve ser seguida em comparação com o controlador híbrido histerético da literatura e tem mais chances de seguir pela direção de rotação mais curta. Este estudo foi apresentado no XII Simpósio Brasileiro de Automação Inteligente - SBAI 2015 e o respectivo artigo está publicado online, disponível em <http://swge.inf.br/SBAI2015/anais/413.pdf>.
3. Apresenta-se uma outra estratégia de controle de atitude de corpo rígido, híbrido e global, que é robusto a ruídos de medição (ou seja, não há *chattering*) por meio do controlador denominado bimodal (veja Capítulo 5). Ele é apropriado para casos em que a velocidade angular inicial e final são zero e tem a atitude representada por quatérnio. Porém, ele também apresenta vantagens para condições iniciais genéricas. Dentre os controladores globais, presume-se que ele seja o mais interessante quando o nível de ruído na medição da atitude é expressivo como, por exemplo, quando sensores/componentes de baixo custo são usados ou quando o sistema está imerso em ambientes onde há muito ruído eletromagnético. O controlador possui duas variáveis de estado lógicas binárias. Por conseguir adaptar a banda de histerese, ele reduz a região onde o controlador híbrido histerético determina a direção de rotação mais longa, sem comprometer a robustez, sendo uma solução intermediária em termos de custo entre o controlador descontínuo e o híbrido histerético. Um artigo sobre este estudo foi publicado na revista Journal of the Franklin Institute.

4. Propõe-se um controle de sincronização de atitude distribuído para uma rede de corpos rígidos (agentes) representada por um grafo não direcionado e conexo (cíclico ou acíclico) que apresente uma estabilidade global e assintótica (veja Capítulo 6). Devido às inerentes interações entre os agentes, o projeto do controlador é muito mais desafiador. Na literatura, a grande maioria dos controladores sugerem leis de realimentação de estado contínuas ou descontínuas. Como no caso restrito a um único corpo rígido estes tipos de estratégias de controle levam o sistema a apresentar problemas bem conhecidos como estados instáveis, fenômeno *unwinding* e *chattering*, é esperado que, no caso de sistemas multiagente, haja problemas de desempenho ainda piores. Para resolver estes problemas, o controlador proposto usa como base o controlador histerético híbrido da literatura com uma variável lógica binária e uma restrição mais forte para o parâmetro banda de histerese. Um artigo a respeito deste estudo foi submetido à revista *International Journal of Systems Science*.

5. Propõe-se uma estratégia de controle híbrido global para resolver o problema cinemático de rotação e translação de um corpo rígido e seja robusto a ruídos de medição (veja Capítulo 7). O controlador híbrido baseado em dual quatérnio sugerido na literatura estende o controlador histerético baseado em quatérnio que, como se sabe, tem um região do espaço de estados onde a lei de controle força o movimento para a direção de rotação mais longa, gastando-se mais energia que o necessário. A estratégia proposta adapta o controlador de atitude bimodal do Capítulo 5 ao sistema de pose de um corpo rígido a fim de reduzir, em média, o tempo de estabilização ou consumo de energia. Neste contexto, o problema de consumo de energia é mais grave, pois o movimento de rotação e translação estão acoplados, consumindo mais energia (veja Capítulo 7). Este estudo foi apresentado no *American Control Conference - ACC 2017* e o respectivo artigo foi publicado nos anais do evento.

B

PROOFS OF SOME LEMMAS

In this appendix, the lemmas used along the text are demonstrated.

Lemma B.1 Euler's equation in body coordinates

Let J^b represent the constant inertia matrix calculated in the body frame, τ^b represent the external torque expressed in the body frame and ω^b represent the current angular velocity of the body frame as seen from the reference frame and expressed in the body frame. The dynamic equation, known as the Euler's equation, written in body coordinates, is given by

$$J^b \dot{\omega}^b = S(J^b \omega^b) \omega^b + \tau^b. \quad (\text{B.1})$$

Proof. Consider that variable with a superscript letter b is expressed in the body frame. Absence of this superscript letter indicates the variable is expressed in the reference frame. Taking the time derivative of the angular momentum [65] expressed in the body frame L^b ,

$$L^b = J^b \omega^b, \quad (\text{B.2})$$

$$\dot{L}^b = J^b \dot{\omega}^b. \quad (\text{B.3})$$

As $L = RL^b$, taking its time derivative,

$$L = RL^b, \quad (\text{B.4})$$

$$\dot{L} = \dot{R}L^b + R\dot{L}^b. \quad (\text{B.5})$$

Using that $\dot{R} = RS(\omega^b)$ [37, page 52], (B.2) and (B.3),

$$\dot{L} = RS(\omega^b)(J^b \omega^b) + R(J^b \dot{\omega}^b). \quad (\text{B.6})$$

As the torque τ equals the time derivative of the angular momentum and $\tau = R\tau^b$,

$$\tau = R \left[S(\omega^b) (J^b \omega^b) + J^b \dot{\omega}^b \right], \quad (\text{B.7})$$

$$J^b \dot{\omega}^b = R^T \tau - S(\omega^b) (J^b \omega^b), \quad (\text{B.8})$$

$$= S(J^b \omega^b) (\omega^b) + \tau^b. \quad (\text{B.9})$$

□

Lemma B.2 Quaternion kinematic equation for the attitude error

Let \mathbf{q} represent the current attitude, $\boldsymbol{\omega}$ be the current angular velocity, \mathbf{q}_d represent the desired attitude and $\boldsymbol{\omega}_d$ be the desired angular velocity. Given that the attitude error is defined as $\mathbf{q}_e = \mathbf{q}_d^* \circ \mathbf{q}$, the kinematic equation for the attitude error is

$$\dot{\mathbf{q}}_e = \frac{1}{2} \mathbf{q}_e \circ (0, \boldsymbol{\omega}_e), \quad (\text{B.10})$$

where $\boldsymbol{\omega}_e = \boldsymbol{\omega} - \mathcal{R}(\mathbf{q}_e)^T \boldsymbol{\omega}_d$.

Proof. Take the time derivative of the attitude error,

$$\mathbf{q}_e = \mathbf{q}_d^* \circ \mathbf{q}, \quad (\text{B.11})$$

$$\dot{\mathbf{q}}_e = \dot{\mathbf{q}}_d^* \circ \mathbf{q} + \mathbf{q}_d^* \circ \dot{\mathbf{q}}. \quad (\text{B.12})$$

Substituting the kinematic equation (2.7) into (B.12),

$$\dot{\mathbf{q}}_e = \left(\frac{1}{2} \mathbf{q}_d \circ (0, \boldsymbol{\omega}_d) \right)^* \circ \mathbf{q} + \mathbf{q}_d^* \circ \left(\frac{1}{2} \mathbf{q} \circ (0, \boldsymbol{\omega}) \right), \quad (\text{B.13})$$

$$= -\frac{1}{2} (0, \boldsymbol{\omega}_d) \circ \mathbf{q}_d^* \circ \mathbf{q} + \frac{1}{2} \mathbf{q}_d^* \circ \mathbf{q} \circ (0, \boldsymbol{\omega}), \quad (\text{B.14})$$

$$= \frac{1}{2} \mathbf{q}_e \circ (0, \boldsymbol{\omega}) - \frac{1}{2} (0, \boldsymbol{\omega}_d) \circ \mathbf{q}_e, \quad (\text{B.15})$$

$$= \frac{1}{2} \mathbf{q}_e \circ [(0, \boldsymbol{\omega}) - \mathbf{q}_e^* \circ (0, \boldsymbol{\omega}_d) \circ \mathbf{q}_e], \quad (\text{B.16})$$

$$= \frac{1}{2} \mathbf{q}_e \circ [(0, \boldsymbol{\omega}) - (0, \mathcal{R}(\mathbf{q}_e^*) \boldsymbol{\omega}_d)], \quad (\text{B.17})$$

$$= \frac{1}{2} \mathbf{q}_e \circ [(0, \boldsymbol{\omega} - \mathcal{R}(\mathbf{q}_e)^T \boldsymbol{\omega}_d)]. \quad (\text{B.18})$$

□

Lemma B.3 Hybrid basic conditions

Let $\bar{x} = (\mathbf{q}_e, \boldsymbol{\omega}) \in X$, $X = \mathbb{S}^3 \times \mathbb{R}^3$, $\bar{x}_2 = (\bar{x}, \bar{h}, m) \in \mathcal{X} \times \{1, -1\} \times \{1, -1\}$ and $\bar{\mathcal{H}}$, defined either in (4.7) or in (5.8), be a closed-loop autonomous hybrid system. The hybrid system $\bar{\mathcal{H}}$ satisfies the hybrid basic conditions (Assumption 6.5 of [49])

(A1) C_2 and D_2 are closed sets;

(A2) $\bar{F}_2 : \mathbb{R}^n \rightrightarrows \mathbb{R}^n$ is outer semicontinuous, locally bounded, convex-valued, and $\bar{F}_2(\bar{x}_2) \neq \emptyset$ for all $\bar{x}_2 \in C_2$;

(A3) $\bar{G}_2 : \mathbb{R}^n \rightrightarrows \mathbb{R}^n$ is outer semicontinuous, locally bounded and $\bar{G}_2(\bar{x}_2) \neq \emptyset$ for all $\bar{x}_2 \in D_2$.

Proof. The hybrid system $\bar{\mathcal{H}}$ satisfies:

- (A1), D_2 is the union of a finite number of closed sets that results in a closed set [66] and C_2 is the intersection of closed sets that results in a closed set [66].
- (A2), \bar{F}_2 is continuous in C_2 . Consequently, it is outer semicontinuous and locally bounded [49,

page 102]. Clearly it is also convex-valued and non empty for every $\bar{x}_2 \in C_2$.

- (A3), the graph of \bar{G}_2 is closed. According to [49, Lemma 5.10], a set-valued mapping is outer semicontinuous if and only if the graph of the mapping is closed. Also \bar{G}_2 is clearly bounded in $[-1, 1]$ and non empty for all $\bar{x}_2 \in D_2$.

□

The purpose of the following lemma is to find the minimum α such that $\mathbf{q} \in \mathcal{M} + \alpha\mathbb{B}$. The idea is to find out a relation between α and η .

Lemma B.4

Let $\mathcal{M} \triangleq \{\mathbf{q} \in \mathbb{S}^3 : \eta = 0\}$ and $\mathbf{q} = (\eta, \boldsymbol{\epsilon}) \in \mathbb{S}^3$ be a fixed attitude. Then, the distance between \mathbf{q} and the set \mathcal{M} is

$$d(\mathbf{q}, \mathcal{M}) = \inf_{\mathbf{q}_w \in \mathcal{M}} \|\mathbf{q} - \mathbf{q}_w\| = \|\mathbf{q} - \mathbf{q}_w^*\| = \sqrt{2 - 2\sqrt{1 - \eta^2}}. \quad (\text{B.19})$$

Proof. Let $\mathbf{q}_w = (0, \boldsymbol{\epsilon}_w) \in \mathcal{M}$. As $\mathbf{q} - \mathbf{q}_w = (\eta, \boldsymbol{\epsilon}) - (0, \boldsymbol{\epsilon}_w) = (\eta, \boldsymbol{\epsilon} - \boldsymbol{\epsilon}_w)$ and $\|\mathbf{q}_w\|^2 = \|(0, \boldsymbol{\epsilon}_w)\|^2 = \|\boldsymbol{\epsilon}_w\|^2$, the problem of finding distance d can be solved by finding $\boldsymbol{\epsilon}_w^*$ which is a solution of

$$\min_{\|\boldsymbol{\epsilon}_w\|^2=1} \|(\eta, \boldsymbol{\epsilon} - \boldsymbol{\epsilon}_w)\|^2.$$

Let $f(\boldsymbol{\epsilon}_w) = \langle (\eta, \boldsymbol{\epsilon} - \boldsymbol{\epsilon}_w), (\eta, \boldsymbol{\epsilon} - \boldsymbol{\epsilon}_w) \rangle$ and $h(\boldsymbol{\epsilon}_w) = \langle \boldsymbol{\epsilon}_w, \boldsymbol{\epsilon}_w \rangle - 1$.

Theorem of Weierstrass [67, page 8] assures existence of a global minimum since $f(\boldsymbol{\epsilon}_w)$ is continuous and the set $\{\boldsymbol{\epsilon}_w \in \mathbb{R}^3 : h(\boldsymbol{\epsilon}_w) = 0\}$ is compact.

$f(\boldsymbol{\epsilon}_w)$ is differentiable and $h(\boldsymbol{\epsilon}_w)$ is continuously differentiable at any point $\boldsymbol{\epsilon}_w \in \mathbb{R}^3$. Also, $\nabla_{\boldsymbol{\epsilon}_w} h(\boldsymbol{\epsilon}_w^*) = 2\boldsymbol{\epsilon}_w^* \neq \mathbf{0}$ is linearly independent and satisfies the regularity condition. Using Lagrange optimality conditions theorem [67, page 52]

$$L(\boldsymbol{\epsilon}_w, \lambda) = f(\boldsymbol{\epsilon}_w) + \lambda h(\boldsymbol{\epsilon}_w).$$

The minimum can be found by solving the system

$$\nabla_{\boldsymbol{\epsilon}_w} L(\boldsymbol{\epsilon}_w^*, \lambda^*) = 0 \quad (\text{B.20})$$

$$\nabla_{\lambda} L(\boldsymbol{\epsilon}_w^*, \lambda^*) = 0 \quad (\text{B.21})$$

From (B.20),

$$-2(\boldsymbol{\epsilon} - \boldsymbol{\epsilon}_w^*) + 2\lambda^* \boldsymbol{\epsilon}_w^* = 0, \quad (\text{B.22})$$

$$(1 + \lambda^*) \boldsymbol{\epsilon}_w^* = \boldsymbol{\epsilon}. \quad (\text{B.23})$$

From (B.23), if $\lambda^* = -1$, it is required that $\boldsymbol{\epsilon} = \mathbf{0}$, that is, $\mathbf{q} = \pm \mathbf{1} = (\pm 1, \mathbf{0})$. In this case, the minimum is achieved for any $\boldsymbol{\epsilon}_w^* \in \mathbb{S}^2$ and the distance $d = \sqrt{2}$.

For $\lambda^* \neq -1$, from (B.23)

$$\boldsymbol{\epsilon}_w^* = \frac{\boldsymbol{\epsilon}}{1 + \lambda^*}. \quad (\text{B.24})$$

From (B.21), $\langle \boldsymbol{\epsilon}_w^*, \boldsymbol{\epsilon}_w^* \rangle = 1$. Substituting (B.24) into this equation,

$$\frac{\langle \boldsymbol{\epsilon}, \boldsymbol{\epsilon} \rangle}{(1 + \lambda^*)^2} = 1, \quad (\text{B.25})$$

$$(1 + \lambda^*)^2 = \langle \boldsymbol{\epsilon}, \boldsymbol{\epsilon} \rangle, \quad (\text{B.26})$$

$$1 + \lambda^* = \pm \sqrt{1 - \eta^2}. \quad (\text{B.27})$$

Thus, substituting (B.27) into (B.24), $\epsilon_w^* = \pm \frac{\epsilon}{\sqrt{1-\eta^2}}$. This results into two possible solutions. Clearly, the solution that minimizes the problem is achieved when $\mathbf{q}_w^* = \left(0, \frac{\epsilon}{\sqrt{1-\eta^2}}\right)$.

The distance d is

$$d(\mathbf{q}, \mathcal{M}) = \|\mathbf{q} - \mathbf{q}_w^*\|, \quad (\text{B.28})$$

$$= \left\| \left(\eta, \left(1 - \frac{1}{\sqrt{1-\eta^2}}\right) \epsilon \right) \right\|, \quad (\text{B.29})$$

$$= \sqrt{\eta^2 + \left(1 - \frac{1}{\sqrt{1-\eta^2}}\right)^2 \|\epsilon\|^2}, \quad (\text{B.30})$$

$$= \sqrt{\eta^2 + \left(1 - \frac{2}{\sqrt{1-\eta^2}} + \frac{1}{1-\eta^2}\right) (1-\eta^2)}, \quad (\text{B.31})$$

$$= \sqrt{2 - 2\sqrt{1-\eta^2}}. \quad (\text{B.32})$$

This equation also holds for $\mathbf{q} = \pm \mathbf{1}$ when $\lambda^* = -1$. Note that the maximum distance is $d = \sqrt{2}$. \square

A geometrical interpretation of distance d is the line segment \overline{PQ} shown in Figure B.1. Let $\mathbf{q} = (m, \epsilon_m)$. Thus, $\|\mathbf{q} - \mathbf{q}_w^*\| = \left\| \left(m, \left(1 - \frac{1}{\sqrt{1-m^2}}\right) \epsilon\right) \right\|$. Since $\left\| \left(1 - \frac{1}{\sqrt{1-m^2}}\right) \epsilon \right\| = |\sqrt{1-m^2} - 1| \left\| \frac{\epsilon}{\sqrt{1-m^2}} \right\| = |1 - \sqrt{1-m^2}|$ is represented by the size of the line segment \overline{QR} and line segment \overline{RP} has size $|m|$, then $\|\mathbf{q} - \mathbf{q}_w^*\|$ has the size of segment \overline{PQ} .

$$\overline{PQ}^2 = \overline{RP}^2 + \overline{QR}^2 \quad (\text{B.33})$$

$$= \sqrt{m^2 + \left(1 - \sqrt{1-m^2}\right)^2} \quad (\text{B.34})$$

$$= \sqrt{2 - 2\sqrt{1-m^2}} \quad (\text{B.35})$$

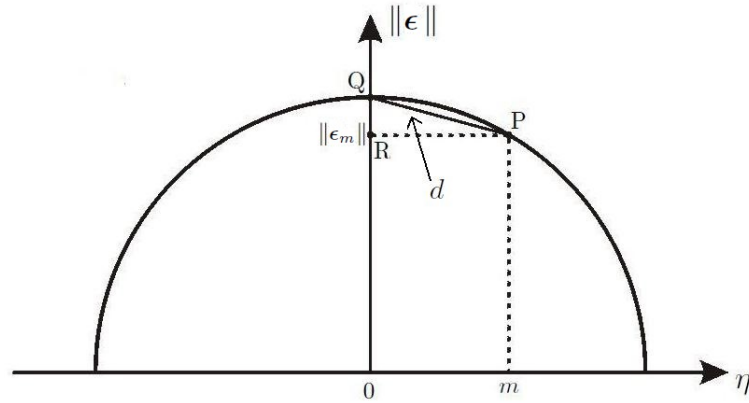


Figure B.1: Geometrical representation of distance d from $\mathbf{q} = (m, \epsilon_m)$.

The lemma that follows looks for the maximum η such that $\mathbf{q} \in \mathcal{M} + \mathbb{B}(0, \alpha)$.

Lemma B.5

Let $\mathcal{M} \triangleq \{\mathbf{q} \in \mathbb{S}^3 : \eta = 0\}$, $\mathbf{q} = (\eta, \boldsymbol{\epsilon}) \in \mathcal{M}^* \triangleq \{(\mathcal{M} + \mathbb{B}(0, \alpha)) \cap \mathbb{S}^3\}$ and $\alpha > 0$. Then

$$|\eta| < \alpha \sqrt{1 - \frac{\alpha^2}{4}}. \quad (\text{B.36})$$

Proof. Let α^* be the distance between \mathbf{q} and \mathcal{M} . From Lemma B.4, $\alpha^* = \sqrt{2 - 2\sqrt{1 - \eta^2}}$, which depends only on η . As $\mathbb{B}(0, \alpha)$ is an open ball, $\alpha > \alpha^*$ and $\mathbf{q} \in \mathcal{M}^*$,

$$\sqrt{2 - 2\sqrt{1 - \eta^2}} < \alpha, \quad (\text{B.37})$$

$$2 - 2\sqrt{1 - \eta^2} < \alpha^2, \quad (\text{B.38})$$

$$\sqrt{1 - \eta^2} > 1 - \frac{\alpha^2}{2}, \quad (\text{B.39})$$

$$1 - \eta^2 > 1 - \alpha^2 + \frac{\alpha^4}{4}, \quad (\text{B.40})$$

$$\eta^2 < \alpha^2 - \frac{\alpha^4}{4}, \quad (\text{B.41})$$

$$|\eta| < \alpha \sqrt{1 - \frac{\alpha^2}{4}}. \quad (\text{B.42})$$

□

Lemma B.6

Let $|\eta| < m$, $\beta \in (0, 1)$ and $\eta_r = -\eta + \beta(\eta - \text{sgn}(\eta)m)$. Then $\text{sgn}(\eta + \eta_r) = -\text{sgn}(\eta)$.

Proof.

$$\eta_r = -\eta + \beta(\eta - \text{sgn}(\eta)m), \quad (\text{B.43})$$

$$\eta + \eta_r = \beta(\eta - \text{sgn}(\eta)m). \quad (\text{B.44})$$

Multiplying both sides of (B.44) by $\text{sgn}(\eta)$,

$$\text{sgn}(\eta) (\eta + \eta_r) = \beta(\text{sgn}(\eta)\eta - \text{sgn}(\eta)\text{sgn}(\eta)m). \quad (\text{B.45})$$

Since $\text{sgn}(\eta)\eta = |\eta|$ and $\text{sgn}(\eta)\text{sgn}(\eta) = 1$,

$$\text{sgn}(\eta) (\eta + \eta_r) = \beta(|\eta| - m). \quad (\text{B.46})$$

Using the constraints of the lemma, $|\eta| < m$ and $\beta > 0$,

$$\text{sgn}(\eta) (\eta + \eta_r) < 0. \quad (\text{B.47})$$

Hence, $\text{sgn}(\eta + \eta_r) \neq \text{sgn}(\eta)$ or $\text{sgn}(\eta + \eta_r) = -\text{sgn}(\eta)$. □

Lemma B.7

Let $\mathbf{q} = (\eta, \boldsymbol{\epsilon}) \in \mathbb{S}^3$ be a fixed attitude and $\mathbf{Q}_e = (\eta_e, \boldsymbol{\epsilon}_e) \in \mathbb{H}$ be a measurement noise with η_e fixed. Given that $|\eta| < 1$ and $|\eta + \eta_e| < 1$, the minimum magnitude of noise, $\|\mathbf{Q}_e^*\|$, such that $\mathbf{q} + \mathbf{Q}_e^*$ still represents an attitude, is achieved when

$$\mathbf{Q}_e^* = \left(\eta_e, \left(\sqrt{\frac{1 - (\eta + \eta_e)^2}{1 - \eta^2}} - 1 \right) \boldsymbol{\epsilon} \right). \quad (\text{B.48})$$

Proof. The problem requires to find \mathbf{Q}_e^* that is a solution of

$$\min_{\|\mathbf{q} + \mathbf{Q}_e\|^2 = 1} \|\mathbf{Q}_e\|.$$

Since $\|\mathbf{Q}_e\|^2 = \eta_e^2 + \|\boldsymbol{\epsilon}_e\|^2$ and η_e is known and fixed, minimizing $\|\mathbf{Q}_e\|$ is equivalent to minimizing $\|\boldsymbol{\epsilon}_e\|^2$. As $\mathbf{q} + \mathbf{Q}_e = (\eta + \eta_e, \boldsymbol{\epsilon} + \boldsymbol{\epsilon}_e)$, the minimization problem above is equivalent to

$$\min_{\|\boldsymbol{\epsilon} + \boldsymbol{\epsilon}_e\|^2 = 1 - (\eta + \eta_e)^2} \|\boldsymbol{\epsilon}_e\|^2.$$

Let $f(\boldsymbol{\epsilon}_e) = \langle \boldsymbol{\epsilon}_e, \boldsymbol{\epsilon}_e \rangle$ and $h(\boldsymbol{\epsilon}_e) = \langle \boldsymbol{\epsilon} + \boldsymbol{\epsilon}_e, \boldsymbol{\epsilon} + \boldsymbol{\epsilon}_e \rangle - 1 + (\eta + \eta_e)^2$.

Theorem of Weierstrass [67, page 8] assures existence of a global minimum since $f(\boldsymbol{\epsilon}_e)$ is continuous and the set $\{\boldsymbol{\epsilon}_e \in \mathbb{R}^3 : h(\boldsymbol{\epsilon}_e) = 0\}$ is compact.

$f(\boldsymbol{\epsilon}_e)$ is differentiable and $h(\boldsymbol{\epsilon}_e)$ is continuously differentiable at any point $\boldsymbol{\epsilon}_e \in \mathbb{R}^3$. Also, $\nabla_{\boldsymbol{\epsilon}_e} h(\boldsymbol{\epsilon}_e^*) = 2(\boldsymbol{\epsilon} + \boldsymbol{\epsilon}_e^*)$ is linearly independent since $\boldsymbol{\epsilon} + \boldsymbol{\epsilon}_e \neq \mathbf{0}$ due to restrictions $|\eta + \eta_e| < 1$ and $\|\mathbf{q} + \mathbf{Q}_e\| = 1$. Hence, the regularity conditions are satisfied.

Using Lagrange optimality conditions theorem [67, page 52]

$$L(\boldsymbol{\epsilon}_e, \lambda) = f(\boldsymbol{\epsilon}_e) + \lambda h(\boldsymbol{\epsilon}_e).$$

The minimum can be found solving the system

$$\nabla_{\boldsymbol{\epsilon}_e} L(\boldsymbol{\epsilon}_e^*, \lambda^*) = 0 \quad (\text{B.49})$$

$$\nabla_{\lambda} L(\boldsymbol{\epsilon}_e^*, \lambda^*) = 0 \quad (\text{B.50})$$

From (B.49)

$$2\boldsymbol{\epsilon}_e^* + 2\lambda^*(\boldsymbol{\epsilon} + \boldsymbol{\epsilon}_e^*) = 0, \quad (\text{B.51})$$

$$(1 + \lambda^*)\boldsymbol{\epsilon}_e^* = -\lambda^*\boldsymbol{\epsilon}. \quad (\text{B.52})$$

For $\lambda^* = -1$, $\boldsymbol{\epsilon} = \mathbf{0}$. This solution is not possible due to restriction $|\eta| < 1$.

For $\lambda^* \neq -1$,

$$\boldsymbol{\epsilon}_e^* = -\frac{\lambda^*\boldsymbol{\epsilon}}{1 + \lambda^*} \quad (\text{B.53})$$

$$\boldsymbol{\epsilon} + \boldsymbol{\epsilon}_e^* = \frac{\boldsymbol{\epsilon}}{1 + \lambda^*} \quad (\text{B.54})$$

From (B.50), $\langle \boldsymbol{\epsilon} + \boldsymbol{\epsilon}_e^*, \boldsymbol{\epsilon} + \boldsymbol{\epsilon}_e^* \rangle = 1 - (\eta + \eta_e)^2$. Substituting (B.54) into this equation,

$$\frac{\langle \boldsymbol{\epsilon}, \boldsymbol{\epsilon} \rangle}{(1 + \lambda^*)^2} = 1 - (\eta + \eta_e)^2, \quad (\text{B.55})$$

$$\frac{1 - \eta^2}{(1 + \lambda^*)^2} = 1 - (\eta + \eta_e)^2, \quad (\text{B.56})$$

$$\frac{1}{1 + \lambda^*} = \pm \sqrt{\frac{1 - (\eta + \eta_e)^2}{1 - \eta^2}}. \quad (\text{B.57})$$

Then, substituting (B.57) into (B.54),

$$\epsilon + \epsilon_e^* = \pm \sqrt{\frac{1 - (\eta + \eta_e)^2}{1 - \eta^2}} \epsilon, \quad (\text{B.58})$$

$$\epsilon_e^* = \left(\pm \sqrt{\frac{1 - (\eta + \eta_e)^2}{1 - \eta^2}} - 1 \right) \epsilon. \quad (\text{B.59})$$

From the two possible solutions, the one which minimizes $\|\epsilon_e\|^2$ is

$$\epsilon_e^* = \left(\sqrt{\frac{1 - (\eta + \eta_e)^2}{1 - \eta^2}} - 1 \right) \epsilon. \quad (\text{B.60})$$

□

Lemma B.8

Let $\mathbf{q} = (\eta, \epsilon) \in \mathbb{S}^3$, $0 < \alpha < \sqrt{2}$, $\beta \in (0, 1)$, $m = \alpha \sqrt{1 - \frac{\alpha^2}{4}} > |\eta|$. Given $\mathbf{Q}_e = (\eta_e, \epsilon_e)$, $\eta_e = -\eta + \beta(\eta - \text{sgn}(\eta)m)$, $\epsilon_e = \left(\sqrt{\frac{1 - (\eta + \eta_e)^2}{1 - \eta^2}} - 1 \right) \epsilon$, then the magnitude of \mathbf{Q}_e , $\|\mathbf{Q}_e\|$, is lower than α .

Proof. The first part of the proof calculates $\|\mathbf{Q}_e\|$ as a function of parameters β , m and η .

$$\|\mathbf{Q}_e\|^2 = \eta_e^2 + \left\| \left(\sqrt{\frac{1 - (\eta + \eta_e)^2}{1 - \eta^2}} - 1 \right) \epsilon \right\|^2.$$

Substituting $\|\epsilon\|^2$ by $(1 - \eta^2)$,

$$\|\mathbf{Q}_e\|^2 = \eta_e^2 + \left(\frac{1 - (\eta + \eta_e)^2}{1 - \eta^2} - 2\sqrt{\frac{1 - (\eta + \eta_e)^2}{1 - \eta^2}} + 1 \right) (1 - \eta^2), \quad (\text{B.61})$$

$$= 2 - 2\eta^2 - 2\eta\eta_e - 2\sqrt{1 - (\eta + \eta_e)^2} \sqrt{1 - \eta^2}. \quad (\text{B.62})$$

Now, substituting η_e by its definition,

$$\|\mathbf{Q}_e\|^2 = 2 \left(1 - \eta^2 - \eta(-\eta + \beta(\eta - \text{sgn}(\eta)m)) - \sqrt{1 - (\beta(\eta - \text{sgn}(\eta)m))^2} \sqrt{1 - \eta^2} \right), \quad (\text{B.63})$$

$$= 2 \left(1 - \beta\eta^2 + \beta|\eta|m - \sqrt{1 - \beta^2(\eta - \text{sgn}(\eta)m)^2} \sqrt{1 - \eta^2} \right). \quad (\text{B.64})$$

Multiplying expression $(\eta - \text{sgn}(\eta)m)^2$ by $\text{sgn}(\eta)^2 = 1$,

$$\|\mathbf{Q}_e\|^2 = 2 \left(1 - \beta\eta^2 + \beta|\eta|m - \sqrt{1 - \beta^2(\text{sgn}(\eta)\eta - m)^2} \sqrt{1 - \eta^2} \right), \quad (\text{B.65})$$

$$= 2 \left(1 + \beta|\eta|(m - |\eta|) - \sqrt{1 - \beta^2(m - |\eta|)^2} \sqrt{1 - \eta^2} \right). \quad (\text{B.66})$$

The last part of the proof considers that the inequality $\|\mathbf{Q}_e\| < \alpha$ holds and looks for some inconsistencies. Using Lemma B.4, it follows that $\|\mathbf{Q}_e\|^2 < 2 - 2\sqrt{1 - m^2}$ and

$$2 \left(1 + \beta|\eta|(m - |\eta|) - \sqrt{1 - \beta^2(m - |\eta|)^2} \sqrt{1 - \eta^2} \right) < 2 - 2\sqrt{1 - m^2}, \quad (\text{B.67})$$

$$\sqrt{1-m^2} + \beta|\eta|(m-|\eta|) < \sqrt{1 + \beta^2\eta^2(m-|\eta|)^2 - \beta^2(m-|\eta|)^2 - \eta^2} \quad (\text{B.68})$$

As $m > |\eta|$, both sides of the inequality are non negative and can be squared,

$$\begin{aligned} -m^2 + 2\beta|\eta|(m-|\eta|)\sqrt{1-m^2} &< -\beta^2(m-|\eta|)^2 - \eta^2, \\ 2\beta|\eta|(m-|\eta|)\sqrt{1-m^2} &< -\beta^2(m-|\eta|)^2 + (m+|\eta|)(m-|\eta|). \end{aligned} \quad (\text{B.69})$$

Dividing both sides by $(m-|\eta|)$,

$$2\beta|\eta|\sqrt{1-m^2} < (1-\beta^2)m + (1+\beta^2)|\eta|. \quad (\text{B.70})$$

Squaring both sides again, as both of them are non negative,

$$\begin{aligned} 4\beta^2\eta^2(1-m^2) &< (1-\beta^2)^2m^2 + 2(1-\beta^2)(1+\beta^2)m|\eta| + (1+\beta^2)^2\eta^2, \\ -4\beta^2\eta^2m^2 &< (1-\beta^2)^2m^2 + 2(1-\beta^2)(1+\beta^2)m|\eta| + (1-\beta^2)^2\eta^2. \end{aligned} \quad (\text{B.71})$$

Since the left side of the inequality is negative and the right side is positive, the inequality holds. Thus, it is proved that $\|\mathbf{Q}_e\| < \alpha$. \square

The following lemmas refer to the multi-agent control chapter (Chapter 6).

Lemma B.9

Let $\mathbf{q}_{ij} = (\eta_{ij}, \epsilon_{ij}) = \mathbf{q}_j^* \circ \mathbf{q}_i$ and $R_{ij} = R_j^T R_i = \mathcal{R}(\mathbf{q}_{ij})$. Then $R_{ij}\epsilon_{ij} = \epsilon_{ij}$.

Proof. Using (2.5),

$$\begin{aligned} R_{ij}\epsilon_{ij} &= (I + 2\eta_{ij}S(\epsilon_{ij}) + 2S(\epsilon_{ij})^2)\epsilon_{ij}, \\ &= \epsilon_{ij} + 2\eta_{ij}S(\epsilon_{ij})\epsilon_{ij} + 2S(\epsilon_{ij})^2\epsilon_{ij}. \end{aligned}$$

As $S(\epsilon_{ij})\epsilon_{ij} = \epsilon_{ij} \times \epsilon_{ij} = 0$,

$$R_{ij}\epsilon_{ij} = \epsilon_{ij}.$$

\square

Lemma B.10

Let $J_i = J_i^T > 0$, $k_{Gi} > 0$, $a_{ij} > 0$, $\bar{x}_i = (\mathbf{q}_{i0}, \boldsymbol{\omega}_i, h_i) \in \bar{X} \triangleq \mathbb{S}^3 \times \mathbb{R}^3 \times \{1, -1\}$, $i = 1, 2, \dots, n$, $\bar{x} = (\bar{x}_1, \bar{x}_2, \dots, \bar{x}_n) \in \bar{X}^n$ and $V : \bar{X}^n \rightarrow \mathbb{R}$,

$$V(\bar{x}) = \sum_{i=1}^n 2k_{Gi}(1-h_i\eta_{i0}) + \sum_{i=1}^n \sum_{j=1}^n a_{ij}(1-h_i h_j \eta_{ij}) + \frac{1}{2} \sum_{i=1}^n \boldsymbol{\omega}_i^T J_i \boldsymbol{\omega}_i.$$

Then $V(\bar{x}) = 0 \Leftrightarrow \bar{x} \in \bar{A}$, where

$$\bar{A} = \bigcap_{i=1}^n \bar{A}_i, \quad \bar{A}_i \triangleq \{\bar{x} \in \bar{X}^n : \bar{x}_i = (\mathbf{1}, \mathbf{0}, 1) \text{ or } \bar{x}_i = (-\mathbf{1}, \mathbf{0}, -1)\}.$$

Proof. As J_i is a positive definite matrix, $\boldsymbol{\omega}_i^T J_i \boldsymbol{\omega}_i = 0 \iff \boldsymbol{\omega}_i = \mathbf{0}$. Hence, $\sum_{i=1}^n \boldsymbol{\omega}_i^T J_i \boldsymbol{\omega}_i = 0 \iff \boldsymbol{\omega}_i = \mathbf{0}, i = 1, \dots, n$.

Regarding the first summation, $1 - h_i \eta_{i0} = 0 \iff h_i \eta_{i0} = 1$. Multiplying both sides by h_i and since $h_i^2 = 1$, it follows that $\eta_{i0} = h_i$ and $\mathbf{q}_{i0} = (h_i, \mathbf{0}) = h_i \mathbf{1}$. Therefore, $\sum_{i=1}^n 2k_{G_i}(1 - h_i \eta_{i0}) = 0 \iff \mathbf{q}_{i0} = h_i \mathbf{1}, i = 1, \dots, n$.

Finally, the second summation is a consequence of the previous restriction.

$$\begin{aligned} h_i h_j \eta_{ij} &= h_i h_j (\eta_{j0} \eta_{i0} + \boldsymbol{\epsilon}_{j0}^T \boldsymbol{\epsilon}_{i0}), \\ &= h_i h_j \eta_{j0} \eta_{i0}, \\ &= h_i h_j h_j h_i, \\ &= h_i^2 h_j^2 = 1. \end{aligned}$$

Hence, the summand $1 - h_i h_j \eta_{ij}$ equals 0.

□

C

PUBLICATIONS

The following papers have already been published or submitted:

PEER-REVIEWED JOURNALS

P. P. M. Magro, J. Y. Ishihara, and H. C. Ferreira, “Robust global bimodal rest-to-rest attitude control of rigid body using unit quaternion,” *J. Franklin Inst.*, vol. 354, no. 8, pp. 3554- 3573, 2017.

P. P. M. Magro, and J. Y. Ishihara, “Robust global distributed attitude control for multiple rigid bodies using hybrid controller,” *Int. J. Syst. Sci.*, 2017 (submitted for publication).

PEER-REVIEWED CONFERENCES

P. P. M. Magro, H. T. M. Kussaba, L. F. C. Figueredo, and J. Y. Ishihara, “Dual quaternion-based bimodal global control for robust rigid body pose kinematic stabilization,” *American Control Conference, ACC 2017*, May 2017.

H. M. T. Menegaz, J. Y. Ishihara, and **P. P. M. Magro**, “Unscented Kalman filter for attitude estimation of satellites,” *XII Simpósio Brasileiro de Automação Inteligente, SBAI 2015*, Sep. 2015. Link for the article: <http://swge.inf.br/SBAI2015/anais/375.pdf>.

P. P. M. Magro, J. Y. Ishihara, and H. C. Ferreira, “Controle híbrido robusto e global de atitude de um corpo rígido usando quatérnions unitários,” *XII Simpósio Brasileiro de Automação Inteligente, SBAI 2015*, Sep. 2015. Link for the article: <http://swge.inf.br/SBAI2015/anais/413.pdf>.